Coherent scattering cross sections of some rare earth compounds at small angles below 10° for 662 keV gamma rays

Search | My Selection | Search History

Clear All | Insert Unicode

Search the INIS Repository

Full-text only | RN:53031819 | Search

Advanced Search

Filters

Results 1 - 1 of 1

All results > Conference Title: 65. DAE-BRNS symposium on nuclear physics

META

Coherent scattering cross sections of some rare earth compounds at small angles below 10° for 662 keV gamma rays

Thulasi, P.V. (Department of Physics, University of Calicut, Calicut 673635 (India)); Joseph, Antony (Department of Physics, University of Calicut, Calicut 673635 (India)); Somashekarappa, H.M. (Centre for Application of Radioisotopes and Radiation Technology, Mangalore University, Mangalagangotri 574199 (India)); Kamat, Vinayak Anand (Centre for Application of Radioisotopes and Radiation Technology, Mangalore University, Mangalagangotri 574199 (India)), E-mail: thulasiabhilash@uoc.ac.in

Proceedings of the DAE-BRNS symposium on nuclear physics. V. 65
2021

Citation | Export

Abstract

[en] Studies on coherent scattering cross-sections have remarkable applications in various fields. But, experimental studies are scarce for small angles below 10° and at low momentum transfer region, due to the difficulty of resolving the coherent scattered peak from the main peak, even using the high resolution detectors. A new method had been suggested by Puttaswamy et al., using a simple geometrical set up, earlier used for gamma ray transmission studies. In the present work, using this method, we have determined the angle integrated total (coherent + incoherent) scattering cross sections of CeO_2; Yb_2O_3; Nd_2O_3; Dy_2O_3 and Gd_2O_3 for 661.6 keV gamma rays, in the angular range of (0 - 4°; 0 - 6°; 0 - 8° and 0 - 10°). From the total scattering cross sections, corresponding angle integrated incoherent scattering cross sections obtained from Evaluated Nuclear Reaction Database (ENDF) library (based on the Non relativistic Hartree-Fock form factor method) is subtracted to obtain the angle integrated coherent scattering cross sections. The obtained angle integrated coherent scattering cross sections are compared with that determined from ENDF database and its variation with effective atomic numbers of the selected rare earth oxides have been studied

Primary Subject	NUCLEAR PHYSICS AND RADIATION PHYSICS (S73)
Source	Gupta, Yogesh K.; Sahu, R.R.; Santra, S.; Gupta, A.K. (Nuclear Physics Division, Bhabha Atomic Research Centre, Mumbai (India)) (eds.); Board of Research in Nuclear Sciences, Department of Atomic Energy, Mumbai (India); [977 p.]; Dec 2021; [2 p.]; 65. DAE-BRNS symposium on nuclear physics; Mumbai (India); 1-5 Dec 2021; Article No. G30
Record Type	Book
Literature Type	Conference
Country of publication	India
Descriptors (DEI)	CERIUM OXIDES, COHERENT SCATTERING, EXCITATION FUNCTIONS, FORM FACTORS, GAMMA RADIATION, NUCLEAR REACTIONS, TOTAL CROSS SECTIONS
Descriptors (DEC)	CERIUM COMPOUNDS, CHALCOGENIDES, CROSS SECTIONS, DIFFERENTIAL CROSS SECTIONS, DIMENSIONLESS NUMBERS, ELECTROMAGNETIC RADIATION, FUNCTIONS, IONIZING RADIATIONS, OXIDES, OXYGEN COMPOUNDS, PARTICLE PROPERTIES, RADIATIONS, RARE EARTH COMPOUNDS, SCATTERING
Language	English
Reference Number	**53031819**
Related Record	53031417
INIS Volume	53
INIS Issue	13

A.H.M.'s
ANJUMAN ARTS, SCIENCE AND COMMERCE COLLEGE,
ANJUMANABAD, BHATKAL-581320
(AFFILIATED TO THE KARNATAKA UNIVERSITY, DHARWAD)

65th DAE BRNS SYMPOSIUM ON NUCLEAR PHYSICS

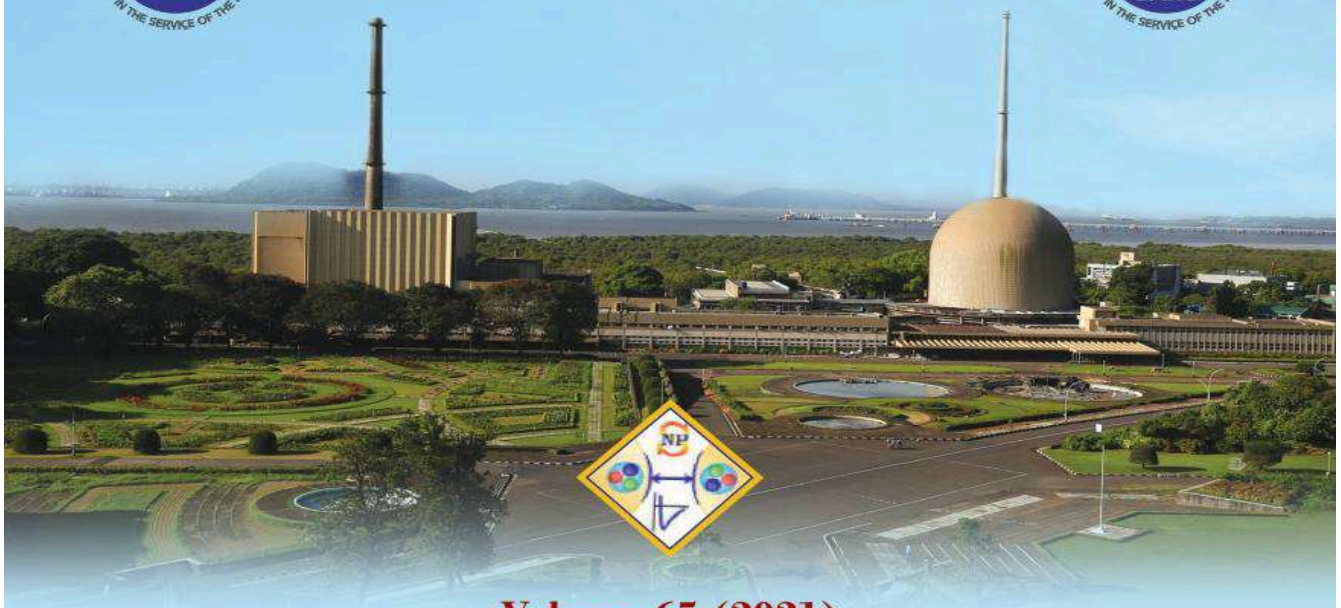

Volume 65 (2021)
DAE Convention Centre Anushaktinagar, Mumbai
December 1 - 5, 2021

Editors
Yogesh K. Gupta, R. R. Sahu,
S. Santra, A. K. Gupta

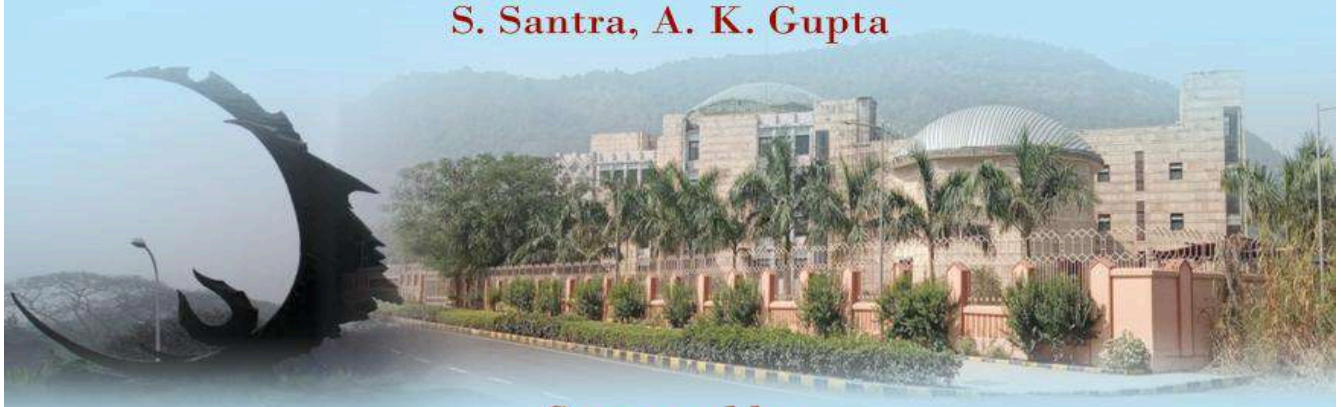

Sponsored by
Board of Research in Nuclear Sciences,
Department of Atomic Energy, Government of India

A.H.M.'s

ANJUMAN ARTS, SCIENCE AND COMMERCE COLLEGE, ANJUMANABAD, BHATKAL-581320

(AFFILIATED TO THE KARNATAKA UNIVERSITY, DHARWAD)

Contact : Yogesh K. Gupta
R. R. Sahu
S. Santra
A. K. Gupta

Printed by : Prudent Arts & Fab Pvt. Ltd.
A-221, TTC Industrial Area,
Opp. Anthony Motors Pvt. Ltd.,
M.I.D.C., Mahape, New Mumbai - 400701
Tel : +91 99302 00043 / 42`

ISBN 818372084-6

Coherent scattering cross sections of some rare earth compounds at small angles below 10^o for 662 keV gamma rays

P V Thulasi[1],* Antony Joseph[1], Somashekarappa H M[2], and Vinayak Anand Kamat[2]
[1] *Department of Physics, University of Calicut, Kerala - 673635, India and*
[2] *Centre for Application of Radioisotopes and Radiation Technology(CARRT), Mangalore University, Mangalagangotri - 574199, India*

Introduction

Studies on coherent scattering cross-sections have remarkable applications in various fields. But, experimental studies are scarce for small angles below 10^o and at low momentum transfer region, due to the difficulty of resolving the coherent scattered peak from the main peak, even using the high resolution detectors. A new method had been suggested by Puttaswamy et al.[1], using a simple geometrical set up, earlier used for gamma ray transmission studies. In the present work, using this method, we have determined the angle integrated total (coherent+ incoherent) scattering cross sections of $CeO_2, Yb_2O_3, Nd_2O_3, Dy_2O_3$ and Gd_2O_3 for 661.6 keV gamma rays, in the angular range of $(0-4^o, 0-6^o, 0-8^o$ and $0-10^o)$. From the total scattering cross sections, corresponding angle integrated incoherent scattering cross sections obtained from Evaluated Nuclear Reaction Database (ENDF) library (based on the Non relativistic Hartree-Fock form factor method) is subtracted to obtain the angle integrated coherent scattering cross sections. The obtained angle integrated coherent scattering cross sections are compared with that determined from ENDF database and its variation with effective atomic numbers of the selected rare earth oxides have been studied.

Estimation of parameters

When perfect narrow beam geometry is ensured, no scattered radiations are assumed to fall on the detector, then the transmitted intensity is represented by I_1. Now, if we allow some scattered radiations also to fall on the detector, it will reduce the value of the mass attenuation coefficient of the scatterer. Let I_2 be the intensity of transmitted plus scattered radiations within a cone of forward acceptance angle θ^0. Then $\Delta\mu$, the corresponding reduction in mass attenuation coefficient, can be expressed by the relation,

$$\Delta\mu = \frac{\ln\left(\frac{I_2}{I_1}\right)}{t} \quad (1)$$

where t is the thickness of the absorber. The total scattering cross section $\Delta\sigma_{sca}$ from 0 to θ^0 in barn/molecule is then given by[2],

$$\Delta\sigma_{sca} = \left(\frac{A}{0.60225}\right)\frac{\Delta\mu}{\rho} barn/molecule \quad (2)$$

where A is the molecular weight and ρ is the density of the scatterer. $\Delta\sigma_{sca}$ constitute both the coherent and incoherent scattering cross sections within the angular range of 0 to θ^0, which is expressed as,

$$\Delta\sigma_{sca} = \int_o^\theta d\sigma_{coh} + \int_o^\theta d\sigma_{incoh} \quad (3)$$

The effective atomic number of the rare earth oxides are obtained from the ratio of the atomic cross section σ_a to the electronic cross section σ_e. Accordingly,

$$\sigma_a = \frac{\mu_c}{N_o \sum_i \frac{\omega_i}{A_i}} \quad (4)$$

$$\sigma_e = \frac{1}{N_o}\sum_i \frac{\omega_i A_i \mu_i}{z_i} \quad (5)$$

In the above equations, N_o, ω_i and μ_i are the Avogadro number, weight fraction and mass

*Electronic address: thulasiabhilash@uoc.ac.in

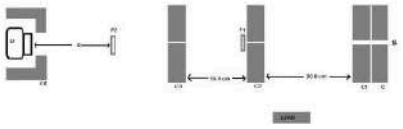

FIG. 1: The experimental setup. S is the source, D is the NaI detector and C, C1, C2 C3, C4 are lead collimators

attenuation coefficient of the i^{th} constituent element of the compound, respectively.Then,

$$Z_{eff} = \frac{\sigma_a}{\sigma_e} \quad (6)$$

Experimental details

In the present study, a ^{137}Cs source with activity of 0.191 GBq and a NaI(Tl) detector of crystal size 76 mm x 76 mm were used.The geometry of the experimental set up used is displayed in Fig 1. First, the scatterer was placed at the position P_1 such that the in-scattering angle was 0.28^o, so that the perfect narrow beam geometry condition has been ensured. No scattered radiations were allowed to reach the detector and pure transmitted beam intensity I_1 was measured. Subsequently, the scatterer was placed at the position P_2 so that the scattered radiations within a forward cone of $0 - \theta^o$ were allowed to reach the detector along with transmitted radiations. The corresponding intensity I_2 was determined, which contains the transmitted as well as scattered photons within an angle θ. From the background subtracted counts of I_1 and I_2, the total scattering cross section $\Delta\sigma_{sca}$ for an angular range of 0- θ^0 was determined . The statistical error estimated in each measurement is less than 0.1% and the error arising from multiple scattering is negligible due to the selection of optimum sample thickness ($\mu t <$ 0.5).

Results and discussion

Angle integrated coherent scattering cross sections of selected rare earth oxides were determined experimentally for 661.6 keV gamma

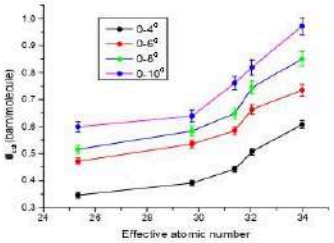

FIG. 2: Variation of coherent scattering cross section with effective atomic number for 661.6 keV gamma rays

rays for small angles below 10^o. The present experimentally determined values of coherent scattering cross sections, agree well with the theoretical angle integrated coherent scattering cross sections of ENDF. The coherent scattering cross section is found to increase with the effective atomic number of rare earth oxides and the variation is displayed in Fig 2.

Acknowledgments

One of the authors, P V Thulasi thank the CARRT centre, Mangalore University, Karnataka, for providing us with the required facilities for conducting the experiment.

References

[1] K S Puttaswamy, Mari Gowda and B Sanjeevaiah, A method for measuring integral scattering cross sections of gamma rays at small angles, Nuclear Instruments and Methods in Physics Research, 224 (1984) 461-468.

[2] L Vinay Kumar and T K Umesh, Small angle scattering of 59.54 keV photons by elemental samples in the atomic number region $13 \leq Z \leq 82$, Journal of Radiation Research and Applied Sciences, 9 (2016) 35-40.

Studies on the effects of Fe3O4-PbO combinations in peroxide vulcanisation of EPDM and shielding 59.54 kev gamma rays

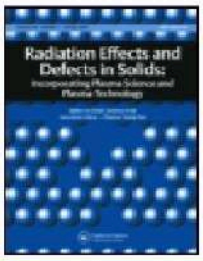

Taylor & Francis

Radiation Effects and Defects in Solids
Incorporating Plasma Science and Plasma Technology

ISSN: (Print) (Online) Journal homepage: https://www.tandfonline.com/loi/grad20

Studies on the effects of Fe_3O_4-PbO combinations in peroxide vulcanisation of EPDM and shielding 59.54 kev gamma rays

Vinayak Anand Kamat, K. Swaroop, K. U. Kiran, K. M. Eshwarappa & H. M. Somashekarappa

To cite this article: Vinayak Anand Kamat, K. Swaroop, K. U. Kiran, K. M. Eshwarappa & H. M. Somashekarappa (2021): Studies on the effects of Fe_3O_4-PbO combinations in peroxide vulcanisation of EPDM and shielding 59.54 kev gamma rays, Radiation Effects and Defects in Solids, DOI: 10.1080/10420150.2021.1935942

To link to this article: https://doi.org/10.1080/10420150.2021.1935942

Published online: 04 Aug 2021.

RADIATION EFFECTS & DEFECTS IN SOLIDS
https://doi.org/10.1080/10420150.2021.1935942

Taylor & Francis
Taylor & Francis Group

Check for updates

Studies on the effects of Fe_3O_4-PbO combinations in peroxide vulcanisation of EPDM and shielding 59.54 kev gamma rays

Vinayak Anand Kamat [a], K. Swaroop [a,b], K. U. Kiran [c], K. M. Eshwarappa [d] and H. M. Somashekarappa [a]

[a]Centre for Application of Radioisotopes and Radiation Technology (CARRT), Mangalore University, Mangalagangotri, KA, India; [b]Department of Studies in Physics, G M Institute of Technology, Davanagere, KA, India; [c]Government Science College (Autonomous), Hassan, KA, India; [d]Department of Studies in Physics, Davanagere University, Davanagere, KA, India

ABSTRACT

This research work presents the preparation of ethylene-propylene-diene-monomer (EPDM) composites filled with different concentrations of lead oxide (PbO) and magnetite (Fe_3O_4). The catalytic role of Fe_3O_4 on peroxide vulcanisation was studied. The morphological studies were done by the FESEM analysis. The evaluation of gamma shielding ability of synthesised composites was done for 59.54 keV gamma rays using a gamma spectrometer. Various shielding parameters, such as percentage attenuation ($\%_{Att}$), linear attenuation coefficient (μ), relaxation length (λ), half value (HVL) and tenth value layer (TVL) thickness, were evaluated for synthesised composites. The obtained results showed that, the shielding ability of the synthesised composites increases with an increase in PbO concentration. Also, the thermal stability of the synthesised composites was studied by TGA and it was found that thermal stability of the synthesised composites decreases with an increase in PbO concentration. Thus by comparing the results of radiation shielding ability and thermal stability, EPDM, with 40 phr PbO and 20 phr Fe_3O_4, can be considered as an ideal shielding material among the synthesised composites.

ARTICLE HISTORY
Received 7 September 2020
Accepted 3 May 2021

KEYWORDS
Polymer composites; radiation shielding; XCOM; MCNP; activation energy

1. Introduction

Radiation technology is widely used in industry, agriculture, aerospace research, food technology and medicine. Hence protection from radiation hazard from all the unnecessary exposure is a must. Preventing harm to the radiation worker or their surroundings from operating equipment, which emits potentially hazardous rays, is important. Shielding materials reduce the intensity of radiation by three nuclear interactions: photoelectric effect, Compton scattering and pair production. The probability of occurrence of these interactions depends upon the energy of incident beam, atomic number (Z) of the material and density of the material used for shielding. The photoelectric effect is predominant with high Z materials and low photon energy (below 0.1 MeV). The probability of Compton scattering

CONTACT H. M. Somashekarappa carrtmu@gmail.com

increases with high 'Z' and for photon energy between 0.6 and 4 MeV. The possibility of pair production will be high for high 'Z' and photon energy which is equal to or greater than 1.022 MeV (*1*,*2*).

Generally, high density materials are more effective in blocking or reducing the intensity of the radiations. However, by increasing the thickness of the low density materials, one can compensate the disparity. Concrete and magnetite are traditionally used for high density radiation shielding. High density hematite is an oxide of iron which is used for gamma/X-ray shielding. Addition of magnetite with steel and magnetite ore to the concrete provides better shielding than the ordinary steel/concrete. Many research attempts were made with alloys, rocks, marbles, steels, polymers, slag, gemstones and glasses for different shielding applications (*3*,*4*). Polymer and rubber, mixed with high atomic number materials, provide better shielding against gamma/X-rays and if they are mixed with hydrogen-rich materials, and also provide effective shielding against fast neutrons also. Polymer and rubber composites are less weight, commercially abundant and produce less secondary radiation than pure metal shields. Because of these advantages polymer composites are used as protective enclosures for devices and radiation workers in hospitals, shielding spacecraft, and nuclear power plants.

WinXCom can generate cross-sections or attenuation coefficients on a standard energy grid, spaced approximately logarithmically, or on a grid specified by the user, or for a mix of both grids (*5*). Auto-Z_{eff}. Direct-Z_{eff}, ZXCOM, and EXABCal software can facilitate easy computation of effective atomic number Z_{eff}, the effective electron density N_{eff} as a function of energy and spectral weighted means (*5*–*8*). MCNP code can be used to calculate photon attenuation by describing the geometry of the attenuator and source term of the gamma source.

Conventionally, high Z and high density metals, such as tungsten (W), lead (Pb), iron (Fe), are used to attenuate gamma photons (*9*,*10*). However, shielding materials having good mechanical strength, flexibility, chemical stability and lightweight are of great importance (*11*,*12*). Szajerski et al. (*13*) fabricated eight different samples of natural rubber (NR) for radiation shielding, which contains Bi (15–35%), W (15%), Gd (0–24%) and Sb (3%). They reported that NR with Bi (50.1 phr), W(50.0 phr), Gd (80.7 phr) and Sb (10.6 phr) is a good shielding material for computed tomographic (CT) X-Rays shielding. Rubber/B_4C (5%)/W (5–30%) composites were fabricated and investigated for gamma (662 keV) and neutron shielding studies by Salami et al. (*14*). They found, gamma and neutron were attenuated by 30% and 18%, respectively for 5% B_4C and 30% W-filled rubber composites. Ahmed et al. (*15*) fabricated lead-filled Nitrile-Butadiene-Rubber (NBR) composites for shielding 0.662 MeV gamma rays. They found linear attenuation coefficient of 0.0478 mm^{-1} and half-value layer (HVL) of 14.5 mm for 75 wt % lead-filled NBR composites. Hussain et al. (*16*) studied gamma attenuation property of polyethylene glycol (PEG)/lead oxide composites for Co-60 gamma rays and found the linear attenuation coefficient of 9.5 cm^{-1} and HVL of 0.07 cm for PEG loaded with 40 wt % PbO. Atta et al. (*17*) synthesised Styrene Butadiene Rubber (SBR-1502)/Montmorillonite clay nanocomposites in the presence of some metal oxides (Fe_2O_3, ZnO, MoO, TiO) for the shielding of gamma rays emitted by ^{137}Cs isotope and reported Molybdenum (II) Oxide (MoO)-treated clay composites show better attenuation coefficient (0.067 cm^{-1}) and HVL (10.34 cm) compared to clay composites treated with other oxides. Klepikov et al. (*18*) investigated Gamma radiation shielding ability of Polystyrene-steel-aluminium composites. They reported that all prepared composites

attenuate gamma rays by 90–98% and 80–97% for 100 and 122 keV gamma energies, respectively.

A radioactive isotope ^{241}Am found its applications in heat and power production in spacecraft, radiotherapy and radiography. There is a need for flexible and lightweight materials to shield gamma rays emitted from ^{241}Am radioactive isotope (*12*,*19*). Ethylene-propylene-diene-monomer (EPDM) has been chosen as a base polymer to prepare flexible composites because of its excellent properties such as low density, saturated and non-polar bonds (*20*). In this study, an attempt has been made to mix lead oxide (PbO) and magnetite (Fe_3O_4) in different ratios with EPDM to enhance the gamma attenuation property. The effects of Fe_3O_4 and PbO combination on peroxide vulcanisation, thermal stability and radiation shielding properties of the synthesised EPDM composites were studied.

2. Materials and methods

2.1. Preparation of samples

2.1.1. Materials

EPDM, with trade name 3045, (ethylene = 56 weight % and diene = 4.7 weight %) belongs to the family of thermoset elastomers and is procured in the form of standard bales from Mitsui Chemicals, Japan. Other processing chemicals, such as antioxident TQ, ISAF black, paraffinic oil, dicumyl peroxide and metal oxide fillers (Fe_3O_4 and PbO), used during the vulcanisation process are described in Table 1.

2.1.2. Compounding

The master batch of EPDM was prepared by mixing raw EPDM rubber with rubber additives such as antidegradent, reinforcing agent, and processing oil in an internal mixer (Francis Shaw, KO MK3, England) for about 5 min and then kept for cooling to room temperature. EPDM-Fe_3O_4-PbO (EMP) composites with desired ratios of Fe_3O_4 and PbO are prepared in laboratory grade two-roll mill with the addition of a vulcanising agent. Five different compounds, EPDM (pristine), L60M0 (PbO-60 phr, Fe_3O_4-0 phr), L40M20 (PbO-60 phr, Fe_3O_4-0 phr), L20M40 (PbO-60 phr, Fe_3O_4-0 phr) and L0M60, were then cured in the hot press under 323 kN pressure at 170°C for their optimum cure time (T_{90}).

2.2. Cure characteristics

The cure characteristics, such as cure time (T_{90}), scorch time (Ts_2), maximum torque (M_h), minimum torque (M_l) and torque difference (M_h-M_l) of the synthesised EMP composites, were studied using the Rubber Process Analyser (RPA 2000, Alpha technologies, USA)

Table 1. Formulation of EPDM composites and their role in compounding.

Materials	Concentration (phr)	Suppliers	Role
EPDM	100	Mitsui chemicals, Japan	Base polymer
Antioxident TQ	1.5	Local suppliers	Antidegradent
ISAF black	30	Philips carbonblack, Kolkata, India	Reinforcing agent
Dicumyl peroxide	3	Peroxide india, Tamil nadu, India	Vulcanising agent
Paraffinic oil	10	Local suppliers	Processing oil
PbO	0–60	Loba chemie, Mumbai, India	Gamma absorber
Fe_3O_4	0–60	KIOCL, Karnataka, India	Gamma absorber

according to ASTM D 2084-01 at vulcanisation temperature of 170°C. The parameter cure rate index (CRI) represents the speed of curing reaction and can be calculated by using Equation (1) (*15*).

$$CRI = \frac{100}{\text{cure time} - \text{scorch time}} \quad (1)$$

2.3. Field emission scanning electron microscopy (FESEM)

Surface morhology of the EMP composites was examined by a field emission scanning electron microscope (ULTRA 55 FESEM, Karl Zeiss, Germany). A small fraction of the synthesised composites were sputtered with gold to avoid electrostatic charging during the image capture. Elemental analysis was performed for all synthesised EMP composites with the Energy-Dispersive X-ray (EDX) spectrometer coupled with FESEM.

2.4. X-ray Diffraction studies (XRD)

X-ray diffraction (XRD) patterns for synthesised EMP composites were obtained by the X-ray diffractometer (Rigaku Miniflex diffractometer using Cu-Kα_1 radiation (1.54060 Å). The diffraction patterns were scanned over 2 θ ranges from 10° to 80° at a scanning rate of 3° min^{-1}.

2.5. Attenuation studies

Attenuation parameters for EPM composites were studied with gamma rays emitted by an americium-241 (^{241}Am-241, activity: $\sim$11.0 GBq) radioactive source and a well-calibrated 76 mm $\times$ 76 mm thallium-activated sodium iodide scintillation detector (scintiSPEC, Thermo Scientific, Germany) coupled with a photomultiplier tube (PMT) and a 2k multichannel analyser (MCA). The detector and radioactive sources are placed in the cylindrical lead case. The sample under investigation is kept 22 cm away from the radioactive source collimator (size = 0.8 cm) and detector collimator (size = 20 cm), respectively (Figure 1). The cylindrical solid lead block, with an outer diameter of 12 cm and a thickness of 5 cm, is used in front of the source and detector. The goodness of shielding used for housing the radioactive source and NaI(Tl) detector was tested by using a RedEye B20 (Thermo Scientific, Germany) survey meter, which showed the counts nearly the same environmental background 30 cm away from the experimental set-up. This observation indicates the photons detected by the detector do not contain any scattered photons at walls of the room. The intensity of transmitted photons (I) through samples and incoming photon intensity (I_0) was detected for 1000 s with and without keeping the samples in-between the radioactive source and NaI (Tl) detector, respectively. Each measurement was repeated four times to reduce the statistical error by a factor of 0.5 (*21*). The whole experimental set-up was kept at the centre of the room on a sturdy wooden table.

Percentage attenuation ($\%_{Att}$) capacity of synthesised composites was calculated by using Equation (2) (*19*,*22*).

$$\%_{Att} = \frac{I_o - I}{I_o} \times 100\% \quad (2)$$

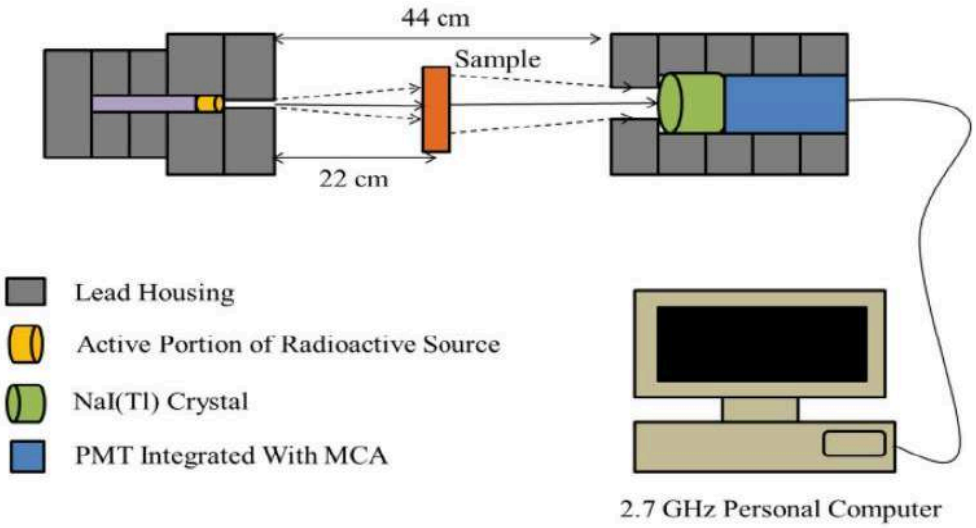

Figure 1. Transmission experimental set-up.

Linear attenuation coefficient (μ) is a physical parameter which represents the probability of gamma interactions per unit length. The value of 'μ' is calculated by using the Beer-Lamberts law (Equation (3)) (*17*,*23*).

$$I = I_o \exp^{-\mu X} \tag{3}$$

Here 'X' is the thickness of the samples. Also the vaules of the attenuation parameters, such as mass attenuation coefficient (μ_m), relaxation length (λ), half value layer thickness (HVL) and tenth value layer thickness (TVL), were obatined from the basic equations from Equation (3) (*12*).

2.6. Thermogravimetric analysis (TGA)

Thermogravimetric analysis (TGA) was performed for all synthesised EMP samples by using a universal thermal analyser (SDT Q 600, WATERS, USA) with a heating rate of 10°C min^{-1} from room temperature to 700°C.

3. Result and discussion

3.1. Cure characteristics

The effect of PbO and Fe_3O_4 concentration on scorch time of peroxide vulcanised EMP composites at 170°C is shown in Figure 2 and results are given in Table 2. The obtained data show an increasing trend in minimum torque (M_l) and maximum torque (M_h) with an increase in Fe_3O_4 content in EMP composites. This indicates the increase in minimum viscosity and maximum viscosity of the synthesised EMP blend compositions (*15*). Also, from Table 2 it is observed that, the values of cross linking density (M_h-M_l) increase with an increase in

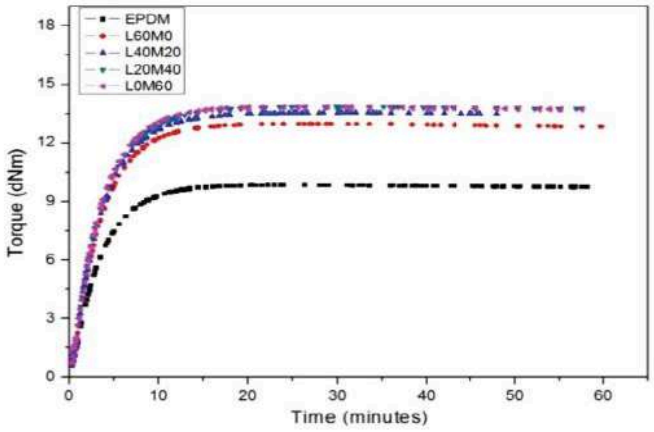

Figure 2. Torque vs. time graph of EPDM composites at 170 °C.

Table 2. Cure charateristics of EPDM composites at 170 °C.

Sample Name	PbO (phr)	Fe_3O_4 (phr)	M_l (dNm)	M_h (dNm)	M_h-M_l (dNm)	Ts_1 (min)	Ts_2 (min)	Tc_{90} (min)	CRI
EPDM	0	0	0.573	9.852	9.279	0.87	1.31	8.39	14.12429
L60M0	60	0	0.601	12.971	12.37	0.75	1.07	8.25	13.92758
L40M20	40	20	0.655	13.549	12.894	0.72	1.04	8.46	13.47709
L20M40	20	40	0.649	13.866	13.217	0.68	0.96	8.67	12.97017
L0M60	0	60	0.674	13.849	13.175	0.71	1.00	8.20	13.88889

Fe_3O_4 concentration in EMP composites. The decreasing trend of cure rate index (CRI) with an increase in Fe_3O_4 content in EMP composites indicates a decrease in activation cites for vulcanisation. This reduces the cure time and thereby speeds up the vulcanisation process. From these observations it can be considered that Fe_3O_4 can acts as a catalyst in the vulcanisation of EMP composites (*15*,*24*).

3.2. FESEM and elemental analysis

FESEM images and EDS spectrum of sythesised EMP composites are shown in Figure 3(a–e). Figure 3(a) indicates the neat EPDM polymer without any impurities and voids on its surface. The surface micrographs of L60M0, L20M40 and L0M60 show fillers (PbO and Fe_3O_4) dispersed over the surface of EPDM matrix. However, in L40M20 samples (Figure 3(c)), fewer filler particles were dispersed on the suface. As the FESEM images cannot differentiate between PbO and Fe_3O_4 filler particles, the dispersion of both PbO and Fe_3O_4 fillers was inhomogenous over the surface of EPDM matrix.

The base polymer EPDM is made up of ethyelene, propylene and diene units. Therefore, the backbone of EPDM contains the repeated units of carbon (C) and hydrogen (H) atoms. The EDS spectrum of pristine EPDM shows pridominent peaks of carbon and oxygen. The hydrogen peak cannot be identified over the pridominent peaks of carbon and oxygen in the EDS spectrum due to the limitaions of the Energy-Dispersive X-ray Spectrophotometer

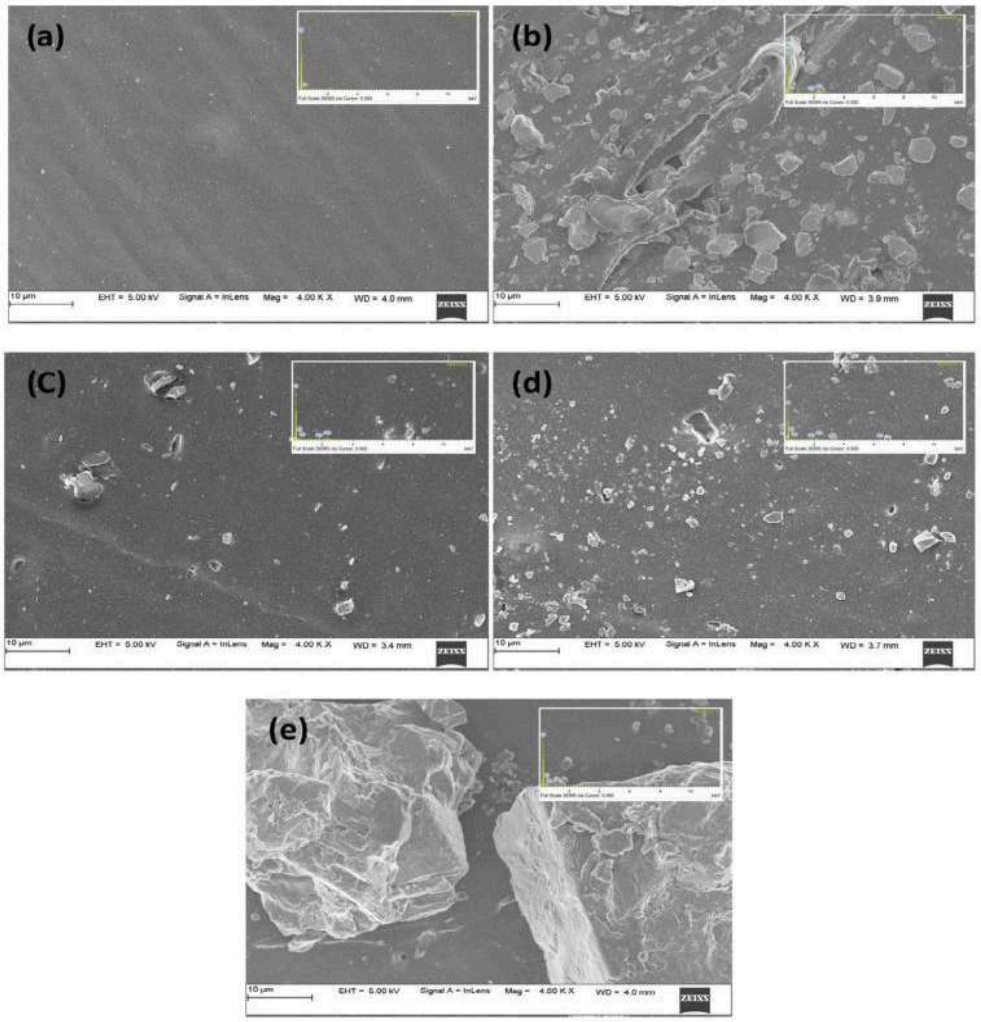

Figure 3. FESEM images and EDS spectrum of (a) EPDM (b) L60M0 (c) L40M20 (d) L20M40 (e) L0M60.

(*25*). However, oxygen peak is due to the peroxide (DCP) used in the vulcanisation process. The predominent peaks of C, O, Fe and Pb in the EDS spectrum of L40M20 and L20M40 samples are due to the presence of both PbO and Fe_3O_4 fillers. Whereas, the Pb peak identified in L60M0 sample and Fe peak identified in L0M60 samples is due to PbO and Fe_3O_4 fillers, respectively.

3.3. X-ray Diffraction (XRD) studies

The diffraction patterns of Fe_3O_4 and PbO used in the preparation of EMP composites are shown in Figure 4(a). For Fe_3O_4 powder, there are characteristic peaks at $2\theta = 30.08°$,

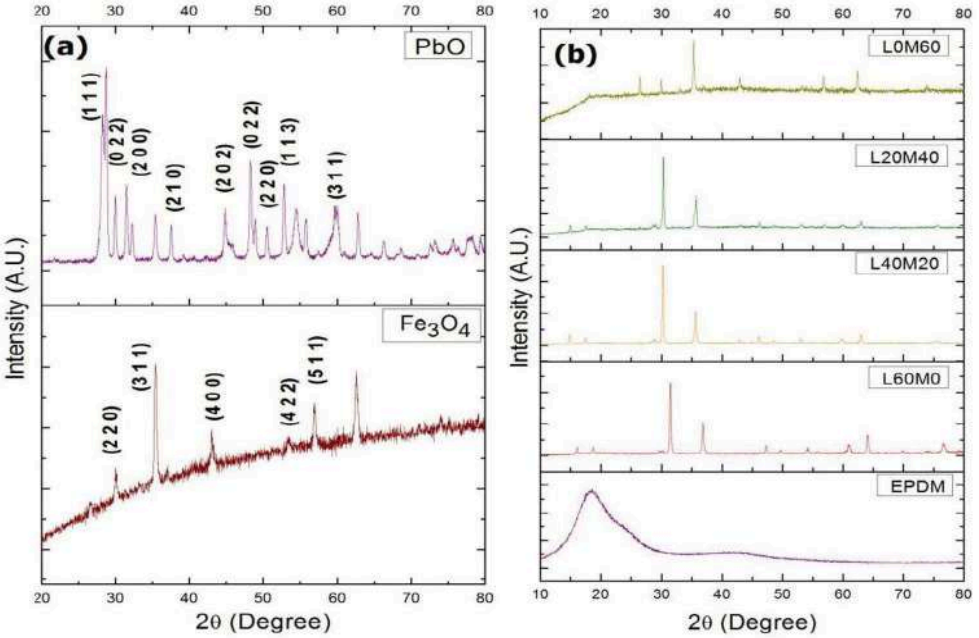

Figure 4. X-Ray diffraction patterns of (a) PbO and Fe_3O_4 (b) EMP composites.

35.32°, 43.12°, 53.38° and 57.02° corresponding to (2 2 0), (3 1 1), (4 0 0), (4 2 2) and (5 1 1) planes of Fe_3O_4, respectively (*26*). For PbO powder, there are characteristic peaks at $2\theta = 31.44°, 36.84°, 46.42°, 47.3°, 49.58°, 54.12°$, and 60.92° corresponsing to (2 0 0), (2 1 0), (2 0 2), (0 2 2), (2 2 0), (1 1 3), and (3 1 1) planes of PbO, respectively. The standard planes indicate Fe_3O_4 and PbO used in this work have a crystalline cubic spinal and tetragonal structure, respectively (*27,28*).

Figure 4(b) shows the X-ray diffractograms obtained for all the EMP composites. The diffractogram of pure EPDM exhibits the broad peak at 18.18° due to its semicrystalline nature. The prominent peaks at $2\theta = 29.96°, 35.28°, 42.82°, 53.3°$ and 56.78° present in L0M60 indicate the presence of Fe_3O_4 fillers in the EPDM matrix. Also, the sharp peaks at $2\theta = 31.44°, 36.84°, 46.42°, 47.3°, 49.58°, 54.12°$ and 60.92° in L60M0 show PbO fillers in the EPDM matrix. As L20M40 and L40M20 samples contain mixtures of Fe_3O_4 and PbO, they shows peaks of both fillers. The semicrystalline nature of the EMP composites decreases with an increase in PbO concentration.

3.4. Attenuation studies

The probability of photon interactions per unit length of synthesised EMP composites was determined and its values are displayed in Table 3. The values of linear attenuation coefficient increase from 0.17997 (EPDM) to 1.95044 cm^{-1} (L60M0) with an increase in PbO concentration for 59.54 keV gamma rays. However, the values of relaxation length decrease

Table 3. Experimental and theortical linear attenuation coefficient (μ) of EMP composites for 59.54 keV gamma rays.

	Linear Attenuation Coefficient (cm^{-1})		
Sample Name	Experimental	XCOM	MCNP
EPDM	0.18 ± 0.01	0.17	0.21
L60M0	1.95 ± 0.04	1.88	1.84
L40M20	1.53 ± 0.01	1.37	1.37
L20M40	0.97 ± 0.01	0.90	0.92
L0M60	0.50 ± 0.01	0.46	0.50

from 5.56146 (EPDM) to 0.51294 cm (L60M0) with an increase in PbO concentration for 59.54 keV gamma rays. This is due to the high interaction cross-section of Pb (*23*). The heighest values of percentage attenuations were exhibited by L60M0 (99.04%) and L40M20 (96.89%) samples out of the synthesised EMP composites.

The experimental values of the linear attenuation coefficients of samples under investigation were compared with the results of Monte Carlo calculations performed using the Monte Carlo N-Particle (MCNP) code. The sample geometries used in MCNP simulation are of the same dimensions which were used for experimental measurement. The F1 tally is used to estimate the number of photons crossing the sample. As many as 1,500,000 histories were tracked to produce reliable confidence intervals (*29*). The estimated relative errror of Monte calculations was less than 6%. Simulated results are presented in Table 3. These results are also compared with the data obtained from online XCOM database (*30*). A slight variation between experimental and therotical values of 'μ' is observed due to the inhomogeniety of PbO and Fe_3O_4 fillers in the EPDM matrix.

Figure 5(b) represents the effect of different filler percentages (PbO and Fe_3O_4) over the percetage attenuation ($\%_{Att}$) capacity of EMP composites for 59.54 keV gamma rays. The behaviour of attenuation percentage curve (Figure 5(b)) is contrary to that of HVL curve (Figure 5(c)). This indicates the improvement of attenuation behaviour of the synthesised EMP composites with an increase in PbO filler concentration.

Furthermore, the values of HVL and TVL decrease with an increase in PbO concentartion. Next to L60M0 composites, L40M20 sample exhibits a good linear attenuation coefficent (1.95044 cm^{-1}) among the synthesised composites. As L40M20 composites contains relatively less PbO content than L60M0 composites they can be considered as better shielding materials among synthesised composites.

3.5. Thermogravimetric analysis (TGA)

Thermogram and the derivative thermogram of EMP composites at a heating rate of 10 °Cmin^{-1} are shown in Figure 6(a,b), respectively. Thermogravimetric curve of pristine EPDM shows that, a minor weight loss starts at 110 °C due to the elimination of moisture content and release of carbon dioxide (CO_2), hydrogen molecule (H_2) and volatile hydrocarbons from EPDM. It is followed by the first stage of degradation which starts at ∼ 440°C ends up at ∼ 470°C. Furthermore, the second stage of degradation starts at 609.50 °C and saturates above 651.69 °C where most of the components of pure EPDM undergo thermal decomposition (Figure 6(a)) (*31*). In comparison with that of EPDM sample degradation

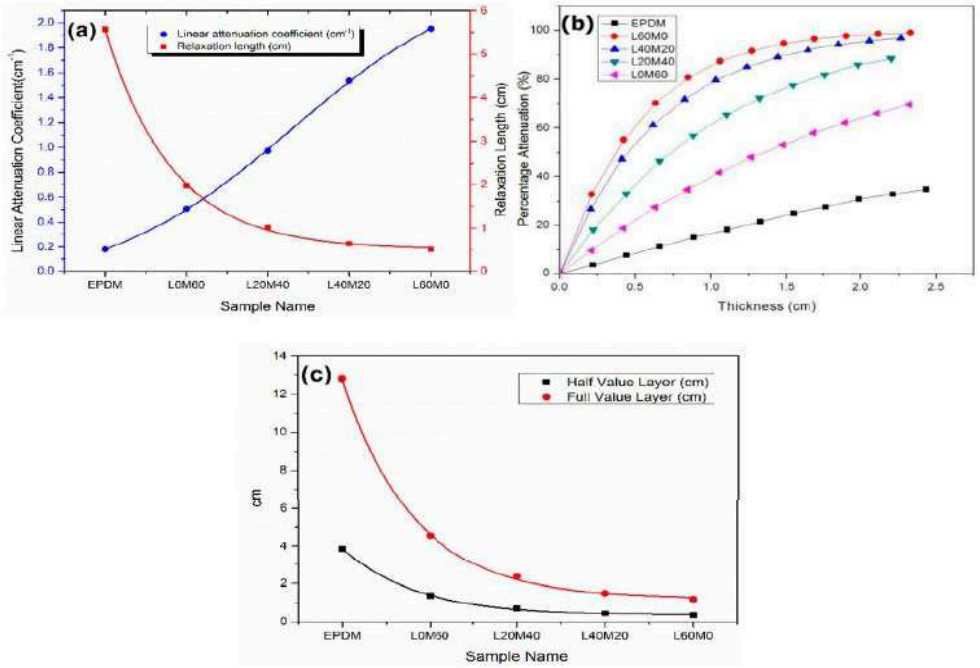

Figure 5. (a) Plot of %Att vs. thickness. Variation of (b) μ, λ (c) HVL and TVL of EMP composites.

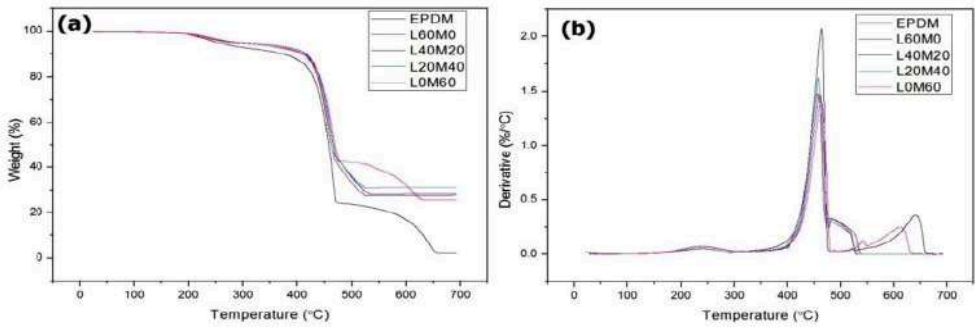

Figure 6. (a) Thermograms and (b) Derivative thermograms of EMP composites.

tempertaure of the EMP composites decreases. Also, among EMP composites the starting point of the first degradation increased from ~ 435°C to ~ 440°C with an increase in Fe_3O_4 concentration. The recidual weight observed for the EPDM composites loaded with metal oxide fillers (PbO and Fe_3O_4) can be due to the presence of high metling point of metal oxide fillers (PbO and Fe_3O_4) which remains even after the complete decomposition of the EPDM.

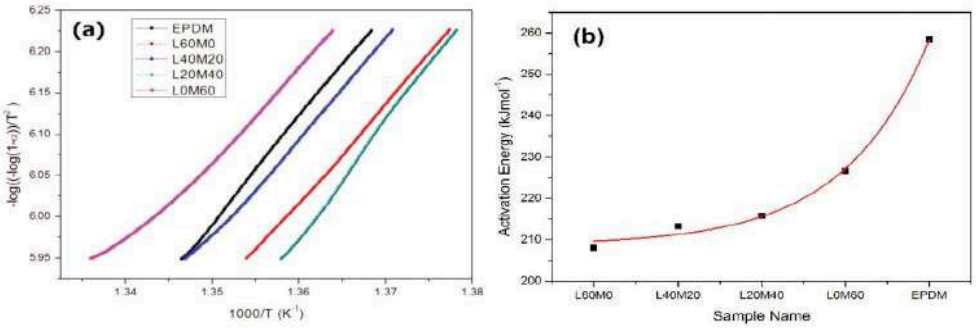

Figure 7. (a) The dependence of $-\log\left(\frac{-\log(1-\alpha)}{T^2}\right)$ vs. $\frac{1000}{T}$ (b) Plot of Activation energy vs. EMP composites.

The temperature (T_{max}), at which maximum degradation occurs, can be determined by using derivative thermograms. From Figure 6(b) it has been observed that all EMP composites have shown good thermal stability up to $\sim$ 322°C. The values of T_{max} increase from $\sim$ 457°C to $\sim$ 463°C with an increase in iron oxide (Fe_3O_4) content. Since Fe_3O_4 acts as a catalyst in EPDM vulcanisation, it may lead to a decrease in unsaturated double bonds in the EPDM network leading to increase the thermal stability of the EMP composites (*24*).

Activation energies of the synthesised EMP composites were determined by using the Coats-Redfern Equation (Equation (4)) (*32,33*).

$$\log\left(\frac{-\log\,(1-\alpha)}{T^2}\right) = \log\frac{R}{\Delta E}\left(1-\frac{2RT}{E}\right) - 0.434\frac{E}{RT} \tag{4}$$

Here 'R' is the gas constant, 'T' is the absolute temperature and 'E' is the activation energy and 'α' is the residual mass of the sample. The slopes of the stright line obtained from the plot (Figure 7(a)) of $-\log\left(\frac{-\log\,(1-\alpha)}{T^2}\right)$ vs. $\left(\frac{1000}{T}\right)$ were used to determine the activation energy of the composites by using Eq. 5.

$$E = 2.303 \times \mathrm{R} \times \text{slope} \tag{5}$$

From Figure 7(b) it has been observed that activation energy of the EMP composites increases with an increase in Fe_3O_4 content. L40M20 sample exhibited relatively more activation energy than L60M0 composite. Therefore, L40M20 sample has relatively more thermal stability than L60M0 composite.

4. Conclusion

The flexible EPDM- Fe_3O_4- PbO composites were synthesised successfully by the melt mixing technique. The Fe_3O_4 used in this work acts as a catalyst in vulcanisation process as well as gamma ray absorber. However, PbO is well known for its gamma-absorbing abilities. The shielding property of all the synthesised EPDM- Fe_3O_4-PbO composites increases with an increase in PbO concentration. All synthesised composites have shown good attenuation

properties for gamma ray of energy 59.54 keV. The percentage attenuation was 99.04% for 2.32 cm-thick L60M0 sheets. Next to this, a 2.26 cm-thick L40M20 exhibits 96.89% attenuation for 59.54 keV gamma rays. Also, L40M20 samples exhibit better thermal stability than L60M0 samples. L40M20 contains relatively less PbO among the other synthesised composites; hence, it can be considered as a better shielding material for space, radiotherapy and power generation applications.

Acknowledgements

The authours are thankful to the Director, Rubber Board Research Institute of India (RRII), Kottayam, for the help in synthesising the EPDM composites and to use lab facility. They are grateful to the Chairman, Department of Physics, Mangalore University, for providing the Amrecium-241 radioactive source to conduct the experiment. They are also thankful to the Coordinator, DST-PURSE programme, Mangalore University for permitting them to use FESEM, DSC and TGA facility.

Disclosure statement

No potential conflict of interest was reported by the author(s).

Notes on contributors

Dr. *Vinayak Anand Kamat* completed his MSc and Ph.D degree from Department of Physics, Mangalore University, Mangalore, Karnataka, India. He has 6 years of research and teaching experience. His main area of research includes gamma radiation shielding properties of polymer composite materials and Thermo Luminescent Dosimeter (TLD) materials. He has more than 10 national and international publications in the field of Nuclear radiation protection and Thermo Luminescent Dosimeters.

Dr. *K. Swaroop* is presently working as Assistant Professor at Department of Physics, G M Institute of Technology, Davanagere, Karnataka, India. He obtained his M.Sc degree in Physics from Kuvempu University and Ph.D in Physics from Mangalore University, Karnataka, India. His main area of research includes hydrogels and hydrogel nanocomposites, gamma irradiation processing of materials, and radiation shielding properties of composite materials. He is having 10 years of research and teaching experience. He has published more than 30 research articles in various journal of national and international repute. He is a reviewer for many international and national journals.

Dr. *K. U. Kiran* did Master Degree and Ph.D from Mangalore University. His area of research is Nuclear Physics. His field of interest include, Gamma backscattering technique using NaI(Tl) detector, Characterization of composite materials using gamma backscattering method, Gamma transmission method to evaluate certain charcterisitcs of materials, Characterization of composite materials using gamma transmission method. Dr. Kiran K U has produced over 20 research papers in the field of Nuclear Physics. Having a teaching experience of over 21 years, Dr. Kiran K U is working as Assistant Professor and Head of the Department of Electronics in Government Science College (Autonomous), Hassan - 573 201, Karnataka. India.

Dr. *K. M. Eshwarappa* is Associate Professor of Physics at Davangere University, Davangere, Karnataka, India. He has authored over 25 publications. He has designed, fabricated and characterised the microtron based photoneutron source for elemental analysis and neutron radiography applications. The current interest of Dr K M Eshwarappa include development of nanocomposites based nuclear radiation shielding materials, nanofluids for industrial applications and gamma backscattering studies for non-destructive testing.

Dr. *H. M. Somashekarappa* is a Professor and formerly heading Medical Physics Division as it's Coordinator and Center-in-Charge of Center for Application of Radioisotopes and Radiation Technology

(CARRT), Mangalore University. His main area of research includes environmental radioactivity, radiation dosimetry, radiation scattering studies, radiation shielding materials, nanocomposite materials, and hydrogel nanocomposite materials for biomedical applications. He authored more than 100 research articles of national and international repute. He has successfully guided 6 PhD students and 3 research students are working under him.

ORCID

Vinayak Anand Kamat http://orcid.org/0000-0002-7591-3571

References

(1) Daniel R., McAlister. Gamma Ray Attenuation Properties of Common Shielding Materials; PG Research Foundation Inc: 1955 University Lane Lisle, IL 60532, USA, 2013. https://www.eichrom.com/wp-content/uploads/2018/01/gamma-ray-attenuation-white-paper-by-d.m.-rev-4.pdf.
(2) Kiran, K.U. Studies on Gamma Back-Scattering Technique for Characterisation of Composite Materials. PhD Thesis, Mangalore University, 2015.
(3) Parminder, K.; Singh, K.J.; Murat, K.; Sonika, T. Study of Environment Friendly Bismuth Incorporated Lithium Borate Glass System for Structural, Gamma-ray and Fast Neutron Shielding Properties. *Spectrochim. Acta, Part A.* **2019**, *223*, 117309.
(4) Büyükyıldız, M.; Kurudirek, M.; Ekici, M.; İçelli, O.; Karabul, Y. Determination of Radiation Shielding Parameters of 304L Stainless Steel Specimens from Welding Area for Photons of Various Gamma ray Sources. *Prog. Nucl. Energy.* **2017**, *100*, 245–254.
(5) Gerward, L.; Guilbert, N.; Jensen, K.B.; Levring, H. WinXCom—A Program for Calculating X-ray Attenuation Coefficients. *Radiat. Phys. Chem.* **2004**, *71*, 653–654.
(6) Taylor, M.L.; Smith, R.L.; Dossing, F.; Franich, R.D. Robust Calculation of Effective Atomic Numbers: The Auto-Z_{eff} Software. *Med. Phys.* **2012**, *39*, 1769–1778.
(7) Un, A.; Caner, T. The Direct-Z_{eff} Software for Direct Calculation of Mass Attenuation Coefficient, Effective Atomic Number and Effective Electron Number. *Ann. Nucl. Energy.* **2014**, *65*, 158–165.
(8) Eyecioglu, O.; Karabul, Y.; El-Khayatt, A.M.; İçelli, O. ZXCOM: A Software for Computation of Radiation Sensing Attributes. *Radiat. Eff. Def. Solids.* **2016**, *171*, 965–977.
(9) Kim, J.; Seo, D.; Lee, B.C.; Seo, Y.S.; William Miller, H. Nano-W Dispersed Gamma Radiation Shielding Material. *Adv. Eng. Mater.* **2014**, *16*, 1083–1089.
(10) Huang, W.; Yang, W.; Ma, Q.; Wu, J. Preparation and Characterization of γ-ray Radiation Shielding $PbWO_4$/ EPDM Composite. *J. Radioanal. Nucl. Chem.* **2016**, *309*, 1097–1103.
(11) Kamat, V.A.; Swaroop, K.; Kiran, K.U.; George, B.; Somashekarappa, H.M. Effect of Hematite-Lead Oxide Combination in Ethylene-Propylene-Diene-Monomer on Shielding 59.54 keV Gamma Rays. *Radiat. Phys. Chem.* **2019a**, *156*, 50–57.
(12) Kamat, V.A.; Swaroop, K.; Kiran, K.U.; Somashekarappa, H.M. Preparation and Characterization of Hematite and Lead Oxide Based Flexible EPDM Composites for Shielding Gamma Rays. *AIP Conf. Proc.* **2019b**, *2115*, 030047. doi:10.1063/1.5112886.
(13) Szajerski, P.; Zaborski, M.; Bem, H.; Baryn, W.; Kusiak, E. Optimization of the Heavy Metal (Bi-W-Gd-Sb) Concentrations in the Elastomeric Shields for Computer Tomography (CT). *J. Radioanal. Nucl. Chem.* **2014**, *300*, 385–391.
(14) Salimi, M.; Amirabad, E.A.; Ghal-Eh, N.; Soltani, Z.; Etaati, G. Fabrication and Radiocharacterization of Boron Carbide and Tungsten Incorporated Rubber Shields. *Int. J. Innovation Appl. Stud.* **2013**, *4*, 437–440.
(15) Ahmed, K.; Nizami, S.S.; Raza, N.Z.; Shirin, K. Cure Characteristics, Mechanical and Swelling Peoperties of Marbel Sludge Filled EPDM Modified Chloroprene Rubber Blends. *Adv. Mater. Phys. Chem.* **2012**, *2*, 90–97.
(16) Rizwan Hussain, Z.-U.-H.; Mohammad, D. A Study of the Shielding Properties of Polyethylene Glycol-Lead Oxide Composite. *J. Islam. Acad. Sci.* **1997**, *10*, 81–84.

(17) Atta, E.R.; Zakaria, K.; M., Madbouly, A.M. Study on Polymer Clay Layered Nanocomposites as Shielding Materials for Ionizing Radiation. *Int. J. Recent Scientific Res.* **2015**, *6*, 4263–4269.
(18) Klepikov, V.F., Prokhorenko, E.M., Lytvynenko, V.V., Zakharchenko, A.A., Hazhmuradov, M.A. Application of Methods of Mathematical Modeling for Determining of Radiation-Protective Characteristics of Polystyrene-Metal Composite Materials. 2016 http://vant.kipt.kharkov.ua/ARTICLE/VANT_2016_3/article_2016_3_123.pdf.
(19) Dubey, K.A.; Chaudhari, C.V.; Suman, S.K.; Raje, N.; Mondal, R.K.; Grover, V.; Murali, S.; Bhardwaj, Y.K.; Varshney, L. Synthesis of Flexible Polymer Shielding Materials for Soft Gamma Rays: Physicomechanical and Attenuation Characteristics of Radiation Crosslinked Polydimethylsiloxane/Bi_2O_3 Composites. *Polym. Compos.* **2016,** *37*, 756–762.
(20) Özdemir, T.; Akbay, İK; Uzun, H.; Reyhancan, İA. Neutron Shielding of EPDM Rubber with Boric Acid: Mechanical, Thermal Properties and Neutron Absorption Tests. *Prog. Nucl. Energy.* **2016,** *89*, 102–109.
(21) Knoll, G.F. *Radiation Detection and Measurement*, 3rd ed.; Wiley: New York, 2000.
(22) Eren Belgin, E.; Aycik, G.A. A Novel Metal Oxide Filled Polyethylene Based Composite Shielding Material for Protection from Harmful Effects of Ionizing Electromagnetic Radiation. *Akademik Platform*. **2014**. 1194–1201. http://isites.info/PastConferences/ISITES2014/ISITES2014/papers/A14-ISITES2014ID188.pdf.
(23) Kamat, V.A.; Swaroop, K.; Kiran, K.U.; Somashekarappa, H.M. Study on the Effect of PbO-Magnetite (Fe_3O_4) on Shielding Properties of EPDM Composites for 662 keV Gamma Rays. *Indian J. Pure Appl. Phys.* **2018,** *56*, 639–642. http://nopr.niscair.res.in/handle/123456789/44849.
(24) El-Tantawy, F.; Bakry, A.; El-Gohary, A.R. Effect of Iron Oxide on the Vulcanization and Electrical Properties of Conductive Butyl Rubber Composites. *Polym. Int.* **2000,** *49*, 1670–1676.
(25) James J., M.; Klaus, K. Application of Electron Probe Microanalysis to the Study of Geological and Planetary Materials. *Microsc. Microanal.* **2001,** *7*, 200–210.
(26) Kong, I.; Ahmad, S.H.; Abdullah, M.H.; Hui, D.; Yusoff, A.N.; Purvanti, D. Magnetic and Microwave Absorbing Properties of Magnetite-Thermoplastic Natural Rubber Nanocomposites. *J. Magn. Magn. Mater.* **2010,** *322*, 3401–3409.
(27) Safarifard, V.; Morsali, A. Sonochemical Syntheses of Nano Lead(II) Iodide Triazole Carboxylate Coordination Polymer: Precursor for Facile Fabrication of Lead(II) Oxide/Iodide Nano-Structures. *Inorg. Chim. Acta.* **2013,** *398*, 151–157.
(28) Arulmozhi, K.T.; Mythili, N. Studies on the Chemical Synthesis and Characterization of Lead Oxide Nanoparticles with Different Organic Capping Agents. *AIP. Adv.* **2013**, 122122.. doi: 10.1063/1.4858419.
(29) Kiran K.U., R.; Eshwarappa, K.M.; Somashekarappa, H.M. Albedo Factors of 123, 320, 511, 662 and 1115 keV Gamma Photons in Carbon, Aluminium, Iron and Copper. *Eur. Phys. J. Plus.* **2016,** *131*, 87.
(30) Berger, M.J.; Hubbell, J.H.; Seltzer, S.M.; Chang, J.; Coursey, J.S.; Sukumar, R.; Zucker, D.S.; Olsen, K. *XCOM: Photon Cross Section Database, Web Version 1.5*; NIST: Washington, DC, 2010, http://physics.nist.gov/xcom.
(31) Zhang, Z.-s.; Xu, J.-s.; Chen, X.; Jiang, J. Studies on Thermal and Mechanical Properties of EPDM Insulation. *Mech. Eng. Control Syst.* **2016**, 66–70. doi: 10.1142/9789814740616_0015
(32) Coats, A.W.; Redfern, J.P. Kinetic Parameters from Thermogravimetric Data. *Nature.* **1964,** *201*, 68–69.
(33) Abdelrazek, E.M.; Elashmawi, I.S. Characterization and Physical Properties of CoCl2 Filled Polyethyl-Methacrylate Films. *Polym. Compos.* **2008**, *29*, 1036–1043. doi: 10.1002/pc.20481

Thermoluminescence Properties of Li Doped TiO2 Nanoparticles Synthesized using Co-precipitation Method

AIP Conference Proceedings

Thermoluminescence properties of Li doped TiO_2 nanoparticles synthesized using co-precipitation method

Cite as: AIP Conference Proceedings **2244**, 090003 (2020); https://doi.org/10.1063/5.0009921
Published Online: 26 June 2020

Kankanady Sharmila, Vinayak Anand Kamath, Kumarswamy Swaroop, and Hiriyur Mallaiah Somashekarappa

Thermoluminescence Properties of Li Doped TiO_2 Nanoparticles Synthesized using Co-precipitation Method

Kankanady Sharmila, Vinayak Anand Kamath, Kumarswamy Swaroop and Hiriyur Mallaiah Somashekarappa*,

Centre for Application of Radioisotopes and Radiation Technology (CARRT), Mangalore University, Mangalagangothri, Karnataka – 574199, India.

*Corresponding author E-mail: carrtmu@gmail.com

Abstract In the present study, lithium (Li) doped titanium dioxide (TiO_2) nanoparticles were synthesised by chemical co-precipitation technique using titanium tetrachloride ($TiCl_4$), sodium hydroxide (NaOH) as a precursor materials and lithium fluoride (LiF) as a dopant. The formation of nanocrystalline structure has been characterized by powder X-ray Diffraction (XRD) and Field Emission Scanning Electron Microscopy (FESEM) for structural and morphological properties. The synthesized TiO_2: Li nanoparticles were annealed at 450 °C and 800 °C. The annealed compounds were irradiated with gamma radiation ranging from 10 Gy to 10 kGy. Thermoluminescent (TL) and dosimetric characteristics of TiO_2 and TiO_2: Li nanoparticles have been studied using Thermoluminescent Dosimeter (TLD) reader. The TL glow curves of TiO_2 and TiO_2: Li nanoparticles have been evaluated for different doses of gamma irradiation. The TiO_2: Li nanoparticle shows higher TL response in comparison with TiO_2 nanoparticles. The more detailed analysis along with results and discussions are presented in this paper.

INTRODUCTION

Thermoluminescence (TL) dosimetry is considered as a reliable and routine method of measuring ionizing and non-ionizing radiation [1]. Titanium dioxide (TiO_2) based ceramics have many desirable and potential applications. The optical and chemical properties of TiO_2 are useful being colorless, transparent possessing a high refractive index, non-toxicity, chemical inertness, photosensitivity and thermoluminescence. It is the combination of its special properties and the ability to tailor the structure that makes TiO_2 based ceramics suitable for a wide range of applications [2]. Interest in titanium dioxide-based ceramics have been increased considerably in recent years as possible TL dosimeters which could be used in a wide variety of research activities and found its applications in ionizing radiation dosimetry [3].

MATERIALS AND METHODS

Lithium (Li) activated TiO_2 nanoparticles have been synthesized by co-precipitation technique using titanium tetrachloride ($TiCl_4$), sodium hydroxide (NaOH) as a precursor materials and lithium Fluoride (LiF) as a dopant. Both $TiCl_4$ and NaOH were mixed in 1:4 mole ratios and 1% of LiF was added to the mixture at room temperature. The white precipitate so obtained was centrifuged, filtered and washed several times by distilled water. The obtained product was dried and sintered at 110 °C until the product was completely dried and further it was calcined at 450 °C and 800°C [4]. The TiO_2 nanoparticles so obtained were characterized using powder X-ray Diffraction (XRD) (Rigaku miniflex 600, USA), Field Emission Scanning Electron Microscopy (FESEM) (ULTRA 55 FESEM, Karl Zeiss, Germany) for structural and morphological properties. Thermoluminescent dosimetric characteristics of TiO_2 nanoparticles have been studied using thermoluminescent dosimeter (TLD) reader (1009I, Nucleonix, India).

Proceedings of the International Conference on Physics of Materials and Nanotechnology ICPN 2019
AIP Conf. Proc. 2244, 090003-1–090003-4; https://doi.org/10.1063/5.0009921
Published by AIP Publishing. 978-0-7354-2003-8/$30.00

RESULT AND DISCUSSION

X-Ray Diffraction Analysis

The diffraction pattern of annealed TiO_2 and TiO_2: Li are shown in Fig. 1(a-d) and it indicates that TiO_2 nanoparticles prepared are nanocrystalline in nature. The prominent diffraction peaks identified at an angle 2θ = 27.40°, 36.06°, 45.18°, 54.35°, 56.48°, 66.19° and 75.16° corresponding to (110),(101), (210),(211), (220), (221) and (320) planes of TiO_2. It shows rutile phase of tetragonal structure which is in good agreement with the JCPDS Card No. 89-4920 [5].

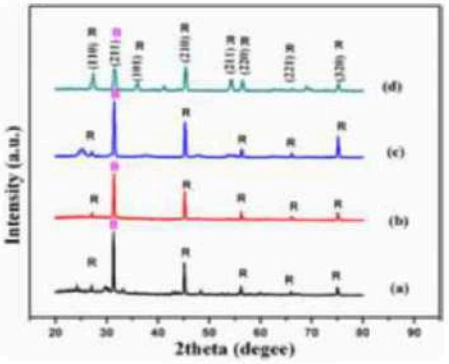

FIGURE 1. XRD spectra of TiO_2 (a), (b) and TiO_2: Li (c), (d) annealed at 450 °C and 800 °C.

Diffraction peaks appeared at 2θ = 31.42° shows presence of brookite crystalline phase along with rutile crystalline phase. The interplanar d-spacing (110) was found to be 3.241 Å and the crystallite size was calculated using Debye-Scherrer's formula which was found to be ~52 nm, ~42 nm, for pure TiO_2 and ~36.5 nm, 18.4 nm for TiO_2: Li which have been annealed at temperature 450 °C and 800 °C. The value of intercrystallite separation is observed to be 3.5624 nm, 3.5513 nm for pure sample annealed at 450 °C and 800 °C respectively. However for doped sample annealed at temperature 450 °C and 800 °C the value of intercrystallite separation was found to be 3.5482 nm, 4.0659 nm. The crystallite size of pure and doped TiO_2 nanoparticles was observed to be decreases with increase in annealing temperature. Intercrystallite separation remains same for the pure TiO_2 and for doped TiO_2 increases in accordance with increase in annealing temperature.

FESEM Analysis

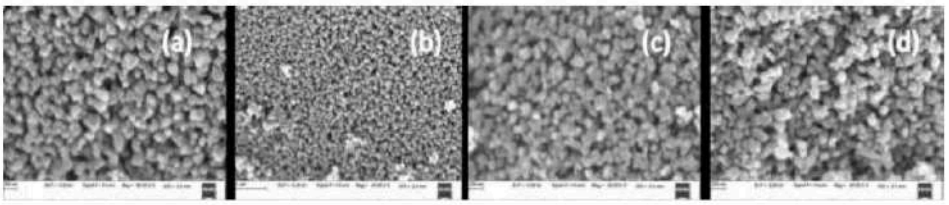

FIGURE 2. Shows the FESEM images of annealed TiO_2 and TiO_2: Li at 450 °C and 800 °C.

Figure 2 shows the SEM micrographs of TiO_2 and Li activated TiO_2 powder annealed at 450 °C and 800 °C. The images of TiO_2 and Li activated TiO_2 nanoparticles have shown the rectangular and hexagonal morphology.

Thermoluminescence Analysis

Thermoluminescent and dosimetric characteristics of TiO_2 and TiO_2: Li nanoparticles have been studied using TLD reader. The synthesized TiO_2 and TiO_2: Li nanoparticles were annealed at 450 °C and 800 °C for 4 hours and subjected to gamma radiation with the dose of 500 Gy. The TL glow curve obtained for TiO_2 and TiO_2: Li nanoparticles annealed at 450 °C and 800 °C are shown in Fig. 3(a) and (b) respectively. It has been observed that the TL intensity of the main peak increases with increase in the annealing temperature in both pure and doped samples. The maximum TL intensity is observed for the samples annealed at 800 °C. The main TL peak is observed around 275 °C and at annealing temperature 800 °C TL peak shows small shift towards low temperature side.

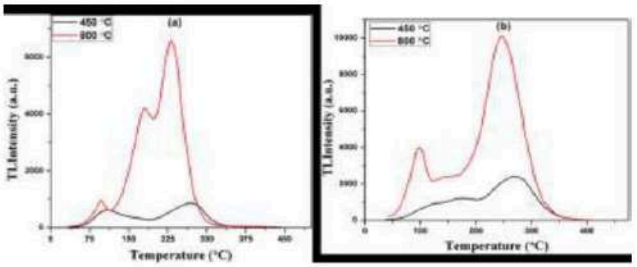

FIGURE 3. TL glow curve annealed at 450 °C and 800°C for (a) TiO_2 and (b) TiO_2: Li.

The effect of Li impurity on the TL properties of TiO_2 has been studied. Fig. 4(a) and (b) shows TL glow curve of TiO_2 and TiO_2: Li samples annealed at 450 °C and 800 °C. Both pure and doped samples were irradiated with gamma radiation of dose 100 Gy and TL intensity of TiO_2: Li is observed to be enhanced two times in comparison with undoped TiO_2. The main TL peak of doped sample shifted towards the higher temperature side in both the annealed temperatures due to the presence of dopant (Li). The effect of doping on the TL intensity of TiO_2 can be observed clearly and it infers that TL intensity of TiO_2: Li is enhances in comparison with undoped TiO_2.

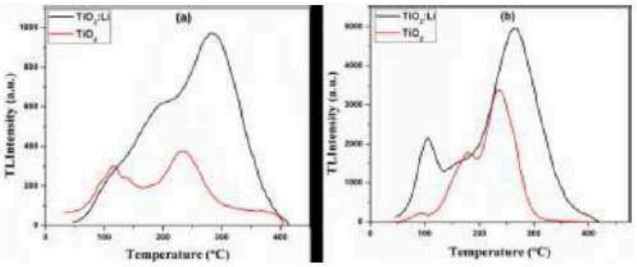

FIGURE 4. TL glow curve of TiO_2 and TiO_2: Li annealed at (a) 450 °C and (b) 800 °C irradiated with the dose of 100 Gy.

Figure 5 (a) and (b) depicts the TL glow curves of gamma irradiated pure TiO_2 at 450 °C and 800°C respectively. However, TL glow curves for TiO_2: Li nanoparticles annealed at 450 °C and 800°C are shown in Fig. 5 (c) and (d) respectively. All the samples were evaluated for different doses 10 Gy, 100 Gy, 500 Gy, 1 kGy, 5 kGy and 10 kGy. Among all the studied cases the TL intensity is observed to be minimum for 10 Gy and maximum for 10 kGy. Thus TiO_2: Li nanoparticles annealed at 800 °C exhibits higher TL intensity in comparison with remaining samples. The TL response is found to be increases with increase in gamma irradiation dose.

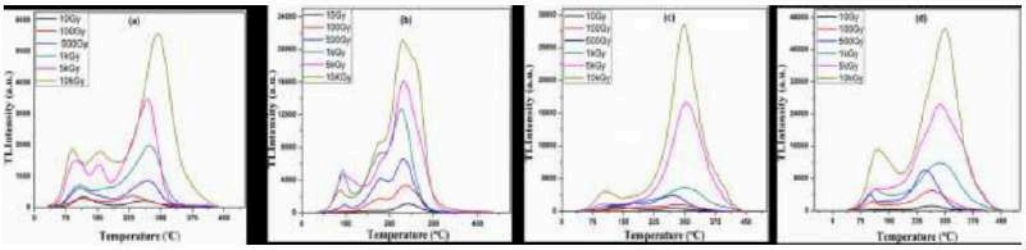

FIGURE 5. TL glow curve of gamma irradiated TiO_2 and TiO_2: Li annealed at 450 °C and 800°C for different doses.

The linearity property for TiO_2 and TiO_2: Li was also studied between 10 Gy to10 kGy and obtained graph is shown in Fig. 6. The TiO_2 and TiO_2: Li nanomaterial shows good linear response for higher doses whereas the slight deviation is observed between 10 to 500 Gy.

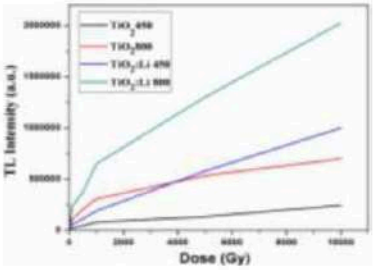

FIGURE 6. Linearity property

CONCLUSION

TiO_2 and TiO_2: Li nanoparticles were successfully synthesized by co-precipitation method. The XRD analysis was carried out for structural characteristics. The crystallite size of all the samples were in a range of 42 to 52 nm. The XRD result shows that the TiO_2 nanocrystals are predominantly in the rutile crystal phase with some traces of brookite phases. The FESEM image has shown rectangular and hexagonal morphology in the form of nano particles. The thermoluminescence glow curves of gamma irradiated TiO_2 nanoparticles have been evaluated for different doses. The synthesized TiO_2 and TiO_2: Li has shown good linearity property between the irradiation doses of 1 kGy to 10 kGy. The TL glow curves of gamma irradiated TiO_2 samples have shown increase in the TL intensity with dose, annealing temperature and doping.

ACKNOWLEDGEMENTS

The authors are grateful to the director of PURSE, Mangalore University, India for providing FESEM experimental facility and DST-FIST, Department of Physics, Mangalore University, India for providing XRD spectroscopy facility.

REFERENCE

1. J.C.A. Vegaa, B.J.A. Nietoa, M.G. Hipolitoc and T.R. Montalvoa, Radiat. Meas. **42**, 613 (2007).
2. X. Chen, G. Gu, H. Liu, Z. Cao, J. Am. Ceram. Soc. **87**, 1035(2004).
3. J. Azorin, Appl. Radiat. Isot. Rev. **83**,187 (2014).
4. P.B. Rathod, K.R. Nemade and S.A.Waghule, Int. J. Chem. Phys. Sci. **4**, 491 (2015).
5. P.M. Shajudheen, K. Viswanathan, K.A. Rani, A.U. Maheswari and S.S. Kumar, World Acad. Sci., Eng. & Technol. Int. J. Chem. & Mol. Eng. **10**, 556 (2016).

Optimization of PbO/Fe3O4/EPDM Flexible Composites for Gamma Shielding Applications

AIP Conference Proceedings

Optimization of PbO/Fe_3O_4/EPDM flexible composites for gamma shielding applications

Cite as: AIP Conference Proceedings **2244**, 040004 (2020); https://doi.org/10.1063/5.0009918
Published Online: 26 June 2020

Vinayak Anand Kamath, Swaroop Kumaraswamy, Kiggal Udayashankar Kiran, and Hiriyur Mallaiah Somashekarappa

A.H.M.'s
ANJUMAN ARTS, SCIENCE AND COMMERCE COLLEGE,
ANJUMANABAD, BHATKAL-581320
(AFFILIATED TO THE KARNATAKA UNIVERSITY, DHARWAD)

Optimization of PbO/Fe_3O_4/EPDM Flexible Composites for Gamma Shielding Applications

Vinayak Anand Kamath[1], Swaroop Kumaraswamy[1], Kiggal Udayashankar Kiran[2] and Hiriyur Mallaiah Somashekarappa[1*],

[1]*Centre for Application of Radioisotopes and Radiation Technology (CARRT), Mangalore University, Mangalagangothri-574 199, Karnataka, India*
[2]*Government Science College (Autonomous), Hassan- 573 201, Karnataka, India*
*Corresponding author: carrtmu@gmail.com

Abstract. This paper presents the synthesis of flexible EPDM composites with different percentage combinations of Fe_3O_4 and PbO. The bonding nature between the metal oxides (Fe_3O_4 and PbO) and the EPDM matrix was examined by FT-IR spectroscopy. The gamma interaction parameters such as linear attenuation coefficient (μ), mass attenuation coefficient (μ_m), half value layer (HVL) and tenth value layer (TVL) thickness have been determined for all synthesised EPDM composites for 123keV, 360 keVand 1173.2keV by using transmission geometry.FT-IRresults shows that nature of interaction between EPDM matrixandmetal oxide fillers (i.e., PbO and Fe_3O_4) is not chemical in nature. The declination in the values of 'μ' and 'μ_m' were observed with increase in gamma energies. The shielding performance of the prepared EPDM composites is observed to be increases with increase in PbO content. HVL and TVL values are observed to be relatively same for all synthesised composites at 1173.2 keV. Among the prepared composites,EPDM loaded with 40 phr of PbO and 20 phr Fe_3O_4(DCPM20) is the optimum combination which contains relatively less content of PbO along with better shielding properties for low energy gamma rays. Thus DCPM20 can serves as a better shielding material for low gamma energies.

INTRODUCTION

A radiation shielding material found its importance in saving the mankind from harmful effectsofionizingradiations (X-ray, γ-ray etc.) [1, 2]. Lead (Pb) is traditionally known as a good radiation shielding material. Researchers in the recent years attempted to synthesize new metal-metal and metal-concrete composites for radiation shielding [3, 4]. Due to heavy weight and lack of flexibility this composites have some limitations. Therefore an attempt has been made by several researchers to prepare the flexible and light weight polymer filled metal oxide composites as a protective radiation shield [5-7].The purpose of present study is to fabricate various concentration of PbO and Fe3O4 filled EPDM composites. The best compatible combination ofPbO and Fe3O4 with EPDM polymer is identified and radiation shielding performance of all prepared EPDM composites were studied for different energy gamma rays. The obtained practical mass attenuation coefficients for prepared EPDM metal oxide composites are compared withtheoretical mass attenuation coefficient obtained fromXCOM database.

EXPERIMENTAL METHODS

Materials

In this study,ethylene propylene diene monomer (EPDM) (Mitsui Chemicals, Japan) was used as a base polymer material. Magnetite (Fe_3O_4) ore which has average particle size less than 150 μm and density 2.85 $gcm^{-3}$was kindly supplied by KIOCL Limited, Panambur Mangalore, India.The lead monoxide (PbO)powder with 99% purity and 9.53 gcm^{-3}density was procured form LOBAChemiePvt. Ltd. Mumbai, India. dicumyl peroxide-98 % (Arkema Peroxides India Private Limited, Tamil Nadu, India) antioxidant-TQ and paraffin oil (procured from local suppliers) were used without any additionalrefinement.

Preparation of Composites

In this study five different samples were prepared, namely pure EPDM (without containing any filler) DCPM60 (0 phr PbO and 60 phr Fe_3O_4), DCPM40 (20 phr PbO and 40 phr Fe_3O_4), DCPM20 (40 phr PbO and 20 phr Fe_3O_4), andDCPM00 (60 phr PbO and 0 phr Fe_3O_4) at the Rubber Board Research Institute of India (RRII), Kottayam. In first step the raw EPDM rubber was compounded with rubber ingradients such as antidegradent (antioxident-TQ) and reinforcing agent (ISAF black). The raw rubber prepared in first step is mixed with vulcanizing agent (DCP) and metal oxide fillers (PbO & Fe_3O_4) in two-roll mill. The cure time is determined for all synthesised EPDM-metal oxide compounds by Rubber Process Analyser (RPA-2000) at 170 °C. The obtained cure time was set into the hot presswith the constant pressure of 323 kN in order to obtain the desired dimension sheets.

Gamma Attenuation Studies

The fraction of initial photon intensity (I0) falls on any material of thickness X will undergo severalinteractionswithatoms, nucleus or electron of target material and thereby loses its energy either by photo electric effect, pair production or by Compton scattering. The rest of intensity (I) transmits through the target material and it is given by Beer-Lamberts equation 1.

$$I = I_o \exp^{-\mu X} \quad \text{---------- (1)}$$

Here 'μ' is the linear attenuation coefficient. The value of 'μ'is experimentally studied by transmission experimental setup. The dependence of 'μ' on gamma energies was evaluated for three different energies namely 123 keV, 360 keV and 1173.2 keV gamma rays by using Co-57 (~25.26 kBq), Ba-133 (~0.6109 MBq), and Co-60 (~2.032 MBq)radioactive sources respectively. The 3"×3"NaI(Tl) detector (scintiSPEC, Thermo Scientific, Germany) is kept at an angle of 180° with respect to the lead shielding containing radioactive source.A cylindrical lead collimator with diameters of 8 mm and 40 mm are used in front of radioactive source and detector respectively. The distance of 440 mm is maintained between the source and detector collimator. The sample is kept exactly at half of the distance between source and detector collimator with the help of polystyrene support which has an extreme low density of 0.00649 gcm-3.

RESULTS AND DISCUSSION

Fourier Transform Infrared Spectroscopic Analysis

The percentage transmission spectrum obtained from Fourier Transform Infrared (FT-IR) spectroscopic analysis between the wave number 400 to 4000 cm-1is shown in the Fig. 1.The peaks obtained at 2954.9cm-1, 2845cm-1, 1452.3cm-1, 1257.5cm-1, 1089.7cm-1, 1018.4cm-1, 794.67cm-1, and 700.16 cm-1in transmission spectrum of pure EPDM is due to the C-H symmetric stretch, C-H asymmetric stretch, mono substituted benzene rings, ketone, C-O stretching vibration, C-H plane in bending vibration, C-H out of plane bending vibration and iso or meta substituted benzene rings respectively [8]. The transmittance peak of all EPDM composites loaded with different proportion of PbO and Fe3O4 are in comparison with that of pure EPDM. Also there are no additional peaks or peak shift is observed for any combination of PbO and Fe3O4 with respect to pure EPDM. This observation indicates the nature of interaction between the EPDM and metal oxide fillers is purely physical.

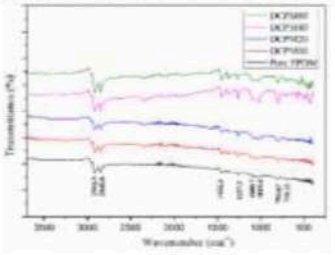

FIGURE 1.FT-IR transmission spectrum of EPDM composites loaded with different proportion of PbO and Fe_3O_4 in comparison with pure EPDM.

Attenuation Studies

Linear Attenuation Coefficient (μ)

The linear attenuation coefficient (μ) is an attenuation parameter represents the number of gamma interactions per unit thickness as the gamma rays passes through the absorber material. The value of 'μ, isdependsupon the absorber density and atomic number. The variation of linear attenuation coefficientas a function of densityis shown in the Fig. 2. From the Fig. 2 it clears that,thevalues of 'μ' varies linearly with density for all the metal oxide loaded EPDM composites.However, the pure EPDM shows the deviation from linearity in Fig. 2 and itcan be ascribed due to the presence of free volume in the polymer network. The value of linear attenuation coefficient for pure EPDM and EPDM composites loaded with different proportion of PbO and Fe3O4 are observed to be decreases with increase in gamma energy.

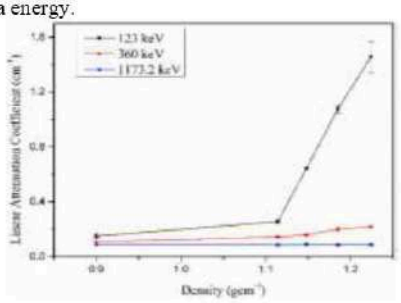

FIGURE 2. Variation of linear attenuation coefficient as a function of density forPure EPDM andEPDM composites loaded with different proportion of PbO and Fe_3O_4.

Mass Attenuation Coefficient (μ_m)

Mass attenuation coefficient (μm) is the density independent attenuation parameter and it can be obtained by dividing the linear attenuation coefficient of absorber material by its density factor. Table 1 represents the mass attenuation coefficients of EPDM and EPDM loaded with different proportion of PbO and Fe3O4 for 123 keV, 360 keV, and 1173.2keV gamma energies. Intable 1the values of mass attenuation coefficient of composites were observed to be increases with increase in the lead oxide concentration. The values of mass attenuation coefficient were also found to be decreased with increase in gamma energy. The highestvalue of attenuation for medium energies (i.e. 123 keV and 360 keV) was observed due to dominancy of photoelectric effect below 500 keV [9]. However at higher energies the attenuation rate is decreases due to pair production and Compton scattering phenomenon.Among the synthesised composites, EPDM with 60 phr of PbO (i.e. DCPM00) has the highest value of mass attenuation coefficient. The theoretical values obtained from XCOM database [10] showsslight deviation from theoretical values and this can be ascribed due to agglomeration of PbO and Fe3O4 fillers within the EPDM matrix.

TABLE 1.Experimental and Theoretical evaluation of mass attenuation coefficient (μm).

Sample name	123 keV		360 keV		1173.2keV	
	μ_m (cm^2g^{-1}) Exp.	μ_m (cm^2g^{-1}) Th.	μ_m (cm^2g^{-1}) Exp.	μ_m (cm^2g^{-1}) Th.	μ_m (cm^2g^{-1}) Exp.	μ_m (cm^2g^{-1}) Th.
Pure EPDM	0.17 ± 0.02	0.16	0.12 ± 0.003	0.11	0.08 ± 0.001	0.066
DCPM60	0.23 ± 0.01	0.18	0.13 ± 0.004	0.11	0.078 ± 0.001	0.063
DCPM40	0.56 ± 0.01	0.46	0.14 ± 0.003	0.12	0.078 ± 0.002	0.064
DCPM20	0.91 ± 0.02	0.74	0.17 ± 0.01	0.14	0.073 ± 0.001	0.064
DCPM00	1.19 ± 0.09	1.01	0.18 ± 0.01	0.16	0.070 ± 0.002	0.065

Half Value Layer (HVL) and Tenth Value Layer (TVL)

The values of HVL and TVL are determined for all synthesized composites at 123 keV, 360 keV and 1173.2 keV gamma rays and it is shown in Fig. 3. From Fig. 3 (a) and (b) it has been observed that, the values of HVL and TVL are observed to be increases with increase in PbO concentration. The values of HVL and TVL are also observed to be decreases with increase in gamma energy. However, at 1173.2 keV the value of HVL and TVL are observed to be almost same for all synthesized EPDM composites which can be attributed due to low gamma interactions at higher energies. As pure EPDM do not contains any metal oxide (PbO and Fe3O4) fillers it has shown highest value of HVL and TVL.

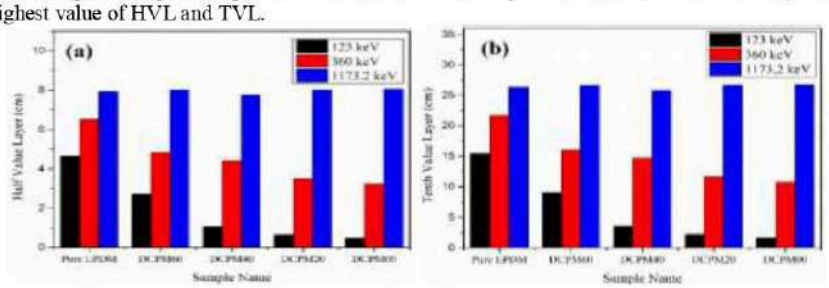

FIGURE 3.(a) Half Value Layer (HVL) and (b) Tenth Value Layer (TVL)forPure EPDM andEPDM composites loaded with different proportion of PbO and Fe_3O_4.

CONCLUSION

EPDM loaded with different concentrations of PbO and Fe_3O_4have been synthesized successfully from melt mixing method. A FT-IR result has shown that the bonding nature between EPDM matrixand metal oxide (PbO and Fe_3O_4) fillers used in this work is purely physical.The value of linear attenuation coefficient (μ) and mass attenuation coefficient(μ_m) of the prepared composites are found to be increase with increase in PbO concentration. A slight variation between the experimental and theoretical mass attenuation coefficient was observed due to the agglomeration of fillers. Among the fabricated EPDM composites, DCPM20 and DCPM00 are found to exhibit relatively better shielding performance for low energy gamma rays. As DCPM20 has relatively less PbO content and it can be considered as good shielding material for low gamma energies.

ACKNOWLEDGEMENT

The authors would like to express their sincere thanks to the Director, Rubber Board Research Institute of India (RRII), Kottayam, for assisting to use lab facility.

REFERENCES

1. K. Singh, S. Singh, A. S. Dhaliwal and Gurmel Singh, Appl. Radiat. Isot.**95**, 174-179 (2015).
2. C. Udagani and B. S. Seshadri, Int. J. Sci. Res.**1**, 68-71 (2012).
3. C. Shuo, B. Mohamed, R. Afsaneh, Radiat. Phys. Chem.,**117**, 12 –22 (2015).
4. P. S. Vishwanath and N. M. Badiger, Int. J. Nucl. Energy Sci. Technol.,**7**, 75–99 (2012).
5. V. Harish, N. Nagaiah and H. G. Harish Kumar, Indian J. Pure Appl. Phys.**50**, 847-850 (2012).
6. Vinayak Anand Kamat, K. Swaroop, K. U. Kiran, H. M. Somashekarappa, AIP Conf. Proc.**2115**, 030047 (2019).
7. Vinayak Anand Kamat, K. Swaroop, K. U. Kiran, G. Benny, H. M. Somashekarappa, Radiat. Phys. Chem. **156**, 50-57 (2019).
8. D. L. Tillier, J. Meuldijk, and C. E. Koning, Polymer (Guildf)., **44**, 7883–7890 (2003).
9. VinayakAnandKamat, K. Swaroop, K. U. Kiran, H. M. Somashekarappa, Indian J. Pure Appl. Phys. **56**, 639–642 (2018).
10. http://physics.nist.gov/xcom. (2018).

Preparation and characterization of bismuth-filled high-density polyethylene composites for gamma-ray shielding

Original Article

Preparation and characterization of bismuth-filled high-density polyethylene composites for gamma-ray shielding

M. Sheela[1,2], Vinayak Anand Kamat[3], K. U. Kiran[4], K. M. Eshwarappa[1,5]

[1]Research and Development Centre, Bharathiar University, Coimbatore, Tamil Nadu, Departments of [2]Physics and [4]Electronics, Government Science College (Autonomous), Hassan, [3]Centre for Application of Radioisotopes and Radiation Technology, CARRT, Mangalore University, Mangalore, [5]Department Studies in Physics, Davanagere University, Davanagere, Karnataka, India

Abstract

An attempt has been made to prepare the nonlead-based gamma shielding materials by adding different weight percentages (0%, 10%, 20%, and 40%) of bismuth in high-density polyethylene (HDPE) matrix. Gamma shielding parameters such as linear attenuation coefficient (μ), mass attenuation coefficient (μ_m), half-value layer, tenth value layer relaxation length (λ), and percentage attenuation were determined for all synthesized samples using 3"×3" NaI (Tl) detector for 59.54 keV energy. The results obtained from attenuation studies have shown that the shielding efficiency of synthesized HDPE+Bi composites increases with an increase in the weight percentage of bismuth. The experimentally obtained mass attenuation coefficient values are compared with Monte Carlo simulation using Monte Carlo N-particle code and XCOM code and are in good agreement with each other. The mechanical parameters such as tensile strength, tensile modulus, and elongation at the break were also determined for synthesized composites. Among the prepared composites, HDPE containing 40 wt% of bismuth (HDPE+40% Bi) has shown good radiation shielding property for 59.54 keV gamma rays along with good mechanical properties. Therefore, HDPE+40% Bi can be considered as a better lead-free shielding material for low-energy gamma rays.

Keywords: Attenuation coefficient, half-value layer, Monte Carlo N-particle, relaxation length, tenth value layer, tensile strength, XCOM

Address for correspondence: Dr. K. M. Eshwarappa, Research Supervisor, Bharathiar University, Coimbatore-641046, Tamilnadu, India.
Associate Professor, Department of Studies in Physics, Davanagere University, Shivagangotri-577007, India.
E-mail: km.eshwarappa@gmail.com

Submission: 05-Sep-2019 **Revision:** 09-Oct-2019 **Accepted:** 22-Oct-2019 **Published:** 27-Jan-2020

INTRODUCTION

Ionizing radiation like gamma radiation is widely used in industry and medicine. However, unwanted exposure to these radiations will cause damage to human life depending on its energy. There are three guidelines for controlling exposure to ionizing radiation (i) minimizing exposure time, (ii) maximizing distance from the radiation source, and (iii) shielding from the radiation source. The shielding material is generally used to reduce the intensity of radiation. There are various shielding techniques depending on the type of radiation. The penetrating power of alpha rays is very less, and they can block by human skin because alpha particles are heavy particles. Therefore, there is no need of shielding against alpha particles. The penetrating

Access this article online

Quick Response Code:

Website: www.rpe.org.in

DOI: 10.4103/rpe.RPE_29_19

How to cite this article: Sheela M, Kamat VA, Kiran KU, Eshwarappa KM. Preparation and characterization of bismuth-filled high-density polyethylene composites for gamma-ray shielding. Radiat Prot Environ 2019;42:180-6.

power of beta particles is higher than alpha particles, so the elements of low atomic number such as aluminum can be used as a shielding material for beta rays. Hydrogenous polymers and boron could play an important role for neutron shielding. Because of high penetrating power, the gamma rays could easily pass through the human body, high-density and high atomic number materials are often used for gamma-ray protection.[1] Lead is particularly well suited for reducing the effect of gamma rays due to its high atomic number, which has its limitations due to its toxicity and heaviness. The polymers loaded with fillers can replace the toxic lead in gamma shielding because they are of low cost, lightweight, mechanical flexibility, and also shielding flexibility, i.e., we can obtain the required shielding effect by varying the filler percentage. These polymer composites can also be used as neutron and X-ray shielding materials.

Several researchers over the globe have fabricated polymer composites for radiation shields and studied the shielding ability. The composites fabricated with 50 wt% aluminum was considered to be good shields for radiological safety aspects.[2] Isophthalic resin bismuth oxide composites are effective gamma radiation shields for the Cs^{137} source.[3] Hematite can enhance the gamma attenuation behavior of pure ethylene-propylene-diene-monomer for 59.54 keV gamma rays.[4] Therefore, the shielding ability of polymer composites is comparable to that of conventional shielding materials. The addition of sepiolite mineral to concretes may be an alternative option that can be used in several radiation protection applications, and experimental results were in good agreement with Monte Carlo N-particle (MCNP) and XCOM results.[5] The polyester steel composites can be used for both neutrons and gamma rays shielding, and the experimental values of the linear attenuation coefficient are compared with MCNP5 code results.[6] High-density polyethylene (HDPE) composed of mainly low Z materials, and its composites with high Z material are good shielding materials for mixed radiation sites such as high energy particle accelerator and at accelerator-based neutron sources.

In the present work, the authors have aimed at studying gamma-ray shielding ability of the shielding material which contains HDPE as the polymer matrix and bismuth as the filler in different weight% (0%, 10%, 20%, and 40%). Because as bismuth is a naturally occurring heavy element placed next to the lead in the periodic table, it has high value of Z and has high density comparable with lead and less toxic compared to lead, it is a right choice for nuclear radiation shielding as a filler and HDPE has good mechanical, thermal and corrosion resistance properties,[7] it was chosen as a polymer matrix.

EXPERIMENTAL METHODS

Materials

In this study, bismuth powder has been used as filler in different weight percentages with the HDPE matrix. This pure bismuth powder (purity-99% and density = 9.8 g/cm^3) was purchased from Sarda Industrial Enterprises, Jaipur, Rajasthan, and the thermoplastic HDPE (density = 0.92 g/cm^3) of injection grade was purchased from Banu Plast, Mumbai.

Preparation of samples

The HDPE composites were prepared by mixing HDPE powder with different weight percentages (0%, 10%, 20%, and 40%) of bismuth thoroughly by the mechanical mixing method. This mixture was molded to the dimension of 30 cm × 30 cm × 0.25 cm in the hydraulic press. The hydraulic press was maintained at the temperature of 180°C with the load pressure of 1000 kg for about 10 min and then the machine was allowed to turn off and rested till the temperature of the hydraulic press falls to 80°C–90°C. Then released the applied load and remove the sample from the mold. Thus, the HDPE+Bi composites were synthesized and cut into required dimensions for further characterization.

Morphological studies

The surface morphology of prepared bismuth-filled HDPE composites was studied using scanning electron microscope (JSM IT 300) at the applied voltage of 15 kV, 3000X resolution.

Gamma attenuation studies

Experimental setup

An experimental set up used for attenuation studies is shown in Figure 1. The Am^{241} source is placed inside the cylindrical lead blocks of 50 mm thick with a hole diameter of 8 and 20 mm for NaI (Tl) detector to avoid the additional contribution of scattered rays in the shielding studies.

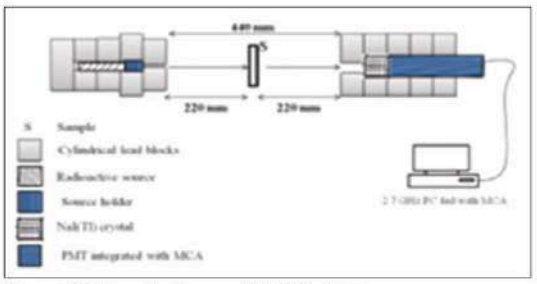

Figure 1: Schematic diagram of NaI (Tl) detector

In this study, the attenuation parameters were determined for energy 59.54 keV bypassing gamma rays through the synthesized polymer composites using well-calibrated 3"×3" NaI (Tl) scintillation detector (Thermo Scientific, Germany) coupled with a photomultiplier tube, preamplifier, amplifier, and PC-based 2k multichannel analyzer (MCA). The entire experimental setup was placed over a wooden table. The data acquisition and analysis were performed by Win (ICx Technologies GmbH, Thermo Scientific, Germany) TMCA 32 software package. The source was placed at a distance of 44 cm from the detector. The polymer composites were placed at a distance of 22 cm from the source. Each measurement was taken for the time duration of 1000 s and 4 trials to reduce the experimental errors by 0.5.

Study of shielding parameters

The parameters such as linear attenuation coefficient (μ), mass attenuation coefficient (μ_m), half-value layer (HVL), tenth value layer (TVL), percentage of attenuation ($\%_{Att}$), and relaxation length (λ) is necessary to know the effectiveness of shielding material.

Beer–Lambert's law $I = I_0 e^{-\mu t}$, where I_0 is the intensity of the gamma rays incident on the target material, I will be the intensity of the gamma rays after passing through the sample of thickness t, and μ is the linear attenuation coefficient, gives the following relation:

$$\mu = -\frac{1}{t}\ln\frac{I}{I_0} \quad (1)$$

$$\mu_m = \frac{\mu}{\rho} \quad (2)$$

Where ρ is the density of the material

$$HVL = \frac{ln2}{\mu} \quad (3)$$

$$\text{TVL} = \frac{ln10}{\mu} \quad (4)$$

$$\lambda = \frac{1}{\mu} \quad (5)$$

The percentage of attenuation is evaluated for different thickness of all samples using the following equation:

$$\%_{Att} = \frac{I_0 - I}{I_0} \times 100 \quad (6)$$

The percentage of the heaviness of the polymer composites compared with other conventional shielding materials could be evaluated using the relation:

$$\%\ \text{heaviness} = \frac{\text{Density of given material}}{\text{Density of lead}} \times 100 \quad (7)$$

Monte Carlo N-particle simulation

MCNP transport code system[8] is used to simulate various physical interactions at a wide energy range. In the literature, there are various MCNP studies on radiation shielding effectiveness for different materials in recent years. The MCNP input file prepared by incorporating source definition, material card, wherein the weight percentage of various elements of samples under study has given and with suitable tally. The weight percentage of different elements of prepared samples were determined by the elemental composition, which was determined by using energy-dispersive X-ray (EDX) spectroscopy.[8] In this study, the MCNP-A General MCNP transport code of version 4A (Los Alamos National Laboratory Report LA-12625,1993, USA) is used to determine μ_m values of HDPE+Bi composites using EDX results.

XCOM software

Theoretical μ_m values can be obtained from the database by Hubbel and Seltzer. Berger and Hubbel developed XCOM[9] software to estimate μ_m values or photon interaction cross-section of a single element, compound or composite mixture in the wide energy region of 1 keV–100 GeV. Different parameters such as interaction coefficients and total attenuation coefficients are determined by the elemental composition of the composite materials. Recently several studies have been used the XCOM software to calculate the values of μ_m in the shielding materials.[9] In this study, by using the results of EDX for HDPE+Bi composites, XCOM of version 1.0.1 has used to determine μ_m values of HDPE/Bi composites for the calculations.

Mechanical studies

Mechanical properties such as tensile strength, Young's modulus, elongation at the break, and the elongation at the peak were studied for the rectangular bar of area 36 mm^2 placed between the grips of Universal Testing Machine (UTM) and was pulled at the speed of 50 mm/min until it broke due to the application of load. The impact strength of the samples was studied using computerized Impact tester and the density of the synthesized HDPE composites was estimated on Archimedes' principle.

RESULTS AND DISCUSSION

Scanning electron microscope analysis

Homogeneous dispersion of the fillers in the polymer matrix is important for the accuracy of measurements.[10] Figure 2a-d shows surface morphological and dispersion of

bismuth within synthesized HDPE composites. Figure 2a shows the neat HDPE matrix without any voids and any other impurities on its surface. The surface morphology of HDPE+Bi composites [Figure 2b] confirms the distribution of filler particles on the HDPE matrix. Agglomeration of fillers was observed in Figure 2c resulted in a decrease in the mechanical strength of the composite. Figure 2d shows the uniform distribution of 40 wt% of the filler in the HDPE matrix. Element analysis for all the composites was performed by using EDX spectroscopy.

Gamma shielding parameters

The shielding parameters of synthesized HDPE+Bi composites evaluated from the transmission experimental setup. For Am^{241} radioactive source, the linear attenuation coefficient (μ) and mass attenuation coefficient (μ_m) were found to increase with the increase in density and wt % of bismuth of synthesized HDPE/Bi composites as shown in Figures 3 and 4 respectively. The HVL, TVL, and the relaxation length found to be decreasing as expected theoretically with the increase in the filler wt% as shown in Figures 5-7, respectively. These values decide the applicability of these materials for radiation shielding applications. Hence, these parameters are necessary to decide which the better shielding material is.[9,10] Figure 8 shows all synthesized composites showed $\%_{Att}$ increases and becomes maximum (≈99%) with the increase in the thickness of the samples and increase in the concentration of bismuth (40 wt%) in the HDPE matrix. This shows that as the weight percentage of bismuth increases its attenuation ability increases for 59.54 keV gamma energy.[4]

Heaviness

The main advantage of polymer composites is its lightness. To verify the heaviness of the HDPE+Bi composites the

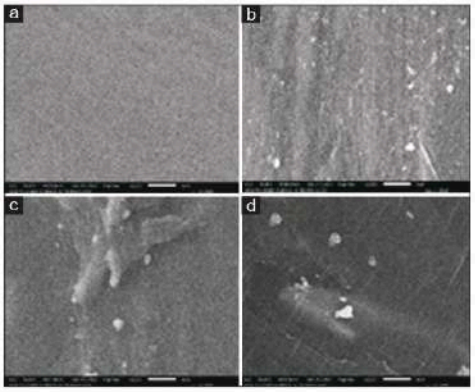

Figure 2: Scanning electron microscope images: (a) Pure high-density polyethylene, (b) High-density polyethylene +10 wt% of bismuth, (c) High-density polyethylene +20 wt% of Bismuth (d) High-density polyethylene +40 wt% of bismuth

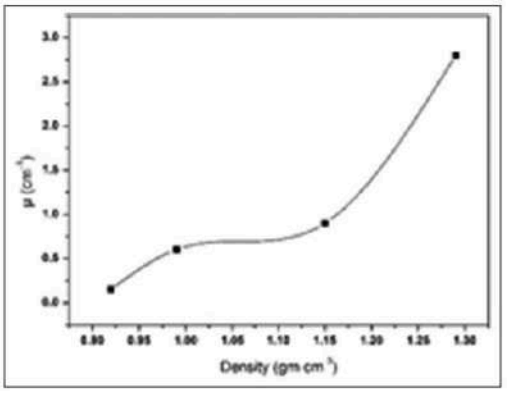

Figure 3: Effect of the density of high-density polyethylene+ Bi composites on linear attenuation coefficient

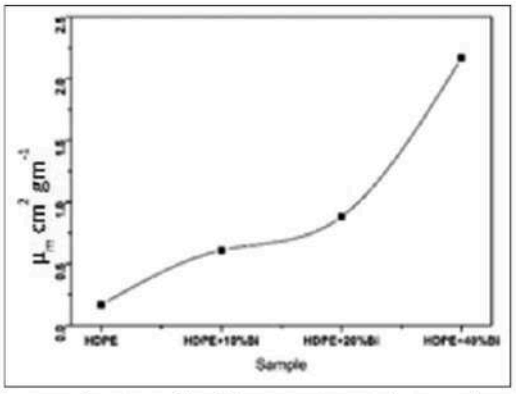

Figure 4: Effect of wt% of Bi on mass attenuation coefficient of high-density polyethylene

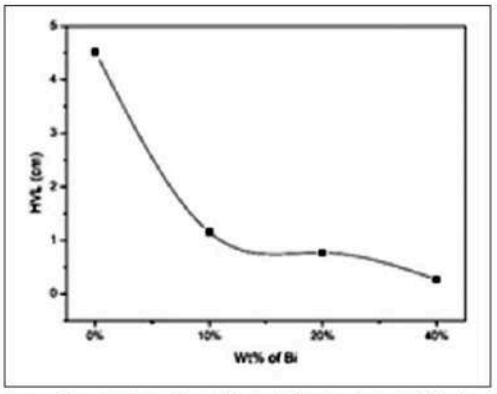

Figure 5: Effect of the wt% of filler on half-value layer of high-density polyethylene

lead was assumed as standard and normalized to 100%. The results of % of heaviness using the relation (7) are as shown in Figure 9. With the lead at 100% heavier than other shielding material under consideration, copper is at 78.83%, aluminum is at 23.8%, carbon is at 19.92%, and iron is at 69.22% heavier of lead. In the case of HDPE+Bi composites, even 40% bismuth-filled composite is only 11.37% of lead, while pure HDPE polymer is only 8.11% of lead. These results prove that the HDPE/Bi composites exhibit excellent lightness when compared with the conventional shielding materials such as lead, copper, aluminum, carbon, and iron and also their performance as radiation shielding materials are appreciable particularly at higher filler concentration (40 wt%) and for low-energy gamma rays.[11]

XCOM and Monte Carlo N-particle simulation results

For the study of shielding properties of the material/composites, the main parameter that has to be determined is the mass attenuation coefficient. The mass attenuation coefficient measures the probability of interaction of a photon with the material. The experimentally obtained mass attenuation coefficient values of HDPE/Bi composites were found to be quite close to those with MCNP and XCOM calculated values as shown in Table 1. The relative error in MCNP simulated results was kept below 5% based on the null hypothesis method. The slight disagreement between calculated and measured values is due to inaccurate nuclear reaction cross-section data, errors in measurement of physical quantities such

Table 1: Comparison between the experimental, XCOM database, and Monte Carlo N-particle calculated values of μ_m

Sample	μ_m (cm^2/g)		
	Experiment	XCOM	MCNP
HDPE	0.167	0.197	0.193
HDPE+10%Bi	0.609	0.711	0.710
HDPE+20% Bi	0.879	1.23	1.22
HDPE+40% Bi	2.168	2.25	2.23

HDPE: High-density polyethylene, MCNP: Monte Carlo N-particle

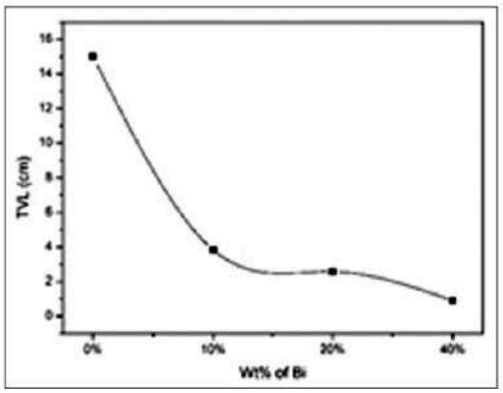

Figure 6: Effect of wt% of Bi on tenth value layer of high-density polyethylene

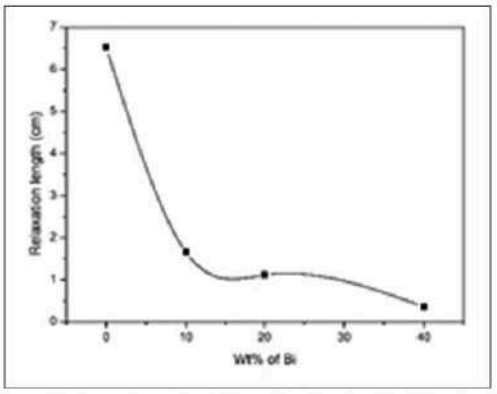

Figure 7: Effect of the wt% of Bi on relaxation length of high-density polyethylene

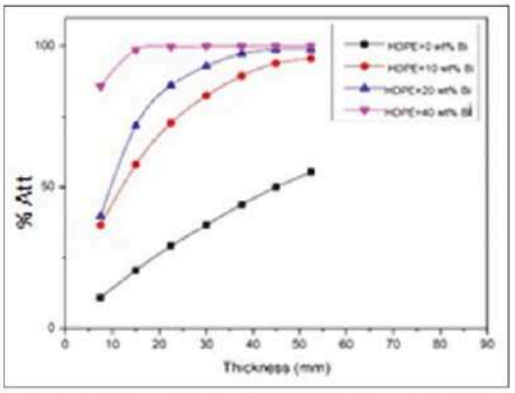

Figure 8: Variation of % Att with the thickness of high-density polyethylene +Bi composites

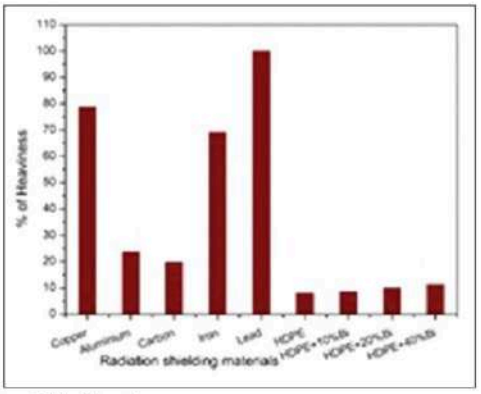

Figure 9: % of heaviness

Table 2: Results of mechanical properties of high-density polyethylene +Bi composites

Sample	Density (g/cm^3)	Tensile strength (MPa)	Young's modulus (G Pa)	Elongation at the break (mm)	Elongation at the peak (mm)	Impact strength (J)
HDPE	0.92	23.4	1.17	19.64	11.04	1.45
HDPE+10% Bi	0.99	24.2	1.58	14.96	10.59	1.4
HDPE+20% Bi	1.15	20.5	1.47	14.89	10.02	1.3
HDPE+40% Bi	1.29	20.6	2.2	14.79	8.93	1.1

HDPE: High-density polyethylene

as dimensions, densities, the elemental composition of the material, and the intensity of sources and it can be seen from Table 1 that the experimental values are less than the theoretical values. It is due to the fact that, uncertainty in experimentally determined weight percent of various elements and also due to uncertainty in reaction cross-section values based on which MCNP and XCOM programs calculate parameters of interest. It could be also due to minute difference geometry of experimental setup and geometry described in the MCNP input file. Although it was tried to design the experiment setup precisely, there were some inaccuracies that were always present, and these affected factors were eliminated in simulation and theoretical calculations.[12]

Mechanical property

The results of the mechanical properties of the prepared HDPE+Bi composites were tabulated in Table 2. This study shows that as the filler concentration increases its tensile strength and Young's modulus of the material of the composites increases, and there is a decrease in elongation at the peak, elongation at the break, and impact strength. As tensile strength represents the resistance of a material to breaking under tension and Young's modulus of the material measures the resistance of a material to elastic deformation under load, the present study results that as the bismuth concentration increases its mechanical strength increases. The details of the study could be found elsewhere.[13]

CONCLUSIONS

In this study, pure bismuth-filled HDPE composites were fabricated successfully by using hydraulic press and their gamma shielding performance, mechanical properties were analyzed. It was found that bismuth was distributed uniformly within the HDPE matrix, as the concentration of bismuth increases its mechanical strength increases. Results obtained from attenuation studies have shown that linear attenuation coefficient, mass attenuation coefficient and percentage attenuation coefficient increase with the increase in filler concentration, HVL, TVL, and λ are observed to decrease with the increase in filler concentration in HDPE matrix for Am^{241} source of energy 59.54 keV. In this study, HDPE with 40 wt% of bismuth shows good shielding properties for 59.54 keV gamma rays. Furthermore, it was found that the experimental values of μ_m are in good agreement with MCNP and XCOM calculated values. This indicates as the filler wt% increases its shielding ability increases and is comparable with the conventional shielding materials such as aluminum and carbon. As per the shielding properties, HDPE+Bi polymer composites can be used as an effective shielding material for 59.54 keV (Am^{241}) energy gamma radiations. Since ^{241}Am has found application in power generation, spacecraft, and radiotherapy, the lightweight HDPE+Bi composite with 40 wt% of Bi can be used as a flexible coat for radiation workers as well as flexible shielding material in space applications.

Financial support and sponsorship

Nil.

Conflicts of interest

There are no conflicts of interest.

REFERENCES

1. Erol A, Pocan I, Yanbay E, Ersöz OA, Lambrecht FY. Radiation shielding of polymer composite materials with wolfram carbide and boron carbide. Radiat Prot Environ 2016;39:3-6.
2. Osman M, Abdel-Monem AM, Mansour Aly FF. Investigation the shielding properties of alumina reinforced composites. JCBPS 2016;6:302-15.
3. Ambika MR, Nagaiah N, Harish V, Lokanath NK, Sridhar MA, Renukappa NM, *et al.* Preparation and characterisation of Isophthalic-Bi2O3 polymer composite gamma for radiation shields. Radiat Phys Chem 2017;130:351-6.
4. Vinayak Anand Kamat K, Swaroop KU, Benny GK, Somashekarappa HM. Effects of hematite-lead oxide combination in ethylene-propylene-dienemonomer on shielding 59.54keV gamma rays. Radiat Phys Chem 2019;156:50-7.
5. Sayyed MI, Tekin HO, Kilicoglu O, Agar O, Zaid MH. Shielding features of concrete types containing sepiolite mineral; Comprehensive study on experimental, XCOM and MCNPX results. Results Phy Elsevier 2018;11:40-5.
6. Osei-Mensah W, Fletcher JJ, Danso KA. Assessment of radiation shielding properties of polyester steel composite using MCNP5. Int J Sci Tech 2016;2:455-7.
7. Khalaf MN. Mechanical properties of filled high density polyethylene. J Saudi Chem Soc 2015;19:88-91.
8. Briesmeister JF. MCNP a General Purpose Monte Carlo N-Particle Transport Code, Ver. 4A. Los Alamos National Laboratory Report LA-12625; 1993.

9. Photon Cross Section Database, WinXcom Version 1.0.1, patch 1 (Build 31), Created by Klaus Bjorn Jensen, Henrik Levring, Nicolas Paul-Marie Guilbert. Offline package.
10. Soylu HM, Yurt Lambrecht F, nErsoz OA. Gamma radiation shielding efficiency of a new lead-free composite material. J Radiational Nucl Chem 2015;305:529-34.
11. Harish V, Nagaiah N, Harish Kumar HG. Lead oxides filled isophthalic resin polymer composites for gamma radiation shielding applications. Ind J Pure Appl Phys 2012;50:847-50.
12. Bagheri R, Moghaddam AK, Yousefnia A. Gamma ray shielding study of barium-bismuth – Borosilicate glasses as transparent shielding materials using MCNP-4C code, XCOM programme and available experimental data. Nucl Eng Technol 2017;49:216-23.
13. Sheela M, Kamat VA, Eshwarappa KM. Mechanical and electrical properties of bismuth filled high-density polyethylene composites. Int J Adv Res Innov Ideas Educ 2019;5:1177-81.

Thermoluminescence Properties of TiO2 Nanoparticles Synthesized using Co-precipitation Method

Thermoluminescence properties of TiO_2 nanoparticles synthesized using co-precipitation method

Cite as: AIP Conference Proceedings **2162**, 020102 (2019); https://doi.org/10.1063/1.5130312
Published Online: 29 October 2019

K. Sharmila, Vinayak Anand Kamat, K. Swaroop, and H. M. Somashekarappa


Thermoluminescence Properties of TiO_2 Nanoparticles Synthesized using Co-precipitation Method

K. Sharmila, Vinayak Anand Kamat, K. Swaroop and H. M. Somashekarappa[a)]

Centre for Application of Radioisotopes and Radiation Technology (CARRT), Mangalore University, Mangalagangothri, Karnataka – 574199, India

[a)]Corresponding author. E-mail: carrtmu@gmail.com

Abstract. In the present study, Titanium dioxide (TiO_2) nanoparticles have been synthesised using co-precipitation technique using titanium tetrachloride and sodium hydroxide as a precursor materials. The TiO_2 nanoparticles so obtained were characterized using powder X-ray Diffraction (XRD) and Scanning Electron Microscopy (SEM) for structural and morphological properties. The TiO_2 nanoparticles were annealed at 450 °C, 500 °C, and 550 °C. The synthesised compounds were irradiated with gamma radiation ranging from 200 Gy to 1 kGy. Thermoluminescentand dosimetric characteristics of TiO_2 nanoparticles have been studied using Thermoluminescent Dosimeter (TLD) reader (Model No: 1009I). The thermoluminescence (TL) glow curves of TiO_2 nanoparticles have been evaluated for different doses of gamma irradiation. The TL response of these nanoparticles shows the increasing trend with increasing of annealing temperature. The more detailed analysis along with results and discussions are presented in this paper.

INTRODUCTION

Thermoluminescence (TL) dosimetry is considered as a standard and regular method of measuring ionizing and non-ionizing radiation. Thermoluminescence dosimetry is used in many scientific and applied fields such as radiation protection, radiotherapy clinic, industry, and environmental and space research, using many different materials [1]. Titanium dioxide (TiO_2) is a wide band gap (3.2eV) semiconductor which has got significant application due to its non-toxicity, chemical inertness, photosensitivity and thermoluminescence properties. TiO_2 is been used as a prominent thermoluminescent material used by the researchers and use of TiO_2 as thermoluminescent dosimeters has increased considerably in the recent years [2].

MATERIALS AND METHODS

TiO_2 nanoparticles have been synthesized by co-precipitation technique using titanium tetrachloride ($TiCl_4$) and sodium hydroxide (NaOH) as precursor materials. Both $TiCl_4$ and NaOH were mixed in 1:2, 1:3, and 1:4 molar ratios at room temperature. The white precipitate so obtained was centrifuged, filtered and washed several times by distilled water. The obtained product was dried and sintered at 110 °C until the product was completely dried and further it was calcined at 450 °C [3]. The TiO_2 nanoparticles so obtained were characterized using powder X-ray Diffraction (XRD)(Rigaku miniflex 600, USA),Field Emission Scanning Electron Microscopy (FESEM)and Energy Dispersive Spectroscopy (EDS) analysis (ULTRA 55 FESEM, Karl Zeiss, Germany) for structural and morphological properties. Thermoluminescentdosimetric characteristics of TiO_2 nanoparticles have been studied using thermoluminescent dosimeter (TLD) reader (1009I, Nucleonix, India).

Proceedings of the International Conference on Advanced Materials
AIP Conf. Proc. 2162, 020102-1–020102-4; https://doi.org/10.1063/1.5130312
Published by AIP Publishing. 978-0-7354-1907-0/$30.00

RESULT AND DISCUSSION

X-Ray Diffraction Analysis

The diffraction pattern of prepared TiO_2 with 1:2, 1:3 and 1:4 mole ratios of precursor are shown in figure 1 (a-c) andit indicates that TiO_2 nanoparticles prepared are nanocrystalline in nature. The prominent diffraction peaks identified at an angle 2θ=27.78°, 36.25°, 41.51°, 44.07°, 54.53°, 56.80°,62.77°,64.55° and 69.44° corresponding to (110), (101), (111), (210), (211), (220),(002), (310)and (301) planes of TiO_2. It shows rutile phase of tetragonal structure which is in good agreement with the JCPDS Card No. 89-4920 [4].

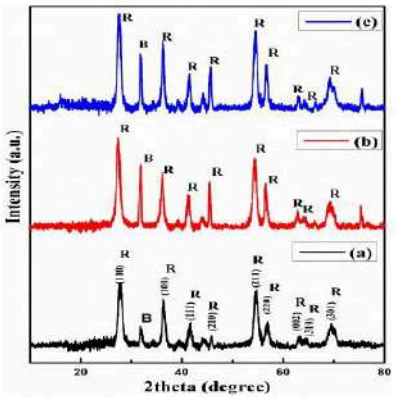

FIGURE 1. XRD spectra of TiO_2 prepared with the precursors mole ratio (a) 1:2, (b) 1:3, (c) 1:4.

Diffraction peaks appeared at 2θ = 31.73° shows presence of brookite crystalline phase along with rutile crystalline phase. The interplanar d-spacing (110) was found to be 3.241 Å and the crystallite size was calculated using Debye-Scherrer's formula which was found to be ~11 nm, ~12 nm, ~23 nm for 1:2, 1:3, and 1:4moleratios respectively. Intercrystallite separation 4.0710 nm, 4.0461 nm, 3.5376 nm with respect to the precursor mole ratio (a) 1:2, (b) 1:3, (c) 1:4. Crystallite size of TiO_2 nanoparticles increases with increase in NaOH concentration and intercrystallite separation decreases with increase in NaOH concentration.

FESEM and EDS Analysis

Figure 2 shows the SEM micrographs of TiO_2 powder calcined at 450 °C. All the images of TiO_2 nanoparticles synthesized at different mole concentration of precursors have shown the granular morphology. The Figure 3 shows the Energy Dispersive Spectroscopy (EDS) analysis of prepared TiO_2 powder which shows the presence of Ti and O, with no trace of any impurities.

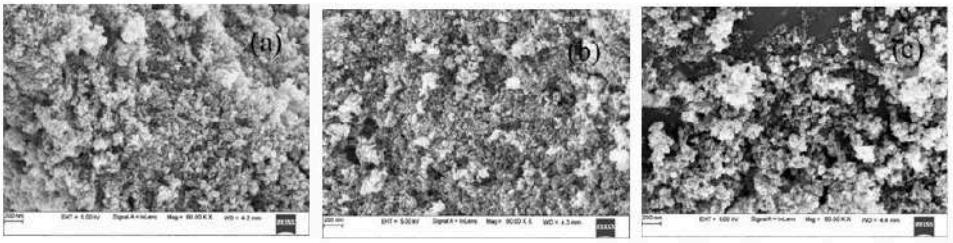

FIGURE 2. Shows the FESEM images of TiO_2 prepared with the precursors mole ratio (a) 1:2, (b) 1:3, (c) 1:4.

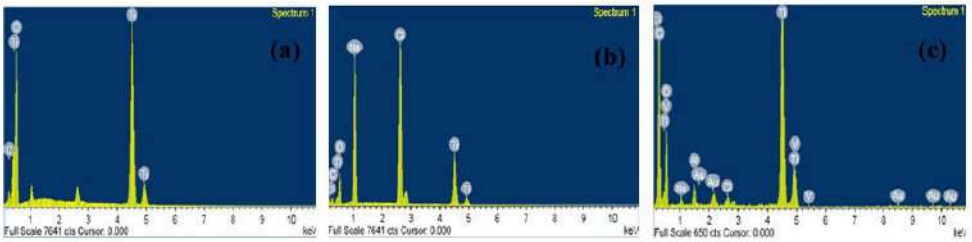

FIGURE 3. EDS analysis of TiO_2 prepared with the precursors mole ratio (a) 1:2, (b) 1:3, (c) 1:4.

Thermoluminescence Analysis

Thermoluminescentand dosimetric characteristics of TiO_2 nanoparticles have been studied using TLD reader.The TiO_2 nanoparticles were annealed atthree different temperatures ranging from 450 °C to 550 °C for 2 hours.Figure.4 (a to c)shows the TL glow curve of TiO_2 nanoparticles prepared at precursors mole ratio. It is observed that the TL intensity of the main peak increases with increase in the annealing temperature. The maximum TL intensity is observed for the sample annealed at 550 °C. The TL peak corresponding to 1:2, 1:3, and 1:4 ratio of $TiCl_4$:NaOH increased from 259 °C to 264 °C, 261 °C to 276 °C, and 258 °C to 262 °C as the annealing temperature increases from 450 °C to 550 °C respectively as shown in figure 4 (a to c) [5].

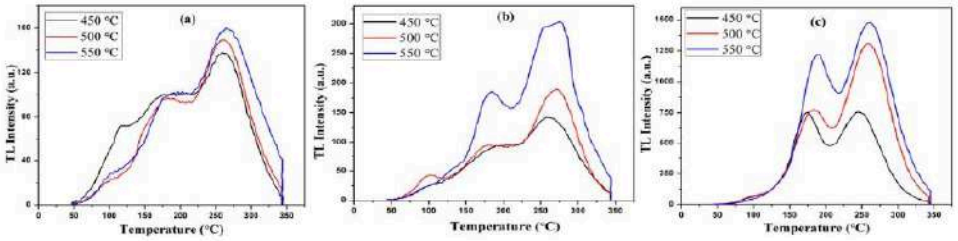

FIGURE 4. TL glow curve of TiO_2 prepared with the precursors mole ratio of (a) 1:2, (b) 1:3, (c) 1:4 for different annealing temperature.

Figure 4(c) exhibits TL peaks for the shallow traps at temperature 175°C, 184°C and 188°C. Thermoluminescence is related to radiation induced defects and due to increase in the thermal energy, electron trapped in the electron trap is released to conduction band and then recombination of electron takes place with the hole found in the hole trap. According Cernea [6] et al, shallow traps will released at low temperatures and deeper traps will released at higher temperatures.TL glow curve intensity of sintered TiO_2 powder was found to be more intense, this intensity is increased as the annealing temperature was increased. The reason for this increasing intensity could be that under irradiation the crystalline TiO_2 ions in the lattice crystal cause defects and thus act as trapping sites by capturing the electrons released by irradiation [2]. Due to ionizing radiation electrons are excited from the valence band to the conduction band. In ionic materials the primary radiolytic reactions resulting from interactions between radiation and the crystal take place at anions e.g. the O^{2-} ions in case of oxides. The deexcitation processes are sufficiently energetic and effective to induce atomic/ionic displacements in the crystal lattice, which leads to the formation of radiation induced defects. The continuous production of free electrons and holes as a result of the exposure to ionizing radiation free electrons and holes can migrate in the crystal until they are trapped by luminescentcenters(trapping sites) in the crystal [7].

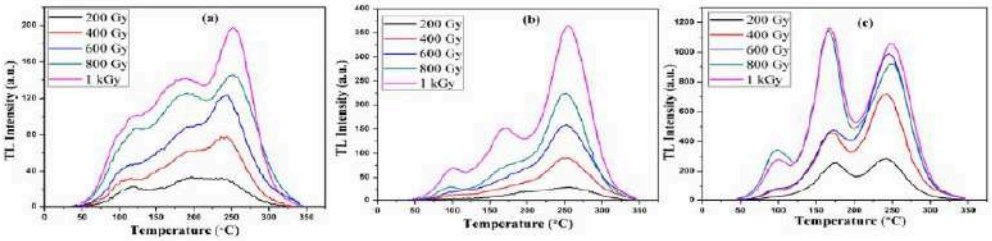

FIGURE 5. TL glow curve of TiO_2 prepared with the precursors mole ratio of (a) 1:2, (b) 1:3, (c) 1:4for different doses of irradiations respectively.

Figure5 shows the TL glow curves of gamma irradiated TiO_2 nanoparticles. All the samples were evaluated for different doses 200 Gy, 400 Gy, 600 Gy, 800 Gy and 1 kGy. In all the three precursor mole ratio the TL intensity is minimum for 200 Gy and maximum for 1 kGy dose. The main TL peak is observed around 245 °C to 255°C for three mole ratios. Among all the studied samples the TiO_2 nanoparticles synthesized at 1:4 mole exhibits better TL glow curve with higher TL intensity. The precursor mole ratios 1:2 and 1:3 gives the prominent TL peak at around 252°C to 255 °C without more deviation in the temperature with respect to the dose. Overall, the results shows increase in TL response with increasing gamma dose and also with increasing precursor's mole ratio.

CONCLUSION

TiO_2 Nanoparticles were successfully synthesized by co-precipitation method. The XRD analysis was carried out for structural characteristics. The crystallite size of all the samples was in a range of 10 to 24 nm. The XRD patterns show that the TiO_2 nanocrystals are predominantly in the rutile crystal phase with some traces of brookite phases. The FESEM image has shown uniform morphology in the form of nano clusters. EDS spectra confirm the samples purity. The thermoluminescence glow curves of gamma irradiated TiO_2 nanoparticles have been evaluated for different doses. The TL glow curves of gamma irradiated TiO_2 samples have shown increase in the TL intensity with dose and with annealing temperature.

ACKNOWLEDGEMENTS

The authors are grateful to the director of PURSE, Mangalore University, India for providing FESEM experimental facility and DST-FIST, Department of Physics, Mangalore University, India for providing XRD spectroscopy facility.

REFERENCE

1. S.K. Omanwar, K.A. Kopikar and H.S. Virk, Rev. *Defect &Diffus. Forum*. 347, 75 (2014).
2. J.C.A. Vegaa, B.J.A. Nietoa, M.G. Hipolitocand T.R. Montalvoa, Radiat. Meas.42, 613 (2007).
3. P.B. Rathod, K.R. Nemade and S.A.Waghule, Int. J. Chem. Phys. Sci. 4, 491 (2015).
4. V.P.M. Shajudheen, K. Viswanathan, K.A. Rani, A.U. Maheswari and S.S. Kumar, World Acad. Sci., Eng. & Technol. Int. J. Chem. & Mol. Eng. 10, 556 (2016).
5. P. Seth and S. Aggarwal, AIP Conf. Proc.1731, 050109 (2016).
6. M. Cernea, M. Secu, C.E. Secu, M. Baibarac and B.S. Vasile,J. Nanopart. Res.13, 77 (2011).
7. Es, H.J. Van, "Thermoluminescence dating of sediments using mineral zircon," Ph.D. thesis, Groningen University, 2008.

Preparation and Characterization of Hematite and Lead Oxide Based Flexible EPDM Composites for Shielding Gamma Rays

Preparation and characterization of hematite and lead oxide based flexible EPDM composites for shielding gamma rays

Cite as: AIP Conference Proceedings **2115**, 030047 (2019); https://doi.org/10.1063/1.5112886
Published Online: 12 July 2019

Vinayak Anand Kamat, Swaroop K., Kiran K. U., and Somashekarappa H. M.

Preparation and Characterization of Hematite and Lead Oxide Based Flexible EPDM Composites for Shielding Gamma Rays

Vinayak Anand Kamat[1], Swaroop K[1], Kiran K U[2] and Somashekarappa H M[1,a)]

[1]*Centre for Application of Radioisotopes and Radiation Technology (CARRT), Mangalore University, Mangalagangothri-574 199, Karnataka, India*
[2]*Government Science College (Autonomous), Hassan- 573 201, Karnataka, India*

[a)]Corresponding author: carrtmu@gmail.com

Abstract. The present work deals with the synthesis of EPDM-Fe_2O_3-PbO composites with different percentages of Fe_2O_3 and PbO. Gamma attenuation parameters, such as linear attenuation coefficient, mass attenuation coefficient, half value layer thickness and tenth value layer thickness have been evaluated for the synthesised EPDM composites at 123 keV, 360 keV and 661.64 keV energies. It has been observed that the mass attenuation coefficient increases with an increase in PbO filler loading. Also, the mass attenuation coefficient is observed to decrease with an increase in gamma energy for synthesised EPDM-Fe_2O_3-PbO composites. The HVL and TVL thicknesses were found to decrease with increase in PbO concentration. Also, The HVL and TVL are noticed to decrease with a decrease in gamma energy. The synthesised EPDM composites with 60 phr of PbO and EPDM composites contains a combination of 40 phr of PbO and 20 phr Fe_2O_3 shows better-shielding performance for lower energies compared to all other synthesised composites.

INTRODUCTION

Ionizing radiation has found its application in power generation, space technology, medical, industrial and agricultural fields [1]. Researchers have used some high-density metal or metal composites to protect the radiation workers from radiation hazards [2]. Among these, lead (Pb) is one of the most commonly used shielding materials due to high density, high atomic number and low cost [3]. However, due to lack of flexibility and heaviness metallic lead has its own limitations [4]. Thus there is a need for flexible composites which can be used for protective clothing and space applications. As a result of this, several investigators have fabricated a variety of polymer-based composites filled with different metal or metal oxide powder [3-4].

In the present study, ethylene propylene diene monomer/hematite/lead oxide (EHP) composites were fabricated and its gamma shielding parameters were evaluated. These were then compared with theoretically obtained attenuation parameters by using the XCOM database.

EXPERIMENTAL METHODS

Materials

Ethylene propylene diene monomer (EPDM) (with 56 % of ethylene content) is used to prepare the composite material, was procured from Mitsui Chemicals, USA. Hematite (Fe_2O_3) ore with a density of 2.02 g/cm^3 and average particle size of < 150 µm was kindly supplied by KIOCL Limited, Panambur, Mangaluru, India. Lead monoxide (99% pure) with a density of 9.53 g/cm^3 was purchased from LOBA Chemie Pvt. Ltd. Mumbai, India, and ISAF black from Philips Carbon Black Ltd., Kolkata, India. Antioxidant TQ was purchased from local suppliers (analytical grade), dicumyl peroxide-98% (vulcanizing agent) was supplied by Arkema Peroxides India Private

DAE Solid State Physics Symposium 2018
AIP Conf. Proc. 2115, 030047-1–030047-4; https://doi.org/10.1063/1.5112886
Published by AIP Publishing. 978-0-7354-1851-6/$30.00

Limited, Cuddalore, Tamil Nadu, India, and paraffin oil (commercial grade) were procured from local suppliers. All chemicals were used without any further purification.

Preparation of Composites

Masterbatch of EPDM containing 30 phr (parts per hundred rubber) of ISAF black, 10 phr of paraffinic oil and 1.5 phr of antioxidant TQ was prepared in an internal mixer (Francis Shaw, KO MK3) at 100 °C and 70 rpm for 5 minutes 30 seconds. The masterbatch was then mixed with a different proportion of metal oxide powders (Fe_2O_3 and PbO) along with the addition of dicumyl peroxide (98% active) in laboratory two-roll mill. Mixed rubber compound was then moulded into sheets of dimensions 14.8 cm X 14.8 cm X 0.2 cm in a hot press at 170 °C for 10 minutes. The samples so obtained were taken for further characterization. A sample designation and corresponding fillers proportions and its densities are shown in table 1.

TABLE 1. Sample designation with corresponding filler concentration and density.

Sample name	PbO (phr)	Fe_2O_3 (phr)	Density (gcm^{-3})
Pristine	0	0	0.9
P0H60	0	60	1.075
P20H40	20	40	1.12
P40H20	40	20	1.17
P60H0	60	0	1.224

Gamma Attenuation Studies

Attenuation studies for the synthesised composites were carried out by using well calibrated 3" X 3" NaI (Tl) detector (Thermo Scientific, Germany) and ^{57}Co (~0.5 μCi), ^{133}Ba (~17 μCi) and ^{137}Cs (~5 mCi) radioactive sources. A cylindrical lead shield with a hole of 40 mm in diameter is placed in front of the detector. Measurements for all synthesised samples were performed for the duration of 2000 sec. The attenuation parameter such as total linear attenuation coefficient (μ), mass attenuation coefficient (μ_m), half value layer (HVL) and tenth value layer (TVL) for the synthesised EHP composites with known inlet photon intensity (I_0), outlet photon intensity (I) and thickness (x) were obtained by using basic equation 1.

$$I = I_o \exp^{-\mu X} \qquad (1)$$

RESULTS AND DISCUSSION

Morphological Studies

Surface morphological studies for synthesised EHP composites were performed by using Field Emission Scanning Electron Microscopy (FESEM, Carl Zeiss, Germany). Figure 1 (a and b) shows the irregular shape of PbO and Fe_2O_3 fillers. Figure 1 (c) shows surface micrograph of pure EPDM matrix without any voids and impurities.

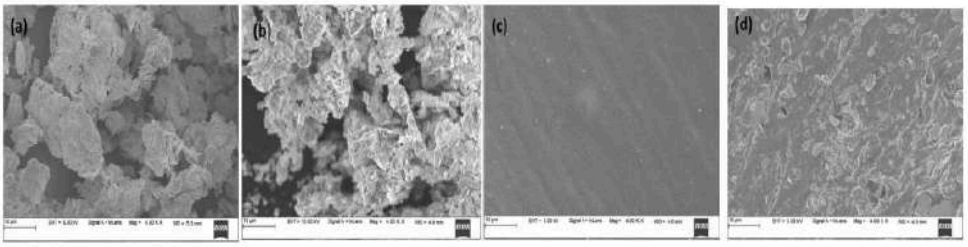

FIGURE 1. FESEM micrographs of (a) PbO, (b) Fe_2O_3, (c) pure EPDM (d) P40H20.

FESEM image (Fig. 1 (d)) of P40H20 indicates the dispersion of PbO and Fe_2O_3 fillers over the surface of the EPDM matrix. This dispersion of the fillers within the polymer matrix may cause opacity for the gamma rays passing through it. Thus, it may lead to the better shielding performance for the EPDM composites filled with the metal oxide fillers compared to the pristine one. Also, Fig. 1 (d) shows the dispersion of the fillers is not uniform and the voids are present on the surface of the EHP composites. This is due to the poor compatibility of the inorganic fillers with organic phase [6].

Attenuation Studies

Linear Attenuation Coefficient (μ)

The interaction probability of gamma rays per unit thickness of the synthesized EHP composites is represented by total linear attenuation coefficient (μ). It is found that the value of 'μ' increases with increase in the density of EHP composites (Fig. 2 (a-b)). This is due to the increase in PbO concentration which may lead to more interaction of gamma rays per unit length [3]. Also, it has been observed that 'μ' value is found to increase with a decrease in incident gamma energy as shown in Fig. 2 (a).

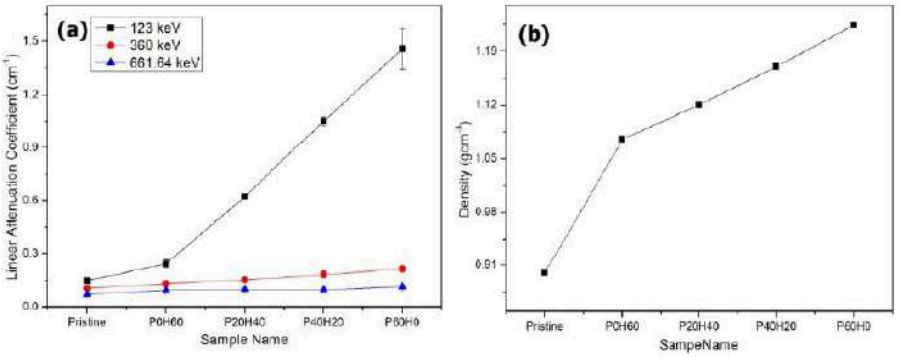

FIGURE 2. Variation of (a) Linear attenuation coefficient and (b) Density with different filler combination of EHP composites.

Mass Attenuation Coefficient (μ_m)

The value of mass attenuation coefficient (μ_m) observed to decreases with an increase in gamma energy (Table 2). The prepared composites exhibit better shielding performance at medium gamma energies (123 keV and 360 keV) compared to high energy (661.64 keV). The highest value of 'μ_m' is obtained for P60H0 samples. Next to that P40H20 composites were also observed to exhibit better shielding property.

TABLE 2. Experimental and Theoretical evaluation of mass attenuation coefficient (μ_m).

Sample name	123 keV		360 keV		661.64 keV	
	μ_m ($cm^2 g^{-1}$) Experimental	μ_m ($cm^2 g^{-1}$) Theoretical	μ_m ($cm^2 g^{-1}$) Experimental	μ_m ($cm^2 g^{-1}$) Theoretical	μ_m ($cm^2 g^{-1}$) Experimental	μ_m ($cm^2 g^{-1}$) Theoretical
Pristine	0.16548	0.1597	0.11805	0.1116	0.08043	0.08647
P0H60	0.22586	0.1788	0.12242	0.108	0.08786	0.08277
P20H40	0.55495	0.4573	0.13767	0.1245	0.08901	0.08549
P40H20	0.89794	0.7358	0.15681	0.141	0.08439	0.0882
P60H0	1.18955	1.014	0.17570	0.1576	0.09270	0.09092

As P40H20 composites contain relatively less PbO content than P60H0 samples, hence P40H20 can be considered as a better shielding material among synthesised composites. The experimental values of 'μ_m' are in good agreement with the theoretical values acquired from the XCOM database [5]. The occurrence of a small

difference in the experimental and theoretical values may be due to uneven dispersion of metal oxide fillers within the EPDM matrix.

Half-Value Layer (HVL) and Tenth Value Layer (TVL)

The HVL and TVL are the thickness of the sample required to reduce the incident intensity to half and tenth of the original value respectively. The HVL and TVL for the synthesised EHP composites are found to decrease with increase in PbO concentration (Fig. 3 (a-b)). Also, it can be seen from the Fig. 3 (a) and Fig. 3 (b) that, the values of HVL and TVL increase with an increase in gamma-ray energies. The least values of HVL and TVL are obtained for P60H0 composites for all the studied gamma-ray energies. The composite, P40H20 has also found to exhibits good HVL and TVL values for all the studied energies as shown in the Fig. 3 (a and b).

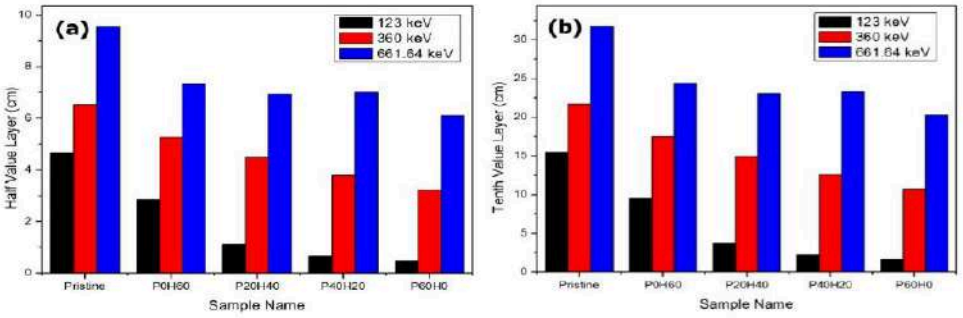

FIGURE 3. (a) Half-value layer (HVL) and (b) Tenth value layer (TVL) of EHP composites.

CONCLUSION

The attenuation parameters for EPDM based metal oxide (PbO and Fe_2O_3) polymer composites developed by melt mixing technique were evaluated. The experimental values of 'μ_m' of prepared EPDM composites were in good agreement with the theoretical values. A small variation between experimental and theoretical values observed may be due to the incompatibility of inorganic fillers (PbO and Fe_2O_3) within organic matrix phase (EPDM). Both P60H0 and P40H20 composites found to exhibit better shielding properties among synthesized composites. Since P40H20 composites contain relatively less concentration of lead than P60H0 composites, it can be recommended as the good shielding materials for lower and medium gamma energies.

ACKNOWLEDGEMENT

The authors express their sincere gratitude to the Coordinator, DST-PURSE program, Mangalore University for permitting to use FESEM facility and the Director, Rubber Board Research Institute of India (RRII), Kottayam, for helping in composites preparation and to use lab facility.

REFERENCES

1. K. Singh, S. Singh, A. S. Dhaliwal and Gurmel Singh, Appl. Radiat. Isot. **95**, 174-179 (2015).
2. A. K. Vinayak, K. Swaroop, K. U. Kiran, G. Benny and H. M. Somashekarappa, Radiat. Phys. Chem. **156**, 50-57 (2019).
3. V. Harish, N. Nagaiah and H. G. Harish Kumar, Indian J. Pure Appl. Phys. **50**, 847-850 (2012).
4. A. K. Vinayak, K. Swaroop, K. U. Kiran and H. M. Somashekarappa, Indian J. Pure Appl. Phys. **56**, 639-642 (2018).
5. http://physics.nist.gov/xcom. (2018).
6. W. Huang, W. Yang, Q. Ma, J. Wu, J. Fan and K. Zhang, J. Radioanal. Nucl. Chem. **309**, 1097-1103 (2016).

Studies on Swelling Behaviour of Radiolytically Synthesised PVA/Gelatin Hydrogels

Studies on swelling behaviour of radiolytically synthesised PVA/gelatin hydrogels

Cite as: AIP Conference Proceedings 2115, 030050 (2019); https://doi.org/10.1063/1.5112889
Published Online: 12 July 2019

K. Swaroop, M. J. Gaana, S. S. Shruthi, Shrinidhi, L. P. Shrikant, A. K. Vinayak, and H. M. Somashekarappa

Studies on Swelling Behaviour of Radiolytically Synthesised PVA/Gelatin Hydrogels

Swaroop K[1], Gaana M J[2], Shruthi S S[2], Shrinidhi[2], Shrikant L P[3], Vinayak A K[1] and Somashekarappa H M[1, a)]

[1]*Centre for Application of Radioisotopes and Radiation Technology (CARRT), Mangalore University, Mangalagangotri-574 199, Mangalore, Karnataka, India*
[2]*Post Graduate Studies & Research in Physics, St. Aloysius College, Mangalore-575003, Karnataka, India*
[3]*K S hedge Medical Academy, NITTE University, Deralakatte, Mangalore-575018, Karnataka, India*

[a)]Corresponding author: carrtmu@gmail.com

Abstract. In the present investigation, an attempt was made to synthesise different compositions of PVA/gelatin hydrogels by gamma irradiation technique. A PVA aqueous solution was mixed with a gelatin aqueous solution of similar concentrations at different weight ratios namely, 100/0, 75/25, 50/50, 25/75, and 0/100 respectively and exposed to gamma irradiation dose of 25 kGy. Further, the prepared sample were analysed for structural and morphological characteristics using powder XRD and FESEM analysis respectively. Significant changes in the structural and morphological characteristics were observed for different PVA and gelatin concentration. The swelling studies were carried out at different pH values and the swelling data was fitted to power law expression to know the swelling mechanism of the PVA/gelatin hydrogels. The swelling characteristics of PVA/gelatin hydrogels found to increase with gelatin percentage. The overall result obtained signifies that the PVA/gelatin hydrogels could be used for various biomedical applications such as wound dressing and drug delivery systems.

INTRODUCTION

Hydrogels are promising class of 3-dimensional cross-linked hydrophilic polymers which are widely used in tissue engineering, pharmaceutical, agriculture and biomedical applications. Hydrogels do not dissolve in water at physiological temperature and pH but they can swell extensively in an aqueous medium. Polyvinyl alcohol (PVA) and gelatin are traditionally used synthetic polymers in biomedical applications because of their non-toxic, hydrophilic, and bio-degradable properties [1, 2]. Gamma irradiation technique is one of the widely used crosslinking technique for hydrogel synthesis. Since gamma irradiation does not involve any chemical additives and therefore retains the biocompatibility of the hydrogels [3].

The aim of this work is to develop a biocompatible hydrogels based on the blends of PVA and gelatin using gamma irradiation technique. The synthesised hydrogels were characterized for structural and morphological characteristics using XRD and FESEM analysis. The swelling characteristics of prepared PVA/gelatin hydrogels were studied at different pH values.

MATERIALS AND METHODS

Materials

Polyvinyl alcohol (Mw: 130,000, Sigma Aldrich, USA) and gelatin from porcine skin (Gel strength: 300, Sigma Aldrich, USA) were used for the synthesis of PVA/gelatin hydrogels. The gamma irradiation was carried out using

DAE Solid State Physics Symposium 2018
AIP Conf. Proc. 2115, 030050-1–030050-4; https://doi.org/10.1063/1.5112889
Published by AIP Publishing. 978-0-7354-1851-6/$30.00

Gamma Chamber (GC 5000; BRIT, Mumbai) equipped with cobalt-60 (^{60}Co) source which delivers a dose rate of 4.2 kGy/hr.

Synthesis of PVA/gelatin hydrogels

PVA (5 wt. %) and gelatin (5 wt. %) aqueous solutions were prepared by dissolving 5 g of PVA and gelatin powder respectively in 100 mL of double distilled water at 70 °C under mechanical stirring. PVA and gelatin aqueous solutions were mixed at different concentrations. The ratio of PVA and gelatin was fixed to 100/0, 75/25, 50/50, 25/75, and 0/100 and labelled them as PG1, PG2, PG3, PG4, and PG5 respectively. After mix up the solutions were allowed to cool to room temperature and bubbled with argon gas in an air sealed container to remove the O_2 content. The solutions were then transferred to petri plates of 10 cm diameter separately and subjected to gamma irradiation of 25 kGy at room temperature. The obtained hydrogel samples were dried at 40 °C. The completely dried samples were taken for further characterization.

The PVA/gelatin hydrogels of different compositions were characterized using different techniques. The powder X-ray diffraction (XRD) analysis was performed to characterize the structural properties. The Field Emission Scanning Electron Microscopy was performed for morphological characterization. The swelling ratio and swelling mechanism studies were carried out at different pH values.

RESULT AND DISCUSSION

The XRD analysis was performed for PVA/gelatin hydrogel composites using Rigaku Miniflex diffractometer, USA with Cu-Kα radiation (λ = 0.15418 Å) at 40 kV and 40 mA. The diffraction and '2θ' was set between 10° and 60°. Figure 1 show the XRD pattern of PVA/gelatin hydrogels. It shows a relatively sharp peak at 19.6° for PG1 which can be matched to the (101) reflection plane of the crystalline PVA [4]. A broad peak appeared at 20.3° for PG5 indicates the semi-crystalline nature of gelatin. The intensities of these semi-crystalline peaks appeared to decrease from ~1900 to ~ 800 a.u. with gelatine concentration indicating significant decrease in the crystallinity. Table 1 shows the crystallinity percentage of the studied hydrogels. From these data, one can notice that at small angles the first-order diffraction shifts to the higher angle in comparison to pure PVA hydrogels (PG1). It is obvious that the percentage crystallinity of the hydrogels was found to decrease with increase in gelatin content, which can explain that intermolecular interaction destroyed the regularity by gelatin.

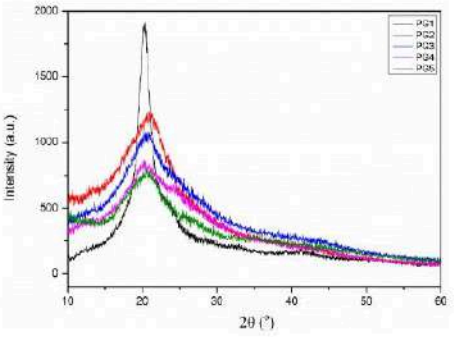

FIGURE 1. XRD analysis of PVA/gelatin hydrogels of different concentrations.

The surface morphology of the PVA/gelatin hydrogels were characterized using FESEM analysis. Figure 2 (a) shows morphology of pure PVA hydrogel (PG1) which shows the plane surface of PVA matrix with no voids or impurities. Figure 2 (b) and 2 (c) shows the morphologies of PG3 and PG5 respectively. These images show that increasing the concentration of gelatin results in porous structure on the surface arrangement of the PVA/gelatin hydrogels. The porous structure of the hydrogels attributes to the volume available for the water adsorption. Significant morphological changes with gelatin concentration which can further results in water adsorption property of the hydrogels.

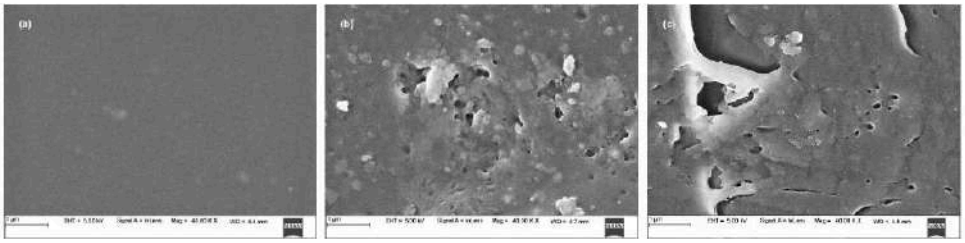

FIGURE 2. FESEM images of PVA/gelatin hydrogels with composition ratio (a) 100/0, (b) 50/50, and (c) 0/100 respectively.

It is known that the application of controlled drug release is directly related to the swelling kinetics of polymer hydrogels. The completely dried and accurately weighed samples were immersed in double distilled water at room temperature until the swelling equilibrium was achieved. The swelling ratio (%S) of the hydrogels was calculated from Eq. (1):

$$\%S = \frac{W_t - W_0}{W_0} X100$$

Where, 'W_t' is the weight of the swollen gel at time 't' and 'W_0' weight of dry hydrogel.

The swelling ratio (%S) of different compositions of PVA/gelatin hydrogels were carried out at different pH values namely 1.5 (acidic), 7 (neutral), and 9.5 (basic) until the samples reached equilibrium swelling. The saturation swelling state of each hydrogel was considered as equilibrium degree of swelling (%EDS) and the values were tabulated in table 1. Fig. 3 (a) shows the swelling ratio of all the studied hydrogels at pH 7 with respect to time. The swelling ratio reaches near equilibrium at about 720 min with a slight increase (10 to 40 %) up to 1440 min and becomes stable thereafter in all the cases. With increase in gelatin content, both swelling rate and %EDS values has increased significantly. It can be seen from table 1 that the %EDS value of all the PVA/gelatin composites has shown maximum at pH 7 when compared to pH 1.5 and 9.5.

The swelling mechanism wherein water diffuses into the hydrogel matrix plays a crucial role in the distinctive application of the hydrogels. The power law expression (equation 2) can be used to determine the nature of water diffusion into the hydrogels.

$$F = kt^n$$

The swelling constant 'k' and diffusion exponent 'n' for double distilled water was estimated using slope of log F vs log t plots (Fig. 3) of PVA/gelatin hydrogels and the values were tabulated in table 1. All the 'n' values of the PVA/gelatin hydrogels studied at different pH values recline between 0.5 to 1 which implicates anomalous (non-Fickian) diffusion mechanism. Anomalous diffusion occurs when the rate of water diffusion and the relaxation rate of polymer matrix are comparable [5].

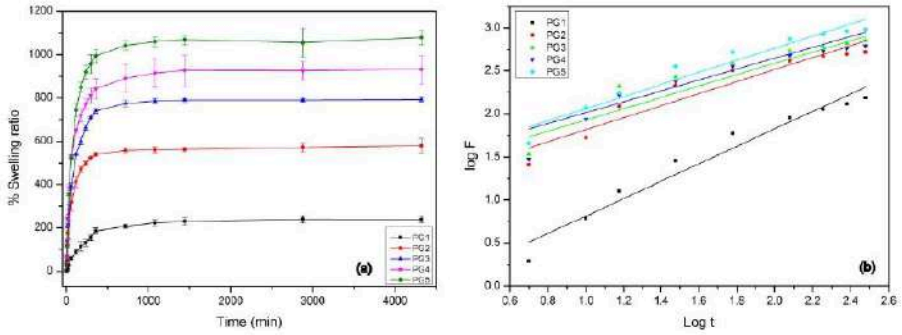

FIGURE 3. Swelling behavior of PVA/gelatin hydrogels (a) Swelling ratio and (b) log F vs log t plot.

Table 1. Effect of polymer compositions on % crystallinity and pH on % EDS of PVA/gelatin hydrogels.

Sample	PVA/gelatin ratio	% crystallinity	% GF	% EDS for different pH		
				Acidic (pH = 1.5)	Neutral (pH = 7)	Basic (pH = 9.5)
PG1	100/0	68.3	68.8 ± 2.91	42.3 ± 11.2	239.1 ± 17. 5	99.3 ± 21.4
PG2	75/25	47.5	53.54 ± 4.32	71.3 ± 7.6	579.6 ± 32.4	135.9 ± 17.8
PG3	50/50	45.0	46.51 ± 3.53	84.9 ± 6.3	791.7 ± 9.6	149.6 ± 33.5
PG4	25/75	43.9	40.69 ± 1.9	98.1 ± 7.6	930.9 ± 63.5	188.1 ± 41.5
PG5	0/100	41.5	32.33 ± 6.52	111.5 ± 13.8	1078.9 ± 32.8	200.4 ± 19.3

CONCLUSION

The PVA/gelatin hydrogels composites were synthesised using gamma irradiation technique and characterized for structural, morphological, and swelling properties. The powder XRD analysis shows that the interference of gelatin in the PVA matrix has led to decrease in the crystallinity of the PVA/gelatin composites. The morphological changes also been observed for PVA/gelatin hydrogels with gelatin concentrations. The formation of pores in the surface of the hydrogel network with gelatin concentration was observed which is helpful in the swelling behaviour of the PVA/gelatin hydrogels. Increase in the gelatin percentage has certainly increased the swelling degree of the hydrogels which could be attributed to decrease in the percentage crystallinity as well as formation of porous structure on the surface of the PVA/gelatin hydrogels. The swelling exponent (n) value of all the samples studied for solutions of different pH were between 0.5 to 1, indicates anomalous water transport mechanism. The PVA/gelatin hydrogels of different concentrations exhibited better swelling ability with tailored functionalities making them a better material for various biomedical application.

ACKNOWLEDGEMENT

The authors express their sincere gratitude to the Coordinator, DST-PURSE program, Mangalore University for permitting to use FESEM facility.

REFERENCES

1. K.S. Anseth , C.N. Bowman, L. Brannon-Peppas, *Biomaterials.* **17**, 1647–1657 (1996).
2. L. Yahia, L. Gritsch, F. L. Motta, S. Chirani and S. Faré, *J. Biomed. Sci.* **4**, 13 (2015).
3. H.L. Abd El-Mohdy, S. Ghanem, *J. Polym. Res.* **16**, 9196 (2009).
4. M.T. Razzak, Zainuddin, Erizal, S.P. Dewi, H. Lely, E. Taty, *Radiat. Phys. Chem.* **55**, 153–165 (1999).
5. A. Kumari, B.S. Kaith, A.S. Singha, S. Kaliac, *Adv. Mater. Lett.* **1**, 123–128 (2010).

MECHANICAL AND ELECTRICAL PROPERTIES OF BISMUTH FILLED HIGH DENSITY POLYETHYLENE COMPOSITES

Vol-5 Issue-3 2019 *IJARIIE-ISSN(O)-2395-4396*

MECHANICAL AND ELECTRICAL PROPERTIES OF BISMUTH FILLED HIGH DENSITY POLYETHYLENE COMPOSITES

Sheela M[1,2], Vinayak Anand Kamat[4], Eshwarappa K M[3,5],

[1]*Assistant Professor, Department of Physics, Government Science College, Hassan, Karnataka, India*
[2]*Research scholar, Bharathiar University, Coimbatore, Tamil Nadu, India*
[3]*Research supervisor, Bharathiar University, Coimbatore, Tamil Nadu, India*
[4]*Research scholar, CARRT, Mangalore University, Mangalore, Karnataka, India*
[5]*Department of PG Studies and Research in Physics, Government First Grade College, Holenarasipura, Karnataka, India*

ABSTRACT

Effect of bismuth filler on mechanical and electrical properties of High Density Polyethylene (HDPE) is described in this study. HDPE composites with different weight percentage of bismuth (0%, 10%, 20% and 40%) were fabricated by using hydraulic press. The mechanical properties like tensile strength, tensile modulus and the elongation at the peak load were studied by using universal testing machine (UTM), impact strength was determined using computerized impact tester and density of the composites were estimated on Archimedes principle. The dispersion of the filler in HDPE was studied using scanning electron microscope (SEM). The density of HDPE has been observed to increase with increase in bismuth concentration. The value of tensile strength and Young's modulus of HDPE become maximum at 10 wt% of bismuth loading and then decreases at 20 wt% of bismuth with HDPE. However, the slight increase in the tensile strength and Young's modulus is observed beyond 20 wt% of bismuth with HDPE. The elongation and impact strength decreases with the increase of bismuth concentration in HDPE. The electrical properties like dielectric constant, dielectric loss, AC conductivity and impedance were studied for synthesized composites using LCR meter for the frequency range 100Hz-1MHz. The dielectric constant increases with the increase in weight percentage of bismuth with HDPE and then slightly decreases for higher frequencies. The AC conductivity increases sharply at higher frequencies but is of very low value ($10^{-10}Sm^{-1}$). The dielectric loss and the impedance decreases with frequency.

Keywords:- *Bismuth, HDPE, tensile strength, tensile modulus, impact strength, dielectric properties, impedance, AC conductivity.*

1. INTRODUCTION

HDPE is known for its greater strength among other polymers. Although the density of HDPE is marginally higher than the other polymers, it has strong intermolecular forces, tensile strength, low moisture absorption chemical and corrosion resistance properties. This polymer has density 0.920 gm/cm^3. Bismuth is a naturally occurring heavy element with atomic weight 83 and atomic mass 209 and high density of 9.8 gm/cm^3. The aim is to study the variation in mechanical properties like density, tensile strength, tensile modulus, impact factor, elongation at the peak and also to study electrical properties like dielectric constant, dielectric loss, AC conductivity and impedance of HDPE when bismuth is added in different weight percentage (0%, 10%, 20%, and 40%) for further study of gamma shielding properties of these composites.

Many researchers have studied the changes in the mechanical and electrical properties of different polymer matrix filled with different fillers. B. Narayanaswamy et al. (2017) investigates the effect of chemical treatment on the physical and mechanical behavior of coconut shell powder and lime stone powder as fillers in different wt% (5%, 7.5% and 10%) reinforced with HDPE matrix. From the study it is observed that the tensile strength of the composite is maximum at 5 wt% of lime stone composite, flexural strength and impact strength of the composites are found to be maximum at 10 wt % of lime stone composite [1]. Daniel Eirasa et al., (2009) evidenced the influence of calcium carbonate nano particles with different weight percentage (3%, 5%, 7% & 10%) on the mechanical properties of polypropylene. The elastic modulus and yield stress increased with the

increase in the addition of calcium carbonate nano particles [2]. Han-Seung Yang et al., (2004) studied the tensile strength and tensile modulus of rice husk filled polypropylene composites, which increase with filler w% and also it is noticed that the composites become brittle at high cross head speed and plastic deformation increases with test temperature [3]. In a study conducted by Iftekhar Ahmad et al. (2010), evidence that, the enhancement in the value of tensile strength and relative elongation for HDPE filled with smallest size fly ash particles. It is also noticed that the tensile modulus and impact resistances are not much dependent on particle size of fly ash fillers [4]. Moayad N. Khalaf, (2015) studied lignocellulose filled HDPE can possess appreciable mechanical strength compared with other fillers [6]. Qingfa Zhang et al., (2018) performed the effect of addition of rice husk biochar/plastic composites to HDPE on mechanical property, in which it was noticed that, with the increase of filler content BPC (biochar/plastic composites) are better than WPC (wood plastic composites) [8].

Waleed A Hussain et al., (2015) found the dielectric constant, dielectric loss and the loss tangent for epoxy/alumina silicate composites increases with the increasing alumina silicate NGK (insulator part as a filler) filler content [10]. As per Dillip K Pradhan et al., (2008) the dielectric relaxation and AC conductivity increase with the increase in plasticizer concentration in plasticized polymer nano composite electrolytes (PPNCEs) [11]. Hence, in the present study an attempt is made to study the effect of bismuth on mechanical and electrical properties of HDPE polymer, and further study on gamma shielding properties of these composites is to be carried out.

2. MATERIALS AND METHODS

2.1 Preparation of samples

The thermoplastic HDPE (injection grade) was selected as the base polymer matrix and it was purchased from Banu plast, Mumbai and the pure bismuth filler was purchased from Sarda Industrial Enterprises, Jaipur, Rajasthan.

The composites were developed by mixing HDPE powder with density 0.920 gm/cm^3 mixed thoroughly with four different weight percentage (0%, 10%, 20%, 40%) of bismuth powder having the density of 9.8 gm/cm^3 by mechanical mixing method. The HDPE-bismuth mixture was taken into the mould with size of 30 cm x 30 cm x 0.3 cm and placed in the hydraulic press at the temperature of about 180 ^{O}C with the load pressure of 1000 kg for about 10 minutes and then the machine was allowed to turn off. The applied load was released after the temperature of the hydraulic press falls to 80^{O}C-90^{O}C. HDPE/Bi composites were then removed from the mould and were then cut into required dimension for the further characterization. The samples are as shown in the fig1.

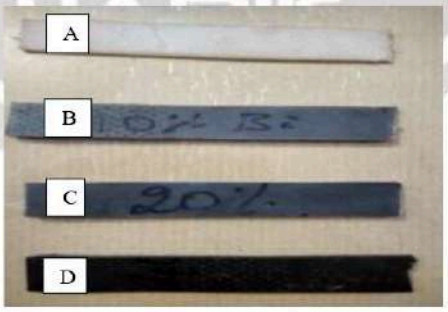

Fig-1: Samples- A) Pure HDPE polymer
B) 90% HDPE + 10% bismuth
C) 80% HDPE + 20% bismuth
D) 60% HDPE + 40% bismuth

2.2 Homogeneity test

The surface morphological and homogeneity of the samples were tested by using scanning electron microscope (JSM IT 300) at applied voltage of 15 kV 1000X resolution.

2.3 Mechanical studies

The mechanical properties of polymer composites such as tensile strength, tensile modulus, and elongation at the peak were studied using universal testing machine (UTM). The rectangular shaped test specimen with dimension 36 sq. mm was used for tensile measurement. Sample was placed between the grips of the UTM and was pulled at the speed of 50 mm/min until it breaks due to the application of load. The impact strength of the specimen was determined by using computerized Impact tester.

2.4 Electrical properties

The AC electrical conductivity and the dielectric properties of HDPE/Bi composites with dimension of 20 mm x15 mm x 2.5 mm were studied by using LCR meter in the frequency range 100 Hz -1 M Hz at 30°C for 1 V. The dielectric constant (ε′), dielectric loss (ε″) and AC conductivity (σ_{ac}) of the synthesised HDPE+Bi composites were calculated by using the following equations (Hussain, W.A. et al., 2019).

$$\varepsilon' = C_p d / \varepsilon_0 A \quad - (1)$$

$$\varepsilon'' = \varepsilon' \tan\delta \quad - (2)$$

$$\sigma_{ac} = \varepsilon' \varepsilon_0 \omega \tan\delta \quad - (3)$$

The dissipation factor D = tan δ= cot θ= 1 / (2πfRpCp), where δ is the loss angle, θ is the phase angle, f is the frequency, Rp is the equivalent parallel resistance, and Cp is the equivalent parallel capacitance, d is the thickness and A is the area of the sample, ε_0 is the permittivity of the free space, ω is the angular frequency.

The complex impedance can be expressed as Z*= Z + i Z', where Z' is the imaginary part of the impedance, Z is the real part of the impedance at different frequencies up to 1MHz. It was measured by Impedance Analyzer.

3. RESULTS AND DISCUSSION

3.1 SEM test

The dispersion of bismuth over the surface of synthesized HDPE composites was examined by using scanning electron microscope (SEM). The SEM image of pure HDPE shows (Fig 2a) the presence of graded ridges and it can cause low mechanical properties compared to HDPE/Bi composites. On addition of 10 wt% of bismuth to HDPE the number of ridges has reduced (Fig 2b). A nonhomogeneous distribution of bismuth particles in HDPE matrix was observed with 20 wt% of bismuth loaded HDPE composites (Fig 2c) and this resulted in decrement of tensile strength and tensile modulus (Iftekhar Ahmad et al., 2010). Fig 2d shows the uniform distribution of the 40 wt% of the filler in HDPE matrix.

Fig-2: SEM images a) HDPE b) HDPE+10% bismuth c) HDPE+20% bismuth d) HDPE+40% bismuth

3.2 Mechanical properties

A. Density

Archimedes principle has been used to determine the density of the prepared composites. From the Fig 3 it is observed that the density of the HDPE has increased with increase in bismuth concentration. This trend is observed due to presence of high density of bismuth (0.92 gm/cm^3 to 1.29 gm/cm^3) fillers.

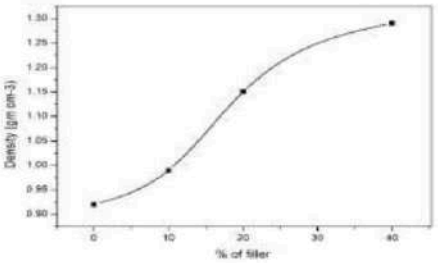

Fig-3: Effect of bismuth on density of HDPE

B. Tensile test

Variation in tensile strength of bismuth loaded HDPE composites is shown in the Fig. 4. It has been observed that there is an increase in tensile strength when HDPE is filled with 10 wt % of bismuth. However, further addition of bismuth at 20 wt% of bismuth leads to decrease in tensile strength. The initial increase and decreasing behaviour in tensile strength of synthesized composites was observed mainly due to surface contact area and nonhomogeneous distribution of bismuth particles at 20 wt% of bismuth added to HDPE. Beyond 20 wt% of bismuth concentration, the increment in tensile strength is observed for synthesized composites due to the homogeneous distribution of bismuth with HDPE (Fig. 2c). The variation in Young's modulus is also similar to tensile strength as shown in Fig. 5. The elongation at peak load of prepared HDPE composites has shown decreasing trend with increase in bismuth weight percentage (Fig. 6) and this can be ascribed to loss in flexibility of HDPE with increment in filler loadings

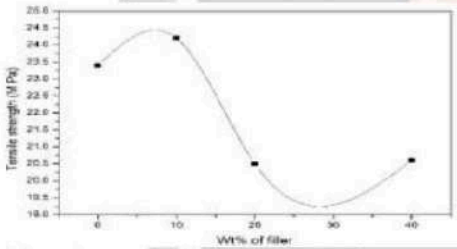

(Moayad N. Khalaf 2015).

Fig-4: Effect of bismuth on tensile strength of HDPE

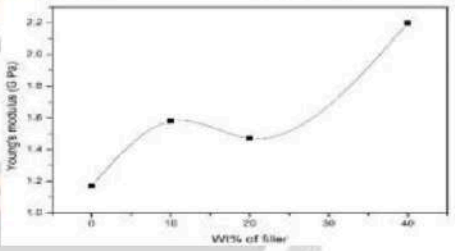

Fig-5: Effect of bismuth on young's modulus of HDPE.

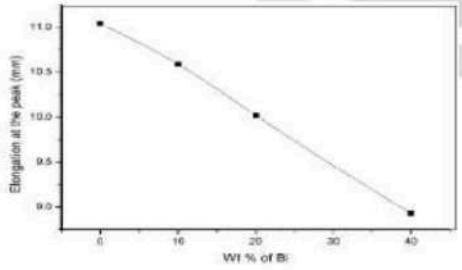

Fig-6: Effect of bismuth on elongation at the peak of HDPE

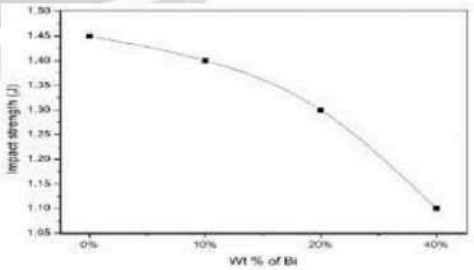

Fig-7: Effect of bismuth on impact strength of HDPE

C. Impact test

Impact strength of HDPE is decreased with the addition of bismuth to HDPE as shown in Fig. 7. This observation is due to decrement in flexibility of the composite with addition of high density bismuth to HDPE

matrix. The material can easily break by the application of external forces at the bismuth and HDPE interface due to weak interaction between them and thus the impact strength of the composites decreases with increment in wt% of bismuth (X-L Wang et al., 2015).

3.3 AC conductivity

The electrical properties were studied by using LCR meter shows that the dielectric constant of the samples increases with the increase in weight percentage of the filler and then slightly decreases with increase in AC frequency as shown in the Fig. 8. This may be due to the fact that the dipolar polarization of HDPE matrix and the interfacial polarization of the HDPE/Bi composites become less in the direction of alternating field at high frequencies. All the samples have shown almost same value of dielectric loss and it decreases with increase in frequency. At higher frequencies the dielectric loss becomes constant as shown in the Fig 9. Fig. 10 shows the AC conductivity remains constant at low frequency and increases sharply with a very narrow range of frequencies in all samples. This may be due to the formation of the conducting phase by the Bismuth filler particle. Fig. 11 shows the decrease in impedance of the sample with increase in bismuth wt % in HDPE composites and with increase in frequency of AC. This is due to the increasing of interfacial polarization (Hussain et al., 2015: Dillip K. Pradhan et al., 2008). Thus the bismuth filled HDPE composites exhibited good dielectric property.

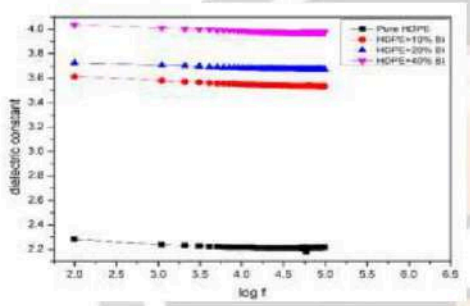

Fig-8: Variation of dielectric constant w r t frequency.

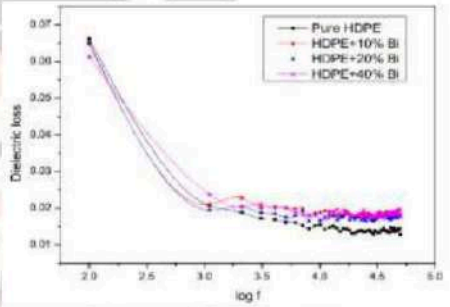

Fig-9: Variation of dielectric loss w.r.t frequency

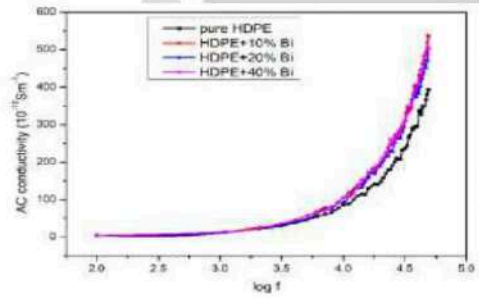

Fig-10: Variation of AC conductivity w.r.t frequency

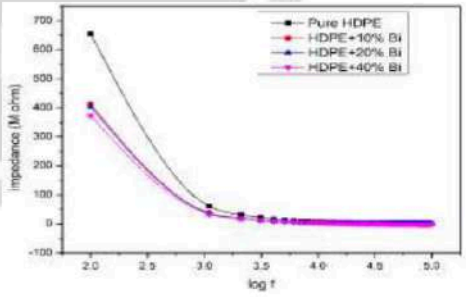

Fig-11: Variation of Impedance w.r.t frequency

4. CONCLUSION

In this study pure bismuth filled HDPE composites were fabricated and their mechanical and electrical properties were analyzed. It was found that bismuth was distributed uniformly within the HDPE matrix. A non-uniform dispersion of the bismuth particles is observed at 20 wt% of bismuth concentration and it tends to decrease in its tensile strength and Young's modulus. Hence, from the present study it is observed that 10 wt% of bismuth is the optimum percentage to be loaded to HDPE to get maximum strength. The dielectric studies and the AC conductivity measurements show that bismuth filled HDPE polymer composites show the sharp increase in ac conductivity at higher frequencies but are of very low value (10^{-10} Sm^{-1}). The value of dielectric constant is observed to increase with the filler weight percentage. The dielectric loss and the impedance of the samples were found to decrease with the frequency. This concludes that the bismuth filled HDPE composites are good dielectrics.

5. ACKNOWLEDGEMENT

The authors are thankful to Dr; Siddaramaiah, Head of the Department of Polymer Science, Sri Jayachamarajendra College of Engineering, Mysore for supporting us in the preparation of the samples and mechanical property studies.

6. REFERENCES

1. Narayana Swamy B, Suresh Babu Y, Tirupati Reddy K, "Mechanical properties of HDPE polymer composites", International Journal of Engineering Science and Computing, January 2017.
2. Daniel Eirasa, Luiz Antonio Pessanb, "Mechanical Properties of Polypropylene/Calcium Carbonate Nanocomposites", Materials Research, Vol. 12, No. 4, 517-522, 2009.
3. Han-Seung Yang, Hyun-Joong Kim, Jungil Son, Hee-Jun Park, Bum-Jae Lee, Taek-Sung Hwang, "Rice-husk flour filled polypropylene composites; mechanical and morphological study", Composite Structures 63 (2004) 305–312.
4. Iftekhar Ahmad and Prakash A. Mahanwar, "Mechanical properties of fly ash filled high density polyethylene", Journal of Minerals & Materials Characterization & Engineering, Vol. 9, No.3, pp.183-198, 2010.
5. Maged A. Osmanand, Ayman Atallah, "Surfactant chain length and tensile properties of calcium carbonate-polyethylene composites", Macromolecular Chemistry and Physics, vol. 208, no. 1, pp. 87– 93, 2007.
6. Moayad N. Khalaf, "Mechanical properties of filled high density polyethylene", Journal of Saudi Chemical Society (2015) 19, 88-91.
7. Ambika M. R., Nagaiah N., Krupashankara M.S., "Study of mechanical strength of polyester-bismuth oxide polymer composites", IJARIIE-ISSN(O)-2395-4396, Vol-2 Issue-1 2016. Vol-1 Issue-5 2016 IJARIIE-ISSN (O)-2395-4396.
8. Qingfa Zhang, Weiming Yi, Zhihe Li, Lihong Wang and Hongzhen Cai, "Mechanical properties of rice husk biochar reinforced high density polyethylene composites", Polymers 2018, 10, 286.
9. Dillip K. Pradhan, Choudhary R. N. P., Samantaray B. K., "Studies of Dielectric Relaxation and AC Conductivity Behavior of Plasticized Polymer Nanocomposite Electrolytes", Int. J. Electrochem. Sci., 3 (2008) 597 – 608.
10. Waleed A. Hussain, Abdullah A. Hussein, Jabar M. Khalaf, Ali H. Al-Mowali, Abdullwahab A. Sultan. "Dielectric Properties and a.c. Conductivity of Epoxy/Alumina Silicate NGK Composites", Advances in Chemical Engineering and Science, 2015, 5, 282-289.
11. X-L Wang, H Ming and H Yin, "Fabrication and properties of HDPE/CF/CaCO3/PE-g-MAH quaternary composites", IOP Conf. Series: Materials Science and Engineering 87 (2015) 012110.

Effects of hematite-lead oxide combination in ethylene-propylene-dienemonomer on shielding 59.54 keV gamma rays

Radiation Physics and Chemistry 156 (2019) 50–57

Contents lists available at ScienceDirect

Radiation Physics and Chemistry

journal homepage: www.elsevier.com/locate/radphyschem

Effects of hematite-lead oxide combination in ethylene-propylene-diene-monomer on shielding 59.54 keV gamma rays

Vinayak Anand Kamat[a], K. Swaroop[a], K.U. Kiran[b], Benny George[c], H.M. Somashekarappa[a,*]

[a] Centre for Application of Radioisotopes and Radiation Technology (CARRT), Mangalore University, Mangalagangotri 574199, Karnataka, India
[b] Government Science College (Autonomous), Hassan 573201, Karnataka, India
[c] Rubber Research Institute of India, Rubber Board, Kottayam 686009, Kerala, India

ARTICLE INFO

Keywords:
Polymer composites
Radiation shielding
Attenuation coefficient
Activation energy

ABSTRACT

Ethylene-propylene-diene-monomer (EPDM) was filled with metal oxides like PbO and Fe_2O_3 and analysed for peroxide vulcanisation kinetics, radiation shielding ability, and thermal stability. Increase in crosslinking density was observed with Fe_2O_3 concentration in the lead oxide-hematite-EPDM (LHE) composites, and radiation shielding property upon addition of total 60 phr fillers was discussed. Among the synthesised composites, P60F0 and P40F20 showed good shielding ability for 59.54 keV gamma rays. All the composites showed good electrical insulation up to 50 kHz AC frequency. Moreover, the P40F20 composite contained relatively less lead content than the P60F0 composite, and also, the mechanical strength and thermal stability of P40F20 was greater than that of the P60F0 composite and therefore, it can be considered as a good shielding material.

1. Introduction

Radiation protection is considered to be one of the necessary aspects for radiation workers, which can be achieved by three parameters, namely, time, distance and shielding. Shielding is most often used to reduce the beam intensity passing through it. Lead (Pb) is one of the highly exploited materials, but has its own limitations. In recent times, polymer composites have gained interest of the scientific community for radiation shielding studies. Based on the application, appropriate fillers and polymer matrix combinations are selected to prepare radiation shielding materials. Some previous investigations on gamma shielding performance of polymers such as Styrene-Butadiene Rubber (SBR) (Abdel-Aziz et al., 1991), polyethylene glycol (Hussain et al., 1997), natural rubber (NR)/SBR blend (Gwaily, 2002), unsaturated polyester (Harish et al., 2009), epoxy (Azman et al., 2013; Eid Gha et al., 2013), loaded with lead oxide and lead ore were reported. Korkut et al. (2013) synthesised epoxy resin filled with ferrochromium slag and evaluated it experimentally and obtained shielding parameters with the Monte Carlo and FLUKA simulations. Dubey et al. (2016) and Ambika et al. (2017) studied the gamma attenuation properties of polydimethylsiloxane and isophthalic resin filled with different concentration of Bi_2O_3. They reported that the shielding ability of the composites increased with the Bi_2O_3 concentration. Kim et al. (2014) synthesised polyethylene coated nano tungsten carbide incorporated with ethylene propylene monomer, which showed enhanced shielding performance up to 75% for ~0.3 MeV gamma rays.

The synthetic elastomer ethylene-propylene-diene monomer (EPDM) because of its saturated and nonpolar chains and least specific gravity (0.86–0.90 kg/m^3) compared with all other rubber materials, exhibited excellent physical properties such as weather and ozone resistance, thermal resistance, dielectric properties, and water and chemical resistance. Furthermore, EPDM has the capacity to include a large concentration of fillers. The appropriate filler loaded EPDM composites found its applications in neutron attenuators, low-level radioactive waste containers and as insulating cable covers in nuclear reactors (Özdemir et al., 2016).

Huang et al. (2016) fabricated lead tungstate ($PbWO_4$) filled EPDM-based polymer composites for shielding gamma rays. They reported that the mass attenuation coefficient of the composites and the tensile strength increased with the increase in $PbWO_4$ concentration (0–400 phr). While selecting polymers for radiation shielding, it is also necessary for the researchers to understand polymer degradation behaviour in the radiation environment. Polymer degradation is mainly influenced by radiation, which will reduce the lifespan of the shielding composite. Hacıoğlu et al. (2013) synthesised two different EPDM compounds with 2,5-di-(t-butyl peroxy)-2,5-dimethylhexane (DMBPHa-aliphatic) and di-(tert-butyl peroxy isopropyl)-benzene (BBPIB-aromatic) peroxide vulcanizing agents. In addition, they studied the irradiation behaviour of EPDM composites at low dose rate (63.16 Gy/h) and high dose rate (993 Gy/h). The sample was irradiated to the highest

* Corresponding author.
E-mail address: carrtmu@gmail.com (H.M. Somashekarappa).

https://doi.org/10.1016/j.radphyschem.2018.10.023
Received 23 June 2018; Received in revised form 17 October 2018; Accepted 26 October 2018
Available online 27 October 2018
0969-806X/

dose of 2156 kGy and it was found that the EPDM compounds could withstand the dose delivered.

Conventional lead aprons have their own drawback such as its heavyweight. In addition, long-term usage of these aprons cause backache and physical fatigue in radiation workers (Özdemir et al., 2018). In the present study, an attempt was made to synthesise flexible lead oxide-hematite-EPDM (LHE) composites with varying concentration of PbO and Fe_2O_3. Also, comparative studies were carried out to evaluate the shielding performance of the synthesised materials and to know the ideal combination of PbO and Fe_2O_3 with EPDM. This work aimed to develop flexible shielding materials, which would possibly found its application in protective clothing for radiation workers, containers for transportation of radioactive sources, containers for radioactive waste management, shielding material in space applications, and many more.

2. Materials and methods

2.1. Fabrication of samples

2.1.1. Materials

The quantity of ethylene propylene diene monomer (EPDM-3045) [ethylene (56 wt%) and diene (4.7 wt%)], antioxidant TQ, ISAF black, paraffinic oil, dicumyl peroxide (DCP), PbO, and Fe_2O_3 used in this work and their suppliers are listed in Table 1.

2.1.2. Synthesis of polymer composites

The EPDM composites were synthesised in two steps. Firstly, the mixing of EPDM with antioxidant TQ, ISAF black, and paraffinic oil was done in an internal mixer (Francis Shaw, KO MK3) for 5 min 30 s at a rotational speed of 70 rpm at 100 °C. Secondly the mixing of high atomic number and high-density metal oxides along with 98% active dicumyl peroxide (DCP) was performed in a two-roll mixing mill. Thus, five flexible LHE composites with five different PbO and Fe_2O_3 combinations were prepared, namely, pristine EPDM (P00), P60F00 (PbO = 60 phr and Fe_2O_3 = 00 phr), P40F20 (PbO = 40 phr and Fe_2O_3 = 20 phr), P20F40 (PbO = 20 phr and Fe_2O_3 = 40 phr) and P00F60 (PbO = 00 phr and Fe_2O_3 = 60 phr).

2.2. Morphological studies

The surface morphological and dispersion of fillers within the LHE composites were analysed using the field emission scanning electron microscope (ULTRA 55 FESEM, Karl Zeiss). Elemental analysis for all the LHE composites was performed using the Energy Dispersive X-ray (EDX) Spectrometer (Karl Zeiss-Sigma) associated with FESEM.

2.3. X-ray diffraction studies (XRD)

The X-ray Diffraction (XRD) was performed with the Rigaku Miniflex diffractometer coupled with the X-ray tube generating Cu-Kα_1 radiation of having a wavelength 1.54060 Å. The X-ray tube was operated with current of 15 mA and voltage of 40 kV. A diffraction spectrum was recorded over the angle (2 θ) from 10° to 80°.

Table 1
Ingredients of EPDM composites.

Ingredients	Content (phr)	Suppliers
EPDM	100	Mitsui Chemicals (Japan)
Antioxidant TQ	1.5	Local Suppliers
ISAF Black	30	Philips Carbon Black Ltd., Kolkata (India)
Paraffinic Oil	10	Local Suppliers
Dicumyl Peroxide (DCP)	3	Peroxide India Pvt. Ltd., Tamil Nadu (India)
PbO	Variable	Loba Chemie Pvt. Ltd., Mumbai (India)
Fe_2O_3	Variable	KIOCL Ltd., Mangaluru (India)

2.4. Study of vulcanisation kinetics

The time required for curing (Tc_{90}) and relative crosslinking density (M_H-M_L) for the synthesised compounds was determined using the Rubber Process Analyser (RPA 2000, Alpha Technologies, USA) as per the procedure of ASTM D 2084-01 at a temperature of 170 °C. LHE composite sheets of thickness 2.0 mm and surface area of 148 mm × 148 mm were prepared in a hot press under pressure of 323 kN and temperature of 170 °C. The sample designation and the corresponding filler concentrations are shown in Table 2.

2.5. Gamma attenuation studies

2.5.1. Experimental setup

A schematic diagram of the experimental setup used for attenuation studies is shown in Fig. 1. The shielding ability of all the synthesised polymer composites can be determined by measuring the gamma rays passing through it. A good and narrow beam geometry was organised by placing a cylindrical lead block of 50 mm thick with a hole diameter of 8 mm for ^{241}Am (source) and 20 mm for NaI(Tl) detector. The gamma spectrometric measurements were carried out by using a well-calibrated 76 mm × 76 mm NaI(Tl) scintillation detector (Thermo Scientific, Germany) integrated with a photomultiplier tube, preamplifier, amplifier, and 2 k multi-channel analyser (MCA). The entire experimental setup was placed over a sturdy wooden table. The data acquisition and analysis were performed with the winTMCA32 software package. A distance of 440 mm was maintained between the ^{241}Am source and the NaI(Tl) detector throughout the experiment. The polymer composite under study was placed at a distance of 220 mm from Americium-241 (^{241}Am ~11.01 GBq) radioactive source. Each measurement was carried out in the time duration of 1000 s and in order to reduce the counting statistical errors by a factor of 0.5, four trials were conducted and the average was taken.

2.5.2. Study of shielding parameters

The intensity of the gamma-ray photons was recorded with and without a sample of known thickness. The interaction probability of the gamma-rays per unit length and other attenuation parameters such as half value layer (HVL) and the relaxation length (λ) of the sample was determined using Eq. (1).

$$I = Io \exp^{-\mu X} \quad (1)$$

where, 'μ' is the linear attenuation coefficient, 'I_0' is the intensity of gamma-rays without any sample and 'I' is the intensity of the gamma-rays, which passes through a sample of thickness 'x'. The percentage attenuation ($\%_{Att}$) as shown by the synthesised LHE composites can also be evaluated using Eq. (2) (Belligin and Aycik, 2014; Dubey et al., 2016).

$$\%_{Att} = \frac{I_o - I}{I_o} \times 100\% \quad (2)$$

2.6. Mechanical properties

Mechanical studies for the synthesised LHE composites were performed using the Universal Testing Machine (UTM, Zwick Roell Z020). The tensile test was performed at room temperature (25 °C) under controlled cross-head speed of 500 mm/min (ASTM D412). Each sample was tested three times and the average values were reported.

Table 2
Effect of PbO and Fe_2O_3 on cure characteristics of peroxide vulcanisation of EPDM at 170 °C.

Sample Designation	PbO (phr)	Fe_2O_3 (phr)	M_L (dNm)	M_H (dNm)	$M_H - M_L$ (dNm)	Ts_1 (min)	Ts_2 (min)	Tc_{90} (min)
P00	0	0	0.573	9.852	9.279	0.87	1.31	8.39
P60F0	60	0	0.601	12.971	12.37	0.75	1.07	8.25
P40F20	40	20	0.696	14.077	13.381	0.69	0.99	8.45
P20F40	20	40	0.761	14.679	13.918	0.65	0.92	8.28
P0F60	0	60	0.796	14.788	13.992	0.60	0.85	7.93

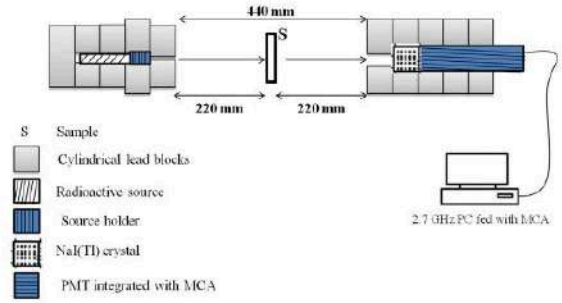

Fig. 1. Schematic representation of experimental set-up for attenuation studies.

2.7. Electrical properties

The AC electrical conductivity studies for the LHE composites were carried out using the Keithley LCR meter. The samples were tested in the frequency range of 40 Hz to 6 MHz at room temperature. Factors such as capacitance (Cp), dissipation factor (tanδ), and resistance (*R*) were utilised to obtain the dielectric constant (ε′), dielectric loss (ε″), and AC conductivity (σ_{ac}) of the synthesised LHE composites by using the following Eqs. Eq. (3–5) (Priyanka et al., 2013).

$$\varepsilon' = \frac{c_p d}{\varepsilon_o A} \tag{3}$$

$$\varepsilon'' = \varepsilon' \tan\delta \tag{4}$$

$$\sigma_{ac} = \varepsilon' \varepsilon_o \omega \tan\delta \tag{5}$$

where, 'ε_0 ' is the permittivity of free space, 'ω' is the angular frequency, and 'A' and 'd' represent the surface area and thickness of the samples, respectively.

2.8. Thermogravimetric analysis (TGA)

The thermal analysis of all the synthesised samples was performed using the universal thermal analyser (SDT Q 600). The thermal behaviour was studied from room temperature to 700 °C under a nitrogen atmosphere with a heating rate of 10 °C/min.

3. Result and discussion

3.1. Morphological studies

Fig. 2(a-e) shows the SEM morphographs and the EDS spectrum obtained for P00, P60F0, P40F20, P20F40, and P0F60. As P00 does not contain any filler, its spectrum shows sharp peaks for C and O. Due to the presence of Fe_2O_3 filler in the P0F60 sample, its EDX spectrum shows only C, Fe, and O elemental peaks. Similarly, P60F0 shows C, Pb, O elemental peaks, since it contains only PbO filler. For the remaining samples (P20F40 and P40F20), the presence of predominant elemental peaks of Pb, Fe, and O was obtained confirming the presence of both PbO and Fe_2O_3 metal oxide fillers in the EPDM matrix. Fig. 2(a) shows the surface morphology of P00 without any impurities and voids. The SEM image of the P60F0 compound [Fig. 2(e)] shows PbO particles spread over the surface of the EPDM matrix. It was also noted that the PbO powders were inhomogeneously dispersed in the EPDM matrix. With the increase in Fe_2O_3 concentration, it was observed that the filler particles had homogeneously dispersed on the surface of the EPDM matrix Fig. 2(b-d). It was observed that the viscosity of the LHE composite increases with the Fe_2O_3 concentration (Table 2) allowing for the impingement of filler particles into the EPDM matrix.

3.2. X-ray diffraction studies (XRD)

The metal oxide fillers (Fe_2O_3 and PbO) and the LHE composites were studied using the powder XRD for structural characterization. The peaks obtained for Fe_2O_3 and PbO by diffraction studies resembled the characteristic peaks obtained from the International Centre of Diffraction Data (ICDD) with card numbers JCPDS-79-1741 and JCPDS-05-0561, respectively as shown in Fig. 3(a). This confirmed that the Fe_2O_3 and PbO used in this work had crystalline monoclinic (Asoufi et al., 2018) and tetragonal (Safarifard and Morsali, 2013; Arulmozhi and Mythili, 2013) structures, respectively.

The diffraction pattern obtained for all the synthesised LHE composites are shown in Fig. 3(b). A broad peak at 18.18° indicated the semi-crystalline nature of the pure EPDM. The sharp peaks at 33.2° (1 0 4), 36.1° (1 1 0), 40.34° (1 1 3), 49.52° (0 2 4), 54.74° (1 1 6), 57.64° (0 1 8), 62.96° (2 1 4), and 64.62° (3 0 0) exhibited by P0F60 was due to the presence of the Fe_2O_3 filler. Also, the prominent peaks at 31.44° (2 0 0), 36.84° (2 1 0), 46.42° (2 0 2), 47.3° (0 2 2), 49.58° (2 2 0), 54.12° (1 1 3), and 60.92° (3 1 1) exhibited by P60F0 was due to the presence of PbO. The remaining samples, P20F40 and P40F20, contained peaks of both the fillers. The intensity of the semi-crystalline peak observed for P00 sample decreased with filler concentration. This indicates, that the crystallinity of the synthesised LHE composites increased with PbO concentration.

3.3. The effect of metal oxides on cure characteristics

The vulcanisation parameters determined using RPA 2000 for the EPDM/metal oxide composites are compiled in Table 2. The values M_L, M_H-M_L, Ts_2, and T_{C90} in Table 2 indicate the viscosity, crosslink density, scorch time, and cure time of the compounds, respectively. Scorch time (Ts_2) is the induction period before the onset of the crosslink formation (vulcanisation). From Table 2 it can be observed, that the viscosity of the samples had increased with Fe_2O_3 concentration. The increment in M_H-M_L values was associated with a decrement in Ts_2 values indicating an increase in the crosslink density of the LHE composites with the increase in Fe_2O_3 concentration (George and Alex, 2014; Özdemir, 2008). The cure time of the LHE composites also decreased with increased Fe_2O_3 concentration. From this, it can be concluded that Fe_2O_3 acts as a catalyst in peroxide vulcanisation (El-Tantawy and Deghaidy, 2000).

3.4. The effect of metal oxides on radiation shielding

The changes in the $\%_{Att}$ values with sample thickness are shown in Fig. 4(a). It was observed that percentage attenuation of the sample increased with the increase in sample thickness. The variation of μ,

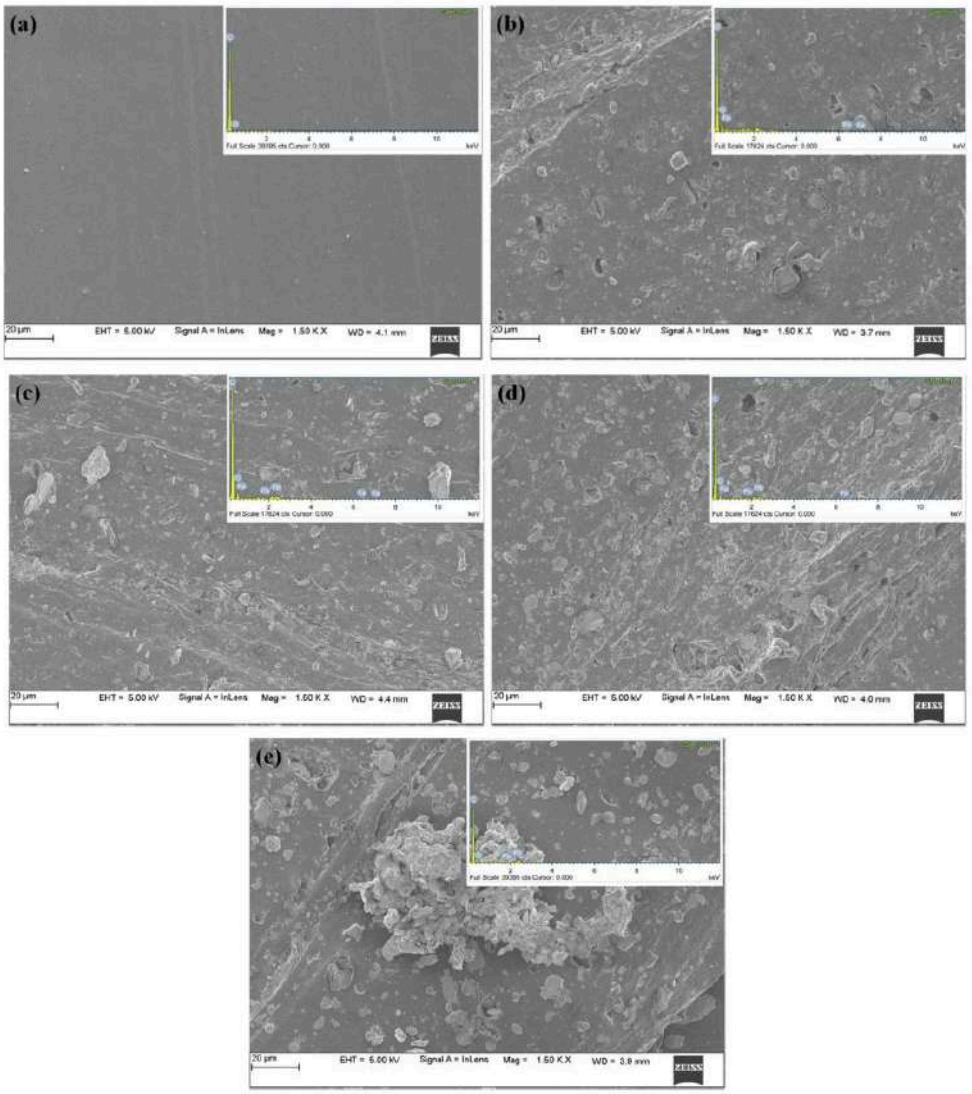

Fig. 2. SEM micrographs and EDS spectrum of (a) P00, (b) P0F60, (c) P20F40, (d) P40F20, and (e) P60F0.

HVL, and relaxation length (λ) with the LHE composites was plotted in Fig. 4(b). It was observed that the value of 'μ' is increased with the PbO concentration. The highest value of 'μ' was obtained for P60F0, as this composition of EPDM contained only PbO. Also, the thickness required to achieve $\%_{Att}$ was less compared with all the other samples. The P60F00 and P40F20 composites showed 99.04$\%_{Att}$ and 95.72$\%_{Att}$, respectively, to 59.54 keV gamma rays. The HVL and relaxation length of the LHE composites was observed to decrease with the increase in PbO concentration. This was due to the presence of high Z materials in the LHE composites (Harish et al., 2012; Kamat et al., 2018). Since the attenuation parameters were studied using narrow beam geometry, the 'build-up' factor was not evaluated in this work.

3.5. Mechanical properties

The mechanical strength of the composites is an important characteristic of various applications. Fig. 5 shows the variation in mechanical properties such as tensile strength, elongation at break, and Young's modulus in the synthesised LHE composites. The values of the tensile strength were observed to increase with the Fe_2O_3 concentration. This may be due to the better interaction between the Fe_2O_3 and polymer matrix than that with PbO. Also, the elongation at break was observed to decrease in the sample containing the fillers compared with the pristine P00. This may be attributed to a decrease in mobility of the polymer chains on the addition of fillers (Huang et al., 2016; Harish et al., 2012). In the present study, the highest $\%_{Att}$ was obtained for only two samples, namely, P60F0 and P40F20, but all the mechanical parameters exhibited by the P40F20 samples were superior to that of the P60F0 composites.

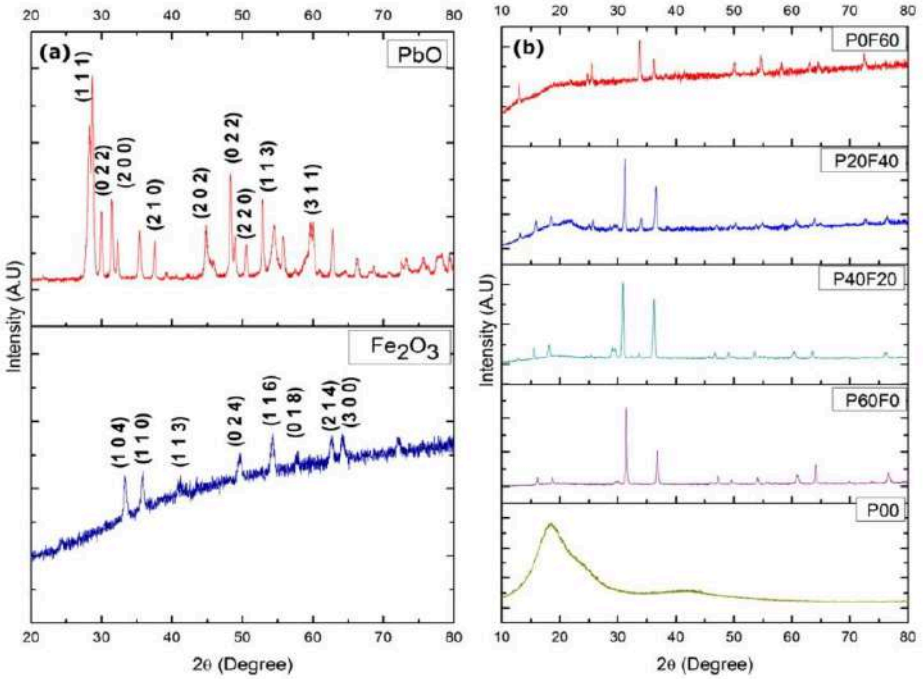

Fig. 3. XRD patterns for (a) PbO and Fe_2O_3 (b) synthesised EPDM composites.

3.6. Electrical properties

The electrical property of the synthesised LHE composites was studied between 40 Hz and 6 MHz AC frequency. The EPDM due to its non-polar and saturated bond acts as a good insulator (Özdemir et al., 2016), but due to the presence of metal oxide fillers (PbO and Fe_2O_3) in its matrix, it may impart some conductivity to the LHE composites. Hence, it is necessary to study the electrical conductivity of the EPDM/metal oxide composites. The variation of dielectric constant (ε'), dielectric loss (ε") and AC conductivity (σ_{ac}) with frequency are given in Fig. 6(a-c). It was observed that all the LHE composites including P00 did not show any conductance up to 50 kHz beyond which there was a sharp rise in AC conductivity. This may be attributed due to the formation of the conducting phase of the metal oxide fillers at high frequency (Kamat et al., 2018). Also in Fig. 6(b), the dielectric constant of all the LHE composites was found to decrease at a lower frequency and saturate at higher frequencies. This variation was associated with the dominance of dipolar and interfacial polarisation at a lower frequency. At higher frequency, it is difficult for the dipoles to orient in the direction of the applied field (Mohapatra Saumya et al., 2008; Hussain et al., 2015). All the LHE composites containing metal oxide fillers showed more dielectric loss compared with that of pristine Fig. 6(c), which may be due to the presence of the moving charge carriers (PbO and Fe_2O_3) (Nithya et al., 2011). Thus, all the LHE composites showed good insulating properties.

3.7. Thermal analysis

The thermograms obtained for all synthesised samples were used to analyse its thermal stability Fig. 7(a & b). There was no significant difference in the thermal stability of the composites observed in Fig. 7(a). All the LHE composites were found to exhibit good thermal

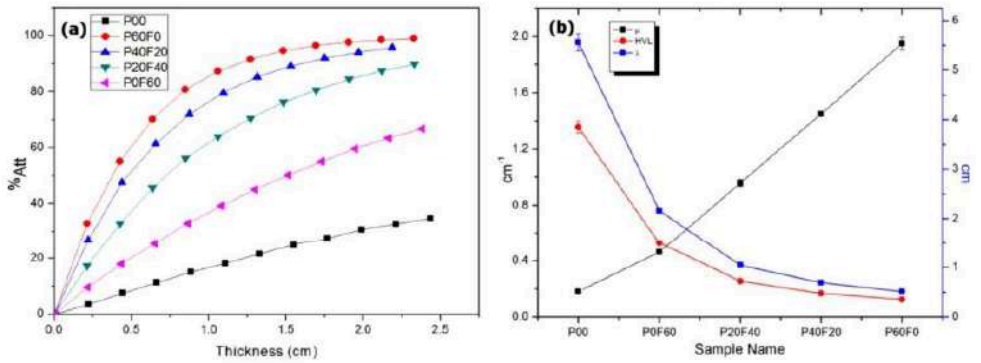

Fig. 4. (a) Plot of $\%_{Att}$ versus sample thickness, and (b) Plot of μ, HVL and λ for LHE composites.

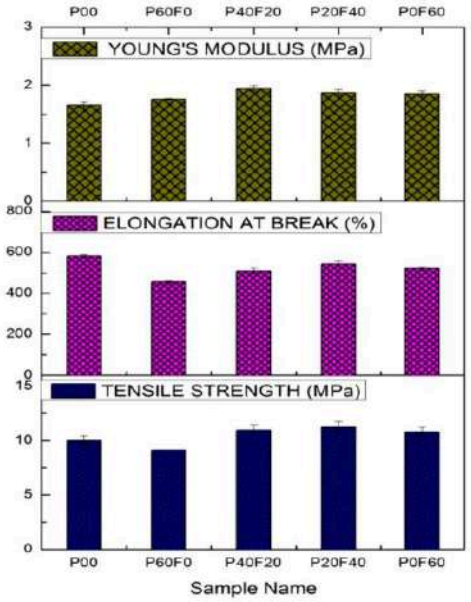

Fig. 5. Variation in Young's modulus, elongation at break and tensile strength of the LHE composites.

stability up to 322.18 °C Fig. 7(b). The temperature at a maximum rate of degradation was observed to increase from 456.97 °C to 459.78 °C with the increment in iron oxide content in the composites. The initial degradation temperature of the LHE composites was also found to increase from 434.36 °C to 438.08 °C with the Fe_2O_3 concentration. This high thermal stability of the LHE composites, with the addition of the Fe_2O_3 fillers, can be attributed to the catalytic action of Fe_2O_3 during vulcanisation. The addition of the Fe_2O_3 fillers leads to a decrease in the unsaturated bonds and thereby, increasing the thermal stability of the LHE composites (El-Tantawy and Deghaidy, 2000).

The data obtained from the TGA was used to calculate the activation energy of the thermal degradation of the LHE composites. The thermal degradation kinetics for all the LHE samples was studied using the Coats-Redfern Equation Eq. (6) (Coats and Redfern, 1964; Abdelrazek and Elashmawi, 2008). Fig. 8(b) represents the variation in activation energy with the change in metal oxide combination. The activation energy depends upon the residual mass of the sample.

$$\log\left(\frac{1-(1-\alpha)^{1-n}}{T^2}\right) = \log\frac{R}{\Delta E}\left(1-\frac{2RT}{E}\right) - 0.434\frac{E}{RT} \tag{6}$$

where, 'R' is the gas constant (8.3136 J/mol K), 'E' is the activation energy of the sample undergoing n^{th} order thermal degradation process, 'T' is absolute temperature, and 'α' is the residual mass, determined using Eq. (7).

$$\alpha = \frac{w_i - w_t}{w_i - w_f} \tag{7}$$

where, 'w_i', 'w_t', and 'w_f' represent initial weight, weight at temperature 't', and final weight of the sample, respectively. By substituting n = 1 in Eq. (6), we get

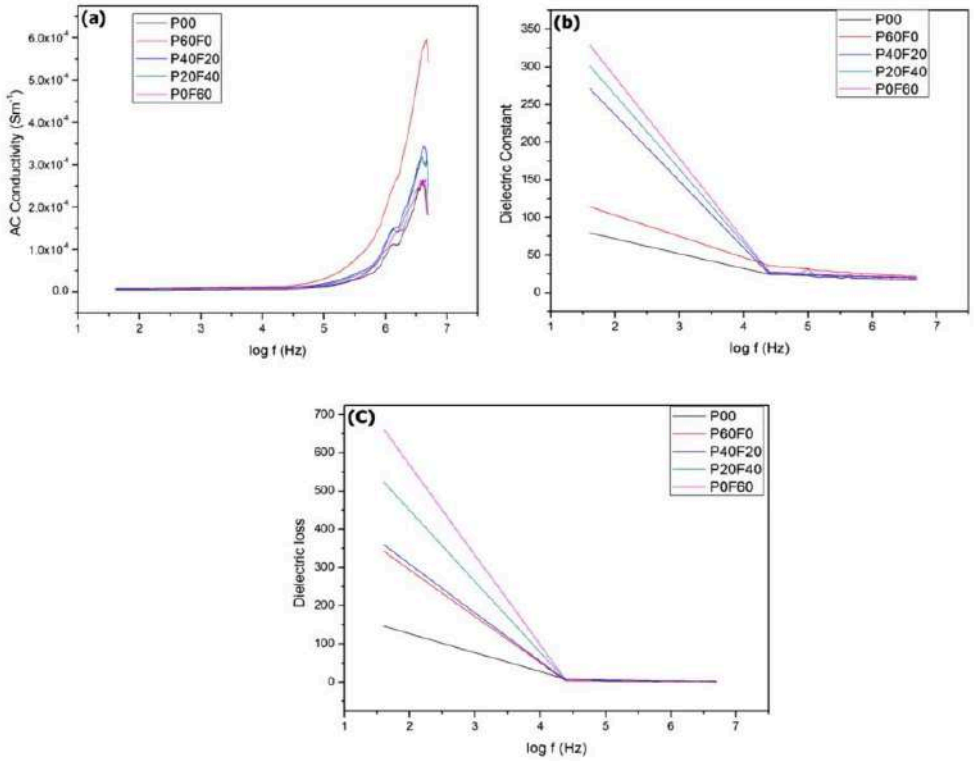

Fig. 6. Plot of (a) AC conductivity (b) dielectric constant, and (c) dielectric loss with respect to frequency for LHE composites.

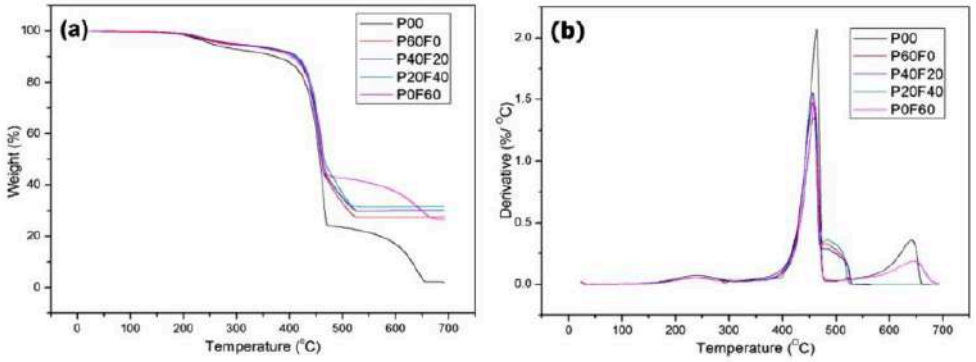

Fig. 7. (a) TG curves, and (b) derivative TG curves of LHE composites.

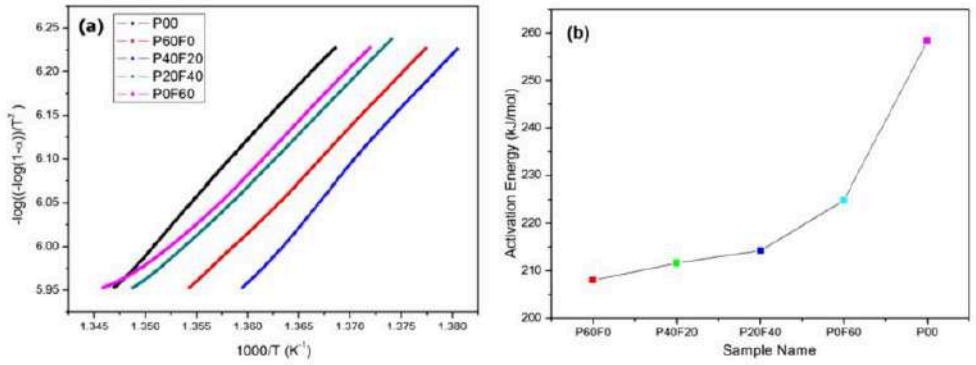

Fig. 8. (a) The dependence of $-\log\left(\frac{-\log(1-\alpha)}{T^2}\right)$ versus $\frac{1000}{T}$, and (b) Plot of Activation energy versus LHE composites.

$$\log\left(\frac{-\log(1-\alpha)}{T^2}\right) = \log\frac{R}{\Delta E}\left(1-\frac{2RT}{E}\right) - 0.434\frac{E}{RT} \quad (8)$$

The activation energy of the samples can be determined by multiplying 2.303 R with the slope obtained from the graph of $-\log\left(\frac{-\log(1-\alpha)}{T^2}\right)$ versus $\left(\frac{1000}{T}\right)$ Fig. 8(a). From Fig. 8(b) it was observed that the activation energy of the sample decreased with the increase in PbO content. The thermal stability of the P40F20 composites was observed to be greater than that of the P60F0 composites.

4. Conclusions

Flexible LHE composites were synthesised successfully using melt mixing techniques. It was observed that the filler, hematite was used to enhance the gamma attenuation behaviour of the pure EPDM,which in turn, acted as a catalyst in the peroxide vulcanisation process. All the synthesised composites showed good attenuation to 59.54 keV gamma rays. The P60F0 flexible sheets of 2.33 cm thickness showed 99.04%$_{Att}$ to 59.54 keV gamma rays. Further, 95.72%$_{Att}$ was observed in 2.19 cm thick P40F20 with a small decrease in PbO content. With reduced PbO concentration, the P40F20 composites showed thermal stability and mechanical strength greater than that of the P60F0 composites and possessed good shielding ability (%$_{Att}$ = 95.72%) for 59.54 keV gamma radiation. Hence, P40F20 can be recommended as a better material for radiation shielding applications with reduced PbO concentration. Since ^{241}Am has found application in power generation, spacecrafts, and radiotherapy, the lightweight EPDM composite with less PbO content (P40F20) can be used as a flexible coat for radiation workers as well as flexible shielding material in space applications.

Acknowledgements

The authors are thankful to the Chairman, Department of Physics, Mangalore University, for providing the ^{241}Am source to conduct the experiment, the Coordinator, DST-PURSE programme, Mangalore University for permitting the use of the FESEM facility and the Head, Microtron Centre, Mangalore University for providing laboratory facility to carry out electrical conductivity studies.

This research did not receive any specific grant from any funding agencies in the public, commercial, or not-for-profit sectors.

References

Abdel-Aziz, M.M., Badran, A.S., Abdel Hakem, A.A., Helaly, F.M., Moustafa, A.B., 1991. Styrene-butadiene rubber/lead oxide composites as gamma radiation shields. J. Appl. Polym. Sci. 42, 1073–1080.

Abdelrazek, E.M., Elashmawi, I.S., 2008. Characterization and physical properties of $CoCl_2$ filled Polyethyl-methacrylate films. Polym. Compos. 1036–1043. https://doi.org/10.1002/pc.20481.

Ambika, M.R., Nagaiah, N., Harish, V., Lokanath, N.K., Sridhar, M.A., Renukappa, N.M., Suman, S.K., 2017. Preparation and characterisation of Isophthalic-Bi_2O_3 polymer composite gamma radiation shields. Radiat. Phys. Chem. 130, 361–368.

Arulmozhi, K.T., Mythili, N., 2013. Studies on the chemical synthesis and characterization of lead oxide nanoparticles with different organic capping agents. AIP Adv. 122122 (2013). https://doi.org/10.1063/1.4858419.

Asoufi, Hassan M., Al-Antary, Tawfiq, M., Awwad, Akl, M., 2018. Green route for synthesis hematite (α-Fe_2O_3) nanopaeticles: toxicity effect on the green peach aphid, Myzus persicae (Sulzer). Environ. Nanotechnol. Monit. Manag. 9, 107–111. <https://www.sciencedirect.com/science/article/pii/S2215153217301824>.

George, Benny, Alex, Rosamma, 2014. Stable free radical assisted scorch control in peroxide vulcanization of EPDM. Rubber Sci. 27, 135–145.

Coats, A.W., Redfern, J.P., 1964. Kinetic parameters from thermogravimetric data. Nature 201, 68–69.

Dubey, K.A., Chaudhari, C.V., Suman, S.K., Raje, N., Mondal, R.K., Grover, V., Murali, S.,

Bhardwaj, Y.K., Varshney, L., 2016. Synthesis of flexible polymer shielding materials for soft gamma rays: physicomechanical and attenuation characteristics of radiation crosslinked polydimethylsiloxane/Bi_2O_3 composites. Polym. Compos. 37, 756–762.

Eid Gha, A., Kany, A.I., El-Toony, M.M., Madbouly, A.M., Bashter, I.I., Gaber, F.A., 2013. Application of epoxy/Pb_3O_4 composite for gamma ray shielding. Arab J. Nucl. Sci. Appl. 46, 226–233.

Eren Belgin, E., Aycik, G.A., 2014. A novel metal oxide filled polyethylene based composite shielding material for protection from harmful effects of ionizing electromagnetic radiation. Akad. Platf. 1194–1201. (http://isites.info/PastConferences/ISITES2014/ISITES2014/papers/A14-ISITES2014ID188.pdf).

El-Tantawy, Farid, Deghaidy, F.S., 2000. Effect of iron oxide on vulcanization kinetics and electrical conductance of butyl rubber. Polym. Int. 49, 1371–1376.

Hacıoğlu, Fırat, Özdemir, Tonguç, Çavdar, Seda, Usanmaz, Ali, 2013. Possible use of EPDM in radioactive waste disposal: long term low dose rate and short term high dose rate irradiation in aquatic and atmosphere environment. Radiat. Phys. Chem. 83, 122–130.

Gwaily, S.E., 2002. Galena/(NR + SBR) rubber composites as gamma radiation shields. Polym. Test. 21, 883–887.

Harish, V., Nagaiah, N., Harish Kumar, H.G., 2012. Lead oxides filled isophthalic resin polymer composites for gamma radiation shielding applications. Indian J. Pure Appl. Phys. 50, 847–850.

Harish, V., Nagaiah, N., Niranjana Prabhu, T., Varughese, K.T., 2009. Preparation and characterization of lead monoxide filled unsaturated polyester based polymer composites for gamma radiation shielding applications. J. Appl. Polym. Sci. 112, 1503–1508.

Hussain, Waleed A., Hussein, Abdullah, A., Khalaf, Jabar, M., Al-Mowali, Ali, H., Sultan, Abdulwahab, A., 2015. Dielectric properties and a.c. conductivity of epoxy/alumina silicate NGK composites. Adv. Chem. Eng. Sci. 5, 282–289.

Kim, Jaewoo, Seo, Duckbong, Lee, Byung Chul, Seo, Young Soo, William Miller, H.., 2014. Nano-W dispersed gamma radiation shielding material. Adv. Eng. Mater. 16, 1083–1089.

Mohapatra Saumya, R., Thakur Awalendra, K., Choudhary, R.N.P., 2008. Studies on dielectric properties of conducting polymer nanocomposite system. Indian J. Eng. Mater. Sci. 15, 347–351.

Nithya, H., Selvasekarapandian, S., Arun Kumar, D., Sakunthala, A., Hema, M., Christopherselvin, P., Kawamura, Junichi, Baskaran, R., Sanjeeviraja, C., 2011. Thermal and dielectric studies of polymer electrolyte based on P(ECH-EO). Mater. Chem. Phys. 126, 404–408.

Azman, Nurul Zahirah Noor, Siddiqi, Salim Ahmed, Hart, Robin, Low, Iv. Meng, 2013. Microstructural design of lead oxide-epoxy composites for radiation shielding purposes. J. Appl. Polym. Sci. 128, 3213–3219.

Özdemir, T., Akbay, İ.K., Uzun, H., Reyhancan, İ.A., 2016. Neutron shielding of EPDM rubber with boric acid: mechanical, thermal properties and neutron absorption tests. Prog. Nucl. Energy 89, 102–109.

Özdemir, T., Güngör, A., Akbay, I.K., Uzun, H., Babuccuoglu, Y., 2018. Nano lead oxide and epdm composite for development of polymer based radiation shielding material: gamma irradiation and attenuation tests. Radiat. Phys. Chem. 144, 248–255.

Priyanka, K.P., Joseph, Sunny, Thankachan, Smitha, Mohammed, E.M., Varghese, Thomas, 2013. Dielectric properties and AC conductivity of nanocrystalline titania. J. Basic. Phys. 2, 4–7.

Hussain, Rizwan, Zia-Ul-Haq, Mohammad, Din, 1997. A study of the shielding properties of polyethylene glycol-lead oxide composite. J. Islam. Acad. Sci. 10, 81–84.

Özdemir, Tonguç, 2008. Gamma irradiation degradation/modification of 5-ethylidene 2-norbornene (ENB)-based ethylene propylene diene rubber (EPDM) depending on ENB content of EPDM and type/content of peroxides used in vulcanization. Radiat. Phys. Chem. 77, 787–793.

Korkut, Turgay, Gencel, Osman, Kam, Erol, Brostow, Witold, 2013. X-ray, Gamma, and Neutron radiation tests on epoxy-ferrochromium slag composites by experiments and Monte Carlo simulations. Int. J. Polym. Anal. Charact. 18, 224–231.

Safarifard, Vahid, Morsali, Ali, 2013. Sonochemical syntheses of nano lead(II) iodide triazole carboxylate coordination polymer: precursor for facile fabrication of lead(II) oxide/iodide nano-structures. Inorg. Chim. Acta 398, 151–157.

Kamat, Vinayak Anand, Swaroop, K., Kiran, K.U., Somashekarappa, H.M., 2018. Study on the effect of PbO-magnetite (Fe_3O_4) on shielding properties of EPDM composites for 662 keV gamma rays. Indian J. Pure Appl. Phys. 56, 639–642.

Huang, Wen, Yang, Wenbin, Ma, Quan, Wu, Juying, Fan, Jinghui, Zhang, Kai, 2016. Preparation and characterization of γ-ray radiation shielding $PbWO_4$/EPDM composite. J. Radioanal. Nucl. Chem. 309, 1097–1103.

Studies on the effect of PbO-magnetite (Fe3O4) on shielding properties of EPDM composites for 662 keV gamma rays

Indian Journal of Pure & Applied Physics
Vol. 56, August 2018, pp. 639-642

Studies on the effect of PbO-magnetite (Fe_3O_4) on shielding properties of EPDM composites for 662 keV gamma rays

Vinayak Anand Kamat[a], Swaroop K[a], Kiran K U[b] & Somashekarappa H M[a]*

[a]Centre for Application of Radioisotopes and Radiation Technology (CARRT), Mangalore University, Mangalagangotri 574 199, India

[b]Government Science College (Autonomous), Hassan 573 201, India

Received 9 May 2018

In the present study different combinations of PbO and Fe_3O_4 in ethylene-propylene-diene monomer (EPDM) matrix have been synthesized and studied the ideal combination for gamma ray shielding. Attenuation parameters such as attenuation coefficient (μ), half value layer (HVL), tenth value layer (TVL), relaxation length (λ) and mass attenuation coefficient (μ_m) have been determined for all samples. It has been found that EPDM with 40 phr of lead oxide and 20 phr of magnetite (DCPM20) has good attenuation ability compared to other synthesized samples for 662 keV gamma rays. Also, DCPM20 has shown better mechanical and AC electrical conductivity properties compared to pure lead-based EPDM composites. Considering all the studied parameters DCPM20 sample has been found to be better radiation shielding material among the studied composites.

Keywords: Attenuation coefficient, HVL, TVL, Relaxation length, AC conductivity

1 Introduction

Gamma radiation is part of electromagnetic radiation which found its great application in industry and medicine[1]. But unwanted exposure to this ionizing radiation will always lead to some severe damages. Research on flexible radiation shielding material is of great interests to protect the workers from these radiations. Incident gamma energy with high atomic number (*Z*) materials gradually reduced by Compton scattering or by electron pair production and vanishes by the photoelectric effect[2]. A further degree of attenuation also depends upon the energy of the incident photon. Ambika *et al.*[3] studied the effect of Bi_2O_3 rate on gamma radiation shielding property of isophthalic resin samples. Otto *et al.*[4] has studied the effect of magnetite ore rate on the gamma radiation shielding properties of concrete samples. Harish *et al.*[5] have studied gamma shielding properties of lead monoxide filled unsaturated polyester based composites. In the present study, different concentrations of PbO and Fe_3O_4 filled EPDM composites were fabricated and their gamma radiation shielding properties were studied.

2 Materials and Methods

2.1 Materials

EPDM is the rubber material used in this work which contains 56% ethylene content, procured from Mitsui Chemicals, USA. ISAF black was procured from Philips Carbon Black Ltd., Kolkata, India. Antioxidant TQ was purchased from local suppliers (analytical grade), dicumyl peroxide-98% (vulcanizing agent) was supplied by Arkema Peroxides India Private Limited, Cuddalore, Tamil Nadu, India and paraffin oil (commercial grade) were procured from local suppliers. Fe_3O_4 (magnetite ore) was kindly supplied by KIOCL Limited., Panambur Mangalore, India. Lead monoxide (99% pure) was purchased from LOBA Chemie Pvt. Ltd. Mumbai, India. All chemicals were used without further purification.

2.2 Sample preparation

In this research work, two fillers namely PbO and Fe_3O_4 were dispersed in EPDM matrix phase. Each sample contains a different proportion of Fe_3O_4 and PbO. Five samples were prepared namely DCPH00 without containing any filler (pristine EPDM), DCPM00 with 60 phr (parts per hundred of rubber) PbO and 0 phr Fe_3O_4, DCPM20 with 40 phr PbO and 20 phr Fe_3O_4, DCPM40 with 20 phr PbO and 40 phr Fe_3O_4 and DCPM60 contains only 60 phr Fe_3O_4. Compounding was performed by melt mixing technique. Mixed compounds were then moulded into sheets of dimensions 14.8 cm×14.8 cm×0.2 cm in a hot press at 170 °C for about 10 min. The samples so obtained were taken for further characterization.

Corresponding author (E-mail: carrtmu@gmail.com)

2.3 Gamma attenuation studies

When initial photon intensity (I_0) passes through a material having thickness X and density ρ, then the intensity of beam transmitted (I) through it is given by Beer-Lamberts law:

$$I = I_0 \exp[-\mu X] \quad \ldots (1)$$

Here, μ is the total linear attenuation coefficient. In this work μ of composite materials was determined for 662 keV energy by using well calibrated 3" × 3" NaI (Tl) detector, coupled to a PC based 2k MCA and ^{137}Cs (~5 mCi) radioactive source. Attenuation parameters such as half value layer (HVL), tenth value layer (TVL) and relaxation length (λ) and mass attenuation coefficient (μ_m) were also evaluated for fabricated samples by using the following equations (Eqs 2-5).

$$\text{HVL} = \frac{\ln 2}{\mu} \quad \ldots (2)$$

$$\text{TVL} = \frac{\ln 10}{\mu} \quad \ldots (3)$$

$$\lambda = \frac{1}{\mu} \quad \ldots (4)$$

$$\mu_m = \frac{\mu}{\rho} \quad \ldots (5)$$

3 Result and Discussion

3.1 Microstructural analysis

Morphological studies were carried out by using field emission scanning electron microscopy (FESEM, Carl Zeiss, Germany). From Fig. 1(a) it was confirmed that PbO granules used in this work having a size varying from 1.985 μm to 3.024 μm, Fig. 1(b) shows the magnetite is having irregular crystals

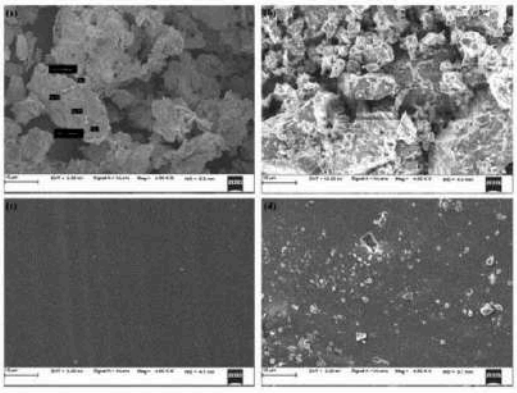

Fig. 1 – FESEM images of (a) PbO, (b) Fe_3O_4, (c) Pristine EPDM (DCPH00) and (d) DCPM40.

shape. Since it was ball milled raw magnetite ore directly obtained from iron ore company, it may contain other impurities like quartz and other minerals[6]. Figure 1(c) shows neat EPDM matrix without any voids and any other impurities on its surface. The surface morphology of DCPM40 (Fig.1(d)) confirms the distribution of filler particles on EPDM matrix. Compatibility of the inorganic filler with organic materials is very low, which may lead to the formation of voids in polymer composites. As fillers dispersed into polymer network prevent passing of gamma photons through matrix vacancies, results in better attenuation of samples loaded with fillers compared to that of pristine (DCPH00). Agglomeration of fillers was observed in Fig. 1(d) leads to modification in the mechanical property of composite samples compared to pure EPDM (DCPH00)[2,3].

3.2 Attenuation studies

Linear attenuation coefficient (μ) replicates the probability of photon interaction per unit thickness of material through which it passes. It was noticed that μ values of all filler combinations increase with respect to pristine DCPH00. Since Pb has high gamma absorption coefficient due to its high atomic number (Z=82), the maximum value of μ was found for DCPM00, which contains 60 phr of lead oxide as a filler material. In the remaining compounds like DCPM20, DCPM40 and DCPM60, μ values are found to be decreasing with decreasing of lead concentration. It has been found that μ value for DCPM00 is slightly higher than that of DCPM20. This may be due to the formation of voids between the inorganic filler (PbO and Fe_3O_4) and an organic phase (EPDM matrix) because of incompatibility. HVL and TVL represent the thickness of the sample required to attenuate the radiation to half and tenth level of incident intensity respectively. The HVL and TVL both were found to decrease for DCPM00 as shown in Fig. 2(a). Relaxation length (λ) is the parameter used to find the length between the two successive gamma interactions. It has been found that λ value tends to decrease for DCPM00 due to high gamma interaction cross-section of Pb compared to Fe (Fig.2(a))[5].

Mass attenuation coefficient (μ_m) is the density-independent parameter, commonly used for comparing the shielding behaviour of different materials regardless of their states. In this study highest value of μ_m is obtained for DCPM20 (0.094 cm^2/g) and DCPM00 (0.093 cm^2/g) among the synthesised composites

(Fig. 2(b)). The values of μ_m obtained for DCPM20 and DCPM00 composites were compared with that of previously reported standard materials for 662 keV gamma rays (Table 1).

3.3 Mechanical studies

Mechanical studies such as tensile test, elongation at break and Young's modulus for synthesised samples have been evaluated by using the universal testing machine (UTM, ZwickRoell Z020) with crosshead displacement rate of 500 mm/min (ASTM D412). From Fig. 3 it has been noticed that tensile strength tends to increase as Fe_3O_4 content increases in samples. This increment in tensile strength may be due to strong bonding force between filler and EPDM matrix. The highest value of elongation at break has been found for the pristine (DCPH00) sample. This may be due to the possibility of free movement of polymer chains. But when fillers are added to polymer matrix mobility of polymer chain ceases, due to the strong interaction between matrix phase and filler phase which leads to decrement in elongation at break[2,5].

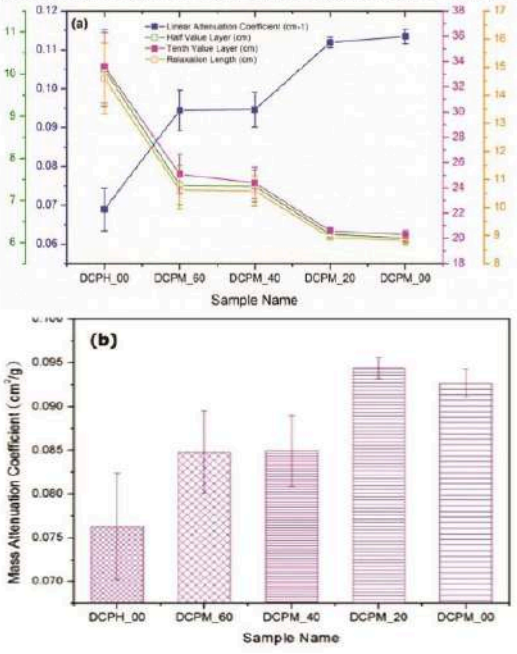

Fig. 2 – (a) Variation of HVL, TVL, λ and μ, and (b) μ_m with different filler combination.

Table 1 – Comparison of μ_m values with the standard shielding materials.

Shielding material	μ_m (cm^2/g)
Lead	0.100[7]
Barite	0.076[8]
Aluminium	0.075[9]
Copper	0.075[9]
85% Barite + 15% colemanite	0.077[8]
DCPM20	0.094
DCPM00	0.093

3.4 Electrical properties

AC electrical conductivity and dielectric properties were studied for all the synthesised samples using Keithley LCR meter. The frequency range from 40 Hz to 6 MHz was selected for AC conductivity and dielectric measurements. From Fig. 4(a) it is clear that all Fe_3O_4 based samples do not show AC conductivity at low-frequency range and this trend continues up to 50 kHz. Conductivity increases sharply as frequency rises from 50 kHz, this can be ascribed to the formation of conducting phase of fillers (PbO and Fe_3O_4). However, DCPM00 starts conducting from 25 kHz. At lower frequencies, dipolar polarization and interfacial polarization are dominant which leads to decrease in the dielectric constant (Fig. 4(b)). At higher frequencies possibility of the orientation of dipoles decreases. It is also found that dielectric loss is more for all samples compared to pristine

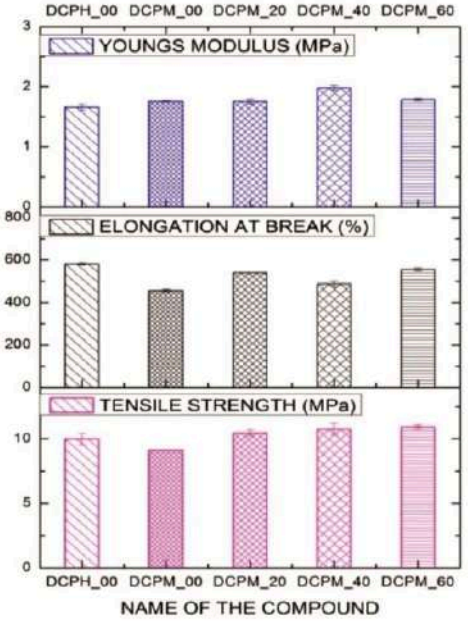

Fig. 3 – Comparison of Young's modulus, elongation at break and tensile strength of samples.

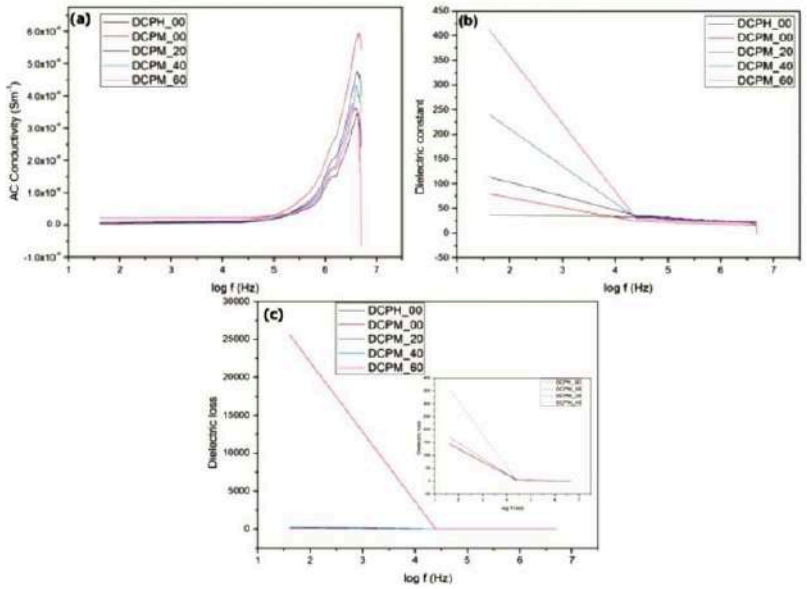

Fig. 4 – Comparison of (a) AC conductivity, (b) dielectric constant and (c) dielectric loss of samples.

DCPH00 due to the addition of mobile charge carriers (PbO and Fe_3O_4) as shown[3] in Fig. 4(c).

4 Conclusions

The EPDM composites with a different combination of PbO and Fe_3O_4 were synthesised for attenuation studies and found DCPM20 composition as a better radiation shielding material compared to others. This may be due to high interaction cross-section of Pb and Fe. Inorganic fillers (PbO and Fe_3O_4) have low interaction with EPDM (organic phase) matrix, and agglomeration of fillers will create voids in the polymer matrix leads to modification in the mechanical property. Also, DCPM20 composites have shown good insulation up to 50 kHz AC frequency. By considering, the gamma attenuation, mechanical and electrical properties of the DCPM20 composite, it is found to be the better radiation shielding material compared to other composites.

Acknowledgement

Authors are thankful to the Coordinator, DST-PURSE program, Mangalore University for permitting to use FESEM facility, the Head, Microtron Centre, Mangalore University for permitting to use electrical conductivity studies and the Director, Rubber Board Research Institute of India (RRII), Kottayam, for helping in synthesising of composites and to use lab facility.

References

1 Sayyed M I, *Chinese J Phys*, 54 (2016) 408.
2 Wen H, Wenbin Y, Quan M, Juying W, Jinghui F & Kai Z, *J Radioanal Nucl Chem*, 309 (2016) 1097.
3 Ambika M R, Nagaiah N, Harish V, Lokanath N K, Sridhar M A, Renukappa N M & Suman S K, *Radiat Phys Chem*, 130 (2017) 351.
4 Otto B & Gür A, *Int J Phys Sci*, 8 (2013) 310.
5 Harish V, Nagaiah N & Harish K H G, *Indian J Pure Appl Phys*, 50 (2012) 847.
6 Boris R, Agnes K & Jörg F, *Meteorit Planet Sci*, 52 (2016) 1495.
7 Eren Belgin E, Aycik G A, Kalemtas A, Pelit A, Dilek D A & Kavak M T, *Radiat Phys Chem*, 115 (2015) 43.
8 Demir F, Budak G, Sahin R, Karabulut A, Oltulu M & Un A, *Ann Nucl Energy*, 38 (2011) 1274.
9 Leclair P, Gamma Ray Attenuation, 2010 Available from http://pleclair.ua.edu//PH255/templates/formal/formal.pdf.